ASTES

Advances in Science, Technology & Engineering Systems Journal

Editorial

Advances in Science, Technology and Engineering Systems Journal (ASTESJ) is an online-only journal dedicated to publishing significant advances covering all aspects of technology relevant to the physical science and engineering communities. The journal regularly publishes articles covering specific topics of interest.

Current Issue features key papers related to multidisciplinary domains involving complex system stemming from numerous disciplines; this is exactly how this journal differs from other interdisciplinary and multidisciplinary engineering journals. This issue contains 10 accepted papers in electrical, computing and IT domains.

Editor-in-chief
Prof. Passerini Kazmersk

CONTENTS

An Application of ANN Model with Bayesian Regularization Learning Algorithm for Computing the Operating Frequency of C-Shaped Patch Antennas

Ahmet Kayabasi[1*], Ali Akdagli[2]

[1]*Engineering Faculty, Department of Electrical-Electronics Engineering, Karamanoglu Mehmetbey University, 70100, Karaman, Turkey*

[2]*Engineering Faculty, Department of Electrical-Electronics Engineering, Mersin University, Ciftlikkoy, Yenisehir, 33343, Mersin, Turkey*

A B S T R A C T

In this paper, an application of artificial neural network (ANN) using bayesian regularization (BR) learning algorithm based on multilayer perceptron (MLP) model is presented for computing the operating frequency of C-shaped patch antennas (CPAs) in UHF band. Firstly, the operating frequencies of 144 CPAs having varied dimensions and electrical parameters were simulated by the XFDTD software package based on the finite-difference time domain (FDTD) method in order to generate the data set for the training and testing processes of the ANN-BR model. Then ANN-BR model was built with data set and while 129 simulated CPAs and remaining 15 simulated CPAs were employed for ANN-BR model training and testing respectively. In order to demonstrate its validity and accuracy, the proposed ANN-BR model was also tested over the simulation data given in the literature. The obtained results show that ANN-BR technique can be successfully used to compute the operating frequency of CPAs without involving any sophisticated methods.

1. Introduction

In the present age of the wireless communication systems are moving towards the miniaturization very rapidly. The patch antennas (PAs) have become popular in wireless communication technology due to their attractive features of low cost, low profile, easy production and conformability to mounting host [1]. By using the substrate materials with high dielectric constant, the smaller antennas can be achieved but this gives rise to decrease the bandwidth and efficiency performances [2]. C-shaped patch antennas (CPAs) formed by slot-loading technique are widely used owing to having better characteristics such as wideband and miniaturized structure [3-5]. In analysis of the traditional PAs techniques such as cavity model [6] and transmission line model [7] are used. However, irregular shaped PAs may not be analyzed with use of these techniques. Simulation and experimental studies are therefore, carried out in analysis and design of irregular shaped

PAs, in general. Powerful simulation tools, which employ electromagnetic methods involving rigorous mathematical formulation and extensive numerical procedures such as finite difference time domain (FDTD) method [8] and method of moment (MoM) [9] are widely utilized; however, the design procedure may be highly time consuming using these tools.

It is well known that current advancements in wireless communication technology have led to increase the use of PAs; hence, simple models should be utilized to analyze their performances such as bandwidth and operating frequency. On the other hand, the operating frequency is of crucial importance in the PA design process because these antennas inherently suffer from the narrow bandwidth. Alternative simple ways should therefore be investigated by taking into consideration that the analysis of the PA is a complex problem because of the fringing fields at the edges. There exist several approaches which vary in accuracy and computational efforts have been proposed to analyze and design PAs. The most widely used can be listed as formulation methods [3-5] and artificial intelligent systems (AIs) [10-15]. Formulation methods are commonly derived with the aid of the optimization

1

algorithm such as genetic, particle swarm, differential evolution etc. The most well-known artificial intelligent systems are the artificial neural network (ANN) [10-13] and the adaptive neuro-fuzzy interference system (ANFIS) [14] and the support vector machine (SVM) [15].

The ANN is a mathematical model inspired by brain's structure. It is an artificial solution to complex and high nonlinear problems. The ANN mimics the working mechanism of the human brain in which highly interconnected neurons and organized into different layers. The neurons contain non-linear type of functions connected mutually by similar synaptic weights. The synaptic weights are weakened or strengthened during the learning process thanks to the learning algorithms such as Levenberg Marquardt (LM), Bayesian regularization (BR), cyclical order incremental update (COIU), Powel-Beale conjugate gradient (PBCG), Fletcher-Powel conjugate gradient (FPCG), Polak-Ribiere conjugate gradient (PRCG), one step secant (OSS) and scaled conjugate gradient (SCG). The performances of the learning algorithms highly depend on the problem, and they should be considered with their own benefits and limitations. BR learning algorithm uptades the weight and bias values according to Levenberg-Marquartd optimization. It minimizes a combination of squared errors and weights and then determines the correct combination so as to produce a network that generalizes well [10].

In our previous works [4-5], a number of approximate formulas with their own simplicity and accuracy have been proposed for calculating the operating frequencies of CPAs. In these formulas, the operating frequency calculation was based on the use of the resonant length equations together with the edge extension dimension and effective relative dielectric constant expressions proposed for rectangular PA (RPA), which leads to more complex the computing process. Several works related to ANN for computing operating frequencies of PAs have been studied in recent years [10-13]. The methods based on ANN were proposed for determining the operating frequency of annular ring [10], E [11], H [12] and L-shaped [13] PAs in the literature. A method of ANN based on MLP model was applied to compute the operating frequencies of annular ring PAs and the constructed model was separately trained with 8 different learning algorithms [10]. The ANN model with Levenberg Marquardt learning algorithm was used to compute the operating frequencies of E, H and L shaped PAs [11-13]. Also in our previous work, ANFIS model has been proposed for predicting the operating frequency of CPAS [14].

In this study, a method of feed forward back propagation (FFBP) ANN model based on multilayered perceptron (MLP) has been designed to compute the operating frequencies of CPAs. In order to create a population data for training and testing the ANN network using bayesian regularization (BR) learning algorithm, the operating frequency values of 144 CPAs operating among 0.33 - 2.92 GHz covering the most bands of GSM, LTE, WLAN and WiMAX standards are determined by means of XFDTD simulation software based on the finite-difference time domain (FDTD) method. In order to provide the generality and stability of the ANN-BR model, the parameters of 129 randomly selected CPAs were utilized to training the models and the 15 remaining's were employed to test the accuracy of the models. The validity of the ANN-BR model is then verified through simulated results of the CPAs reported elsewhere. Furthermore, the proposed model in this study was compared other methods in the literature.

2. Design and Simulation of CPAs

The CPA has a slot with l and w dimensions in the single non-radiating sides of a rectangular patch (LxW) on a substrate of height h with the relative dielectric constant ε_r overall on the ground plane, as shown in Figure 1. Slot loading on the RPA results in a decrease in operating frequency, therefore the operating frequency of the CPA can be reduced effectively.

As shown in Figure 2, in order to determine the operating frequencies, simulations using the XFDTD software package were performed for 144 CPAs with different patch dimensions and various substrate dielectric constant values, as tabulated in Table 1. In the simulations by XFDTD, source wave form was chosen as Gaussian, and the maximum cell size for meshing process was set to 0.7 mm in cubic region. The antennas were supposed to be fed by a coaxial cable with 50 ohm located around $x_0=2(W-w)/3$ and $y_0=(L-l)/2+l$. The antennas operate over the frequency range 0.33 - 2.92 GHz corresponding to the UHF band.
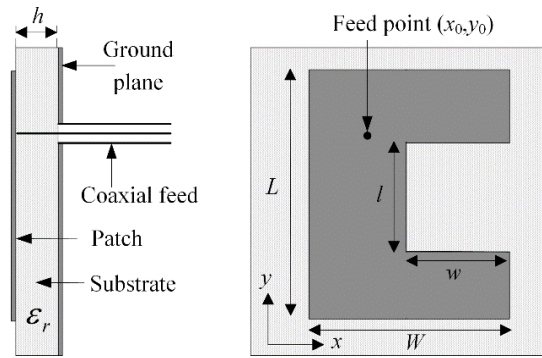
Figure 1: Geometry of CPA
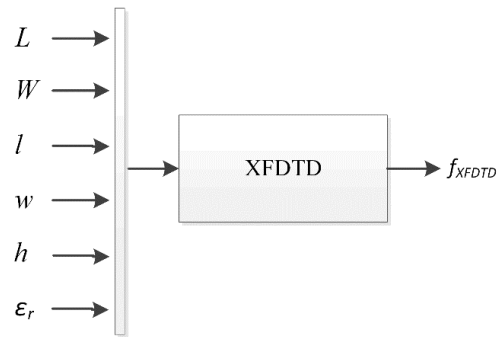
Figure 2: Simulation process by XFDTD

Table 1. The physical and electrical parameters of simulated CPAs

	Patch dimensions (mm)					
	L	W	l	w	h	ε_r
	30	20	7, 12, 15, 20	5, 7, 12, 15	1.6	2.33, 4.28, 9.8
3 x 48	60	40	13, 20, 30, 40	9, 13, 20, 30	3	2.33, 4.28, 9.8
	90	60	20, 30, 40, 60	13, 20, 30, 40	6	2.33, 4.28, 9.8

3. Design of the ANN-BR Model

3.1. Training the ANN-BR Model

The ANN-BR model has been adapted for the computation of the operating frequency of CPAs. As shown in Figure 3, the physical and electrical parameters (L, W, l, w, h and ε_r) of the

antennas were given as input and their respective operating frequency values were given as output for the ANN-BR network.

Thanks to the simulation data, a MLP model of ANN-BR with 3 layers of input, hidden and output layers respectively having 6, 4 and 1 neurons is designed. Whereas the computed operating frequency values are obtained as output from the model of ANN-BR. While the 129 data of simulated 144 CPAs are served to train, and the remaining 15 are used to test the ANN-BR model. The proposed ANN-BR model is given in Figure 4, where f_{XFDTD} and f_{ANN-BR} are the operating frequencies computed by XFDTD packaged software and ANN-BR model, respectively. In the ANN-BR model, "tangent sigmoid" function is used for both input and hidden layers, whereas "purelin" function is utilized for output layer. The BR learning algorithm was used in the ANN model as training algorithm, since it is capable of fast learning and good convergence. The parameters of the ANN model used in this work are tabulated in Table 2. According to (1), the value of the average percentage errors (APE) for the operating frequencies computed by the ANN-BR model was obtained as 0.687% for the 129 CPAs' training data.
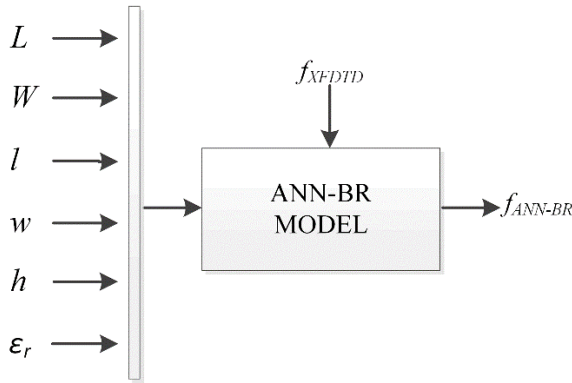
Figure 3: Training process of ANN-BR model
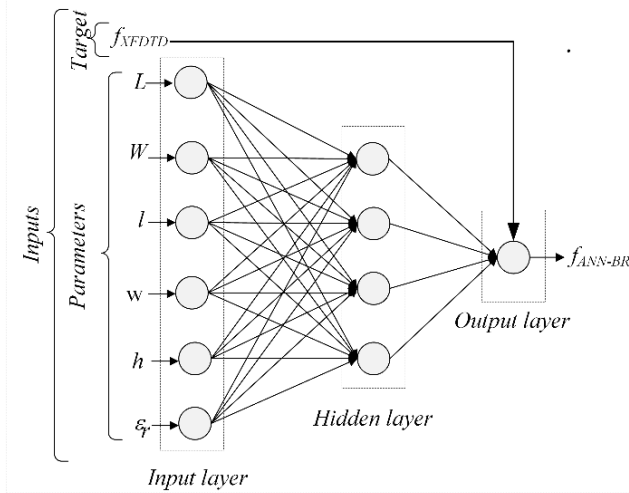
Figure 4: Block diagram of the ANN-BR model

$$APE = \frac{\sum \left| \frac{f_{XFDTD} - f_{ANN-BR}}{f_{XFDTD}} \right| x100}{Total\ antenna\ number} \quad (1)$$

To construct the structure of ANN-BR model, ANN toolbox of MATLAB is used. Training and testing duration take a few seconds after determined parameters that proper with our problem. In the every run process of ANN-BR model, results can be different in each run because initial weights of network is used randomly. The seed value should be fixed to get same result in the every run. For this purpose the seed in the run which is error obtained under desired value is saved. Initial weights of ANN-BR network is fixed by replacing the saved seed value in the program. This method takes time during finding the proper seed value, but after getting the proper seed value, it gives results in a few seconds.

Table 2. The parameters of ANN-BR network

Parameters	Value
Number of input	6
Number of output	1
Epochs	500
Seed value	2084377266
Minimum gradient descent	10^{-10}
Momentum parameter (μ)	0.0001
μ increment	4
μ decrement	0.01
Maximum μ	10^{10}

3.2. The Testing and Verifying the ANN-BR Model

The remainders 15 CPAs from ones used for training process were employed for the test stage and APE value was achieved as 0.757%. This process is shown in Figure 5. The computed operating frequency values and corresponding percentage errors have been given in Table 3. It is clear from the Table 3 that our operating frequencies results are generally in very good agreement with the simulation.
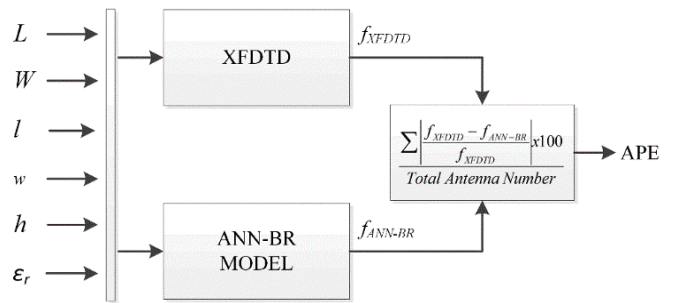
Figure 5: The test process of ANN-BR model

To demonstrate the validity and accuracy of the ANN-BR model, the model was tested against simulation data given elsewhere [3]. The test results are tabulated in Table 4. The values computed with the operating frequency formulas for CPAs given in the literature [4-5] are also given in Table 4. It was observed that the results obtained in this work are better than those predicted by other suggestions. The very good agreement between the simulated values and our computed operating frequency values supports the validity of the ANN-BR model presented here.

Table 3. The operating frequencies determined by ANN-BR model for test process

Antenna number	Patch dimensions (mm)						Operating frequencies (GHz)		Percentage errors (%)
	L	W	l	w	h	ε_r	Simulation	ANN-BR	
1	30	20	15	7	1.6	2.33	2.654	2.656	0.075
2	30	20	7	15	1.6	4.28	1.380	1.378	0.145
3	30	20	20	7	1.6	4.28	2.017	2.030	0.635
4	30	20	12	15	1.6	9.80	0.902	0.895	0.754
5	30	20	20	15	1.6	9.80	0.956	0.951	0.523
6	60	40	30	20	3	2.33	1.164	1.157	0.601
7	60	40	20	9	3	4.28	1.081	1.072	0.805
8	60	40	40	20	3	4.28	0.887	0.911	2.649
9	60	40	30	9	3	9.80	0.721	0.719	0.333
10	60	40	40	30	3	9.80	0.471	0.469	0.425
11	90	60	20	13	6	2.33	0.970	0.980	1.031
12	90	60	40	30	6	2.33	0.776	0.785	1.198
13	90	60	20	40	6	4.28	0.527	0.523	0.816
14	90	60	60	40	6	4.28	0.527	0.524	0.569
15	90	60	60	13	6	9.80	0.499	0.495	0.802
APE									0.757

Table 4. The comparative results for simulated CPAs in the literature [3]

Antenna number	Slot dimensions (mm)		Operating frequencies (GHz)							Percentage errors (%)					
			Sim.	ANN-BR	Calculated			[3]			This Study	[5]	[4]	[3]		
	l	w	[3]	This study	[5]	[4]	For.1	For.2	For.3				For.1	For.2	For.3
1	5	5	1.562	1.61	1.562	1.657	1.502	1.63	—	3.073	0	6.082	3.841	4.353	—
2	10	10	1.445	1.462	1.445	1.497	1.398	1.408	—	1.204	1.315	3.599	3.253	2.561	—
3	15	15	1.286	1.302	1.286	1.334	1.309	1.241	—	1.229	0.467	3.732	1.788	3.499	—
4	20	20	1.13	1.128	1.13	1.178	1.231	1.111	1.002	0.221	0.531	4.248	8.938	1.681	11.33
5	25	25	0.991	0.995	0.991	1.035	1.164	1.008	0.928	0.404	0.908	4.44	17.46	1.715	6.357
6	40	30	0.899	0.905	0.899	0.924	—	0.893	0.856	0.623	1.001	2.781	—	0.667	4.783
7	5	30	0.929	0.936	0.929	0.963	—	1.029	0.904	0.71	0.215	3.66	—	10.764	2.691
8	10	30	0.887	0.888	0.887	0.938	—	—	0.896	0.068	2.706	5.75	—	—	1.015
9	2	30	0.964	0.97	0.964	0.982	—	—	0.91	0.643	1.867	1.867	—	—	5.602
APE										0.908	1.001	1.151	7.055	3.605	5.296

L=60 mm, *W*=40 mm, *h*=1.59 mm, ε_r =2.33, tanδ=0.001, (—): Not available in [3]

4. Conclusion

In this paper, an application of the ANN model which has been used BR learning algorithm is successfully implemented for the prediction of accurate operating frequency of CPAs. XFDTD simulation software based on FDTD was used to define operating frequency of 144 CPAs. ANN-BR model, physically and electrical parameters of 129 CPAs were utilized training data, 15 CPAs were utilized for the test. It was seen that computed results with ANN-BR for training and test data are in a good agreement with the simulation results. The operating frequency results obtained in this study were compared with different simulated and calculated results reported in the literature. The proposed model was achieved the more accurate results as compared to those of the methods proposed in the literature. This ANN model approach is simple and fast modeling which produces more accurate results for the

operating frequency of the CPAs with less computational time and least errors. The most important advantages of ANN model are accuracy and easy to implement for the engineering problems which include the high nonlinearity.

References

[1] R. Garg, P. Bhartia, I. Bahl, A. Ittipiboon, Microstrip Antenna Design Handbook, Londra, Artech House 2001.

[2] K. L. Wong, Compact and Broadband Microstrip Antennas, Wiley, Interscience, 2002.

[3] A. Deshmukh, G. Kumar, "Formulation of resonant frequency for compact rectangular microstrip antennas" Microw. Opt. Techn. Let., **49**: 498–501, 2007.

[4] A. Akdagli, M. B. Bicer, S. Ermis, "A novel expression for resonant length obtained by using artificial bee colony algorithm in calculating resonant

frequency of C-shaped compact microstrip antennas" Turk. J. Electr. Eng. Co., **19**: 597–606, 2011.

[5] A. Toktas, A. Akdagli, M. B. Bicer, A. Kayabasi, "Simple formulas for calculating resonant frequencies of C and H shaped compact microstrip antennas obtained by using artificial bee colony algorithm" J. Electromagnet. Wave., **25**: 1718–1729, 2011.

[6] W. F. Richards, Y. T. Lo, D. D. Harrisson, "An improved theory for microstrip antennas and applications', IEEE T. Antenn. Propag., **29**: 38–46, 1981.

[7] K. Bhattacharyya, R. Garg, "A generalized transmission line model for microstip patches", IEE PROC-H., **132**: 93–98, 1985.

[8] A. Taflove, Computational Electrodynamics: The Finite-Difference Time Domain Method, Boston: Artech House, 1995.

[9] R. F. Harrington, Field Computation by Moment Methods, IEEE Press, Piscataway: NJ, 1993.

[10] A. Akdagli, A. Kayabasi, "An Accurate Computation Method Based on Artificial Neural Networks with Different Learning Algorithms for Resonant Frequency of Annular Ring Microstrip Antennas", J. Comput. Electron., **13**(5): 1014–1019, 2014.

[11] A. Kayabasi, M. B. Bicer, A. Akdagli, A. Toktas, "Computing Resonant Frequency of H-Shaped Compact Microstrip Antennas Operating at UHF Band by Using Artificial Neural Networks", J. Fac. Eng. Archit. Gazi Univ., **26**(4): 833–840, 2011.

[12] A. Akdagli, A. Toktas, A. Kayabasi, İ. Develi, "An application of artificial neural network to compute the resonant frequency of E-shaped compact microstrip antennas", J. Electr. Eng., **64**(5): 317–322, 2013.

[13] A. Kayabasi, A. Toktas, A. Akdagli, M. B. Bicer, D. Ustun, "Applications of ANN and ANFIS to predict the resonant frequency of L-shaped compact microstrip antennas", Appl. Comput. Electrom. **29**(6): 460–469, 2014.

[14] Akdagli A., Kayabasi A., Develi İ. "Computing Resonant Frequency of C Shaped Compact Microstrip Antennas by Using ANFIS", International Int J Electron, **102**(3)**:** 407–417, 2015.

[15] A. Kayabasi, A. Akdagli, "A novel method of support vector machine to compute the resonant frequency of annular ring compact microstrip antennas", Cogent Engineering, **2**(1): 6, 2015.

Ahmet Kayabasi was born in 1980. He received his B.S. and M.S. degrees in Electrical and Electronics Engineering from Selcuk University, Turkey, in 2001, 2005 respectively. In 2015, he received his Ph.D. degree in Electrical and Electronics Engineering from Mersin University, Turkey. From 2001 to 2015, he was a lecturer in the Electronics and Automation Department of Silifke-Tasucu Vocational School of Selcuk University. He has been working as Assistant Professor in the Department of Electrical and Electronics Engineering at Karamanoglu Mehmetbey University. His current research interests include antennas, microstrip antennas, computational electromagnetic, artificial intelligent, and applications of optimization algorithms to electromagnetic problem such as radiation, resonance, and bandwidth. He is a regional editor member of "Advances in Science, Technology and Engineering Systems Journal (ASTESJ)"

Ali Akdagli obtained the B.S., M.S. and Ph.D. degrees from Erciyes University, Kayseri, in 1995, 1997 and 2002 respectively, all in electronic engineering. From 2003 to 2006 he was an assistant professor in the electronic engineering department at Erciyes University. He joined the same department at Mersin University, where he currently works as a professor. He has published more than 90 papers in journals and conference proceedings. His current research interests include evolutionary optimization techniques (genetic algorithm, ant colony optimization, differential evolution, particle swarm optimization, and artificial bee colony algorithms), artificial neural networks and their applications to electromagnetic, microwave circuits, microstrip antennas and antenna pattern synthesis problems. He is an editorial board member of "Recent Patents on Electrical Engineering", International Journal of Computers and Journal of Computational Engineering.

10 Gbps Full Duplex Cost Effective Architecture GPON Network with Single Fiber

Taifoor Ul Islam[1], Aftab Hussain[2], Syed Shees Ashraf[3]

[1]Department of Telecommunication, Institute of Communication Technologies Islamabad, 44000, Pakistan

[2]Department of Electrical Engineering, Swedish College of Engineering and Technology Wah Cantt, 47040, Pakistan

[3]Department of Telecommunication, Institute of Communication Technologies Islamabad, 44000, Pakistan

A R T I C L E I N F O	A B S T R A C T
	In this paper, a full duplex Gigabit Passive Optical Network (GPON) architecture supporting 10Gbps data transmission through single fiber cable network is proposed and demonstrated. A Non Return to Zero Differential Phase Shift Keying (NRZ-DPSK) is utilized for downstream and re-modulate the downstream signal using intensity modulator (on-off keying OOK) in Return to Zero (RZ) format in order to transmit upstream data, sustaining data rate of 10 Gbps/channel is an optimized network in full duplex mode. Simulation results shows that uninterrupted transmission using 50 GHz channel spacing is accomplish over a distance of 25 km.

1. Introduction

A few years ago, internet traffic propensity is shifted from simple web to video based content services [1-2]. The offered copper network is not capable to support such a vast traffic this is the main motive why the complete access network is migrated to Passive Optical Network (PON) [3-4]. Future enabled and highly flexible technology to compile both wireless and wired users in well-ordered method makes PON a promising network [5] solution, provisioning high bandwidth with low CAPEX and OPEX [6].

Time Division Multiplexing-Passive Optical Network (TDM-PON) may be unable to control the continuous growth of high data rate and probable demand of high bandwidth requisite in future. Wavelength Division Multiplexing-Passive Optical Network (WDM-PON) is a possible key solution for offering high data rate on users end and gives optimistic response by escalating growth or demand for broadband application [7]. A Hybrid TDM &WDM format is advance form of PON technology [8], using centralized light source at optical line terminal (OLT) called central office

(CO) and re-modulate the received downstream wavelength for upstream data at optical network unit (ONU) is considered low cost accomplishment [9]. In WDM-TDM-PON different numbers of wavelengths are generated and every single wavelength is utilized on the basis of TDM among numerous ONU's [10]. For that reason, installation of this PON setup results in high resource use and put forward better bandwidth. Similarly, Differential Phase Shift Keying (DPSK) is non-coherent phase shift keying technique that provides improved transmission distance on low power resources and easier circuitry arrangement.

In previous few years different techniques with colorless full duplex transmission for both point to point and broadcast video service were proposed, but the most important weakness was the restriction of uplink data rate up to 2.5Gbps and by means of higher channel spacing of 100GHz [11, 12]. Similarly a network of dual fiber is accomplished of transmitting 10Gbps per channel is measured wastage of assets for both downlink and uplink [13]. A single feeder fiber architecture based on chirp-managed laser (CML) is a enhanced solution for the full duplex transmission because of its economical and petite in size. It can endure dispersion and relay back scattering [14]. This method provides transmission up to 10Gbps in full duplex mode. However it caused drawback of noise factor and signal distortion on the

*Corresponding Author: Taifoor Ul Islam, Department of Telecommunication, Institute of Communication Technologies Islamabad, Pakistan
Tel: +923339621439
Email: engr.taifoor@gmail.com*

receiver end. The above proposed program of ref. 11, 12 and 13 use 60GHz of channel spacing caused definite loss of channel bandwidth. In law, channel spacing should be minimized in order to guarantee more bandwidth.

This paper is an extension of work originally presented in 2015 International Conference on Emerging Technologies (ICET) Peshawar [15]. In this proposed novel approach, we demonstrated a full duplex transmission scheme on single fiber architecture. A 10Gbps data signal used NRZ–DPSK pulse format in downlink, while in uplink 10Gbps data signal is conceded by intensity modulation (IM). This architecture saves the expenditure of second light source at ONU. Simulation results confirmed 10 Gbps downlink data and 10Gbps uplink data with the channel spacing of 50 GHz. We successfully perform the transmission mutually back to back (B2B) and distance over 25km with low bit error rate (BER).

2. Working Principle and Network Architecture

The proposed WDM-PON network architecture is shown in Figure 1.Continuous wave (CW) lasers is used at central office to generate wavelengths from λ_1 to λ_4 for transmission. DPSK modulation is achieved by passing the light into Mach-Zender Modulator (MZM) driven by two complementary outputs of 10 Gbps binary electrical data signal [16]. Four DPSK channels of 10 Gbps are multiplexed and transmitted on full duplex single feeder fiber over a distance of 25 km. On receiver side de-multiplexing is performed and each channel is going towards its nominated ONU. At ONU's half power splitters are used to deliver the data signal to the end user receiver. Whereas, the other half power signal is used to act as carrier signal for the uplink data and re-modulated by Intensity Modulation in OOK format.
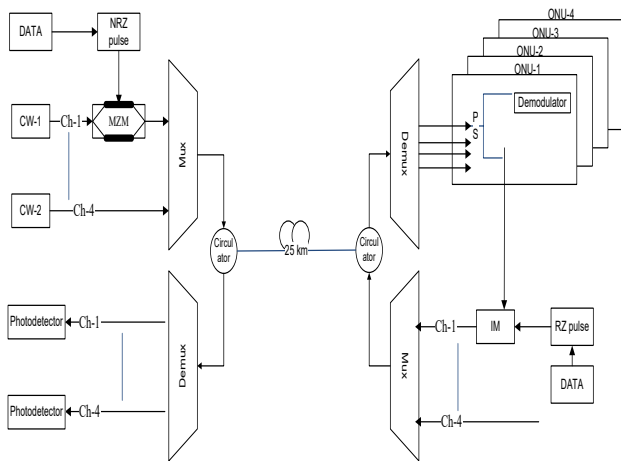

Figure 1 Schematic diagram of proposed WDM-PON Architecture

3. Simulation Setup and Operation

The proposed WDM-PON architecture design full duplex single feeder fiber network with four bi-directional channels of 10 Gbps over a distance 25 km. This model is simulated using Optisystem 7.0 as shown in Figure 2. Four continuous wave lasers are used as a centralized light source to create wavelengths at 1551.3 nm (λ_1), 1551.72 nm (λ_2), 1552.1 nm (λ_3) and 1552.53 nm (λ_4).Visibly evident that channel spacing is 50GHz with the launch power -3 dBm each. Four MZM are used to encode data on these channel

using NRZ-DPSK format. Subsequently, four wavelengths are multiplexed by 4x1 multiplexer with a channel spacing of 50GHz and transmitted over 25km on single feeder fiber architecture. General settings used for Single Mod Fiber (SMF) in simulation model are as follows. Attenuation coefficient (α) is 0.2dB/km, core diameter (ϕ) is set to 80μm2 and dispersion slop is set to zero. The downlink signals are de-multiplexed at receiver side by using1x4 de-multiplexer and forwarded to corresponding ONU. At ONU power splitter is used to tap half power for Mach-Zender Interferometer (MZDI) de-modulator before it is detected on pin receiver. The other half power is given to Mach-Zender Intensity Modulator (IM) driven by 10Gbps uplink data with RZ format. This re-modulated OOK uplink signal is transmitted back to OLT over a distance of 25km on the same fiber. We used pin photo detector with the following specifications; Responsivity (R) is 1A/W and dark current (ID) is 10nA.
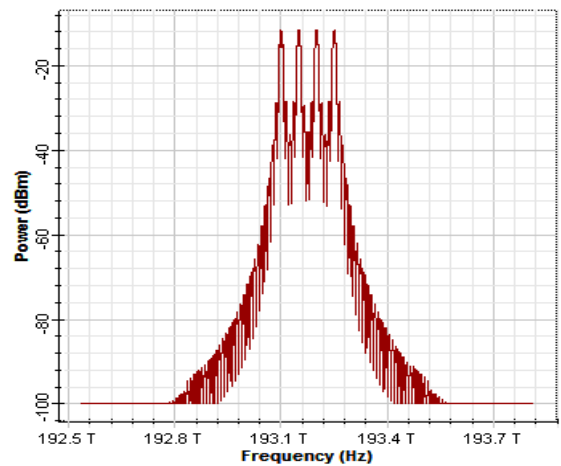
Figure 2 (a) Four downlink DPSK multiplex channels NRZ Based
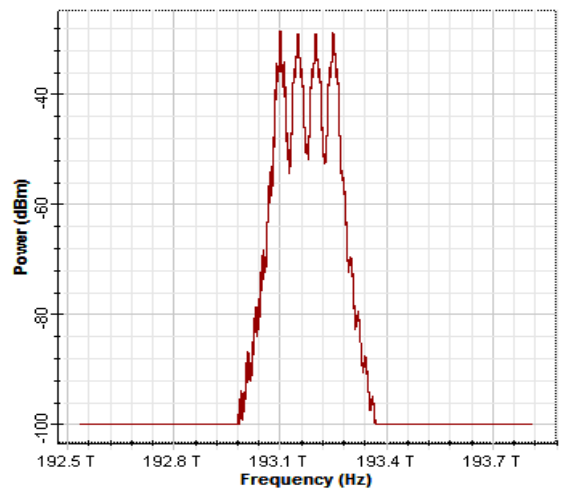
Figure 2 (b) Four downlink DPSK multiplex channels RZ based

4. Performance analysis and results

BER analysis and eye diagram were the main criteria to assess the performance of network. BER as function of received optical power for both uplink and downlink channels are shown in Figure 3. Optical power measured during B2B scenarios in downlink direction at 10^{-9} BER for channels (1, 2, 3 and 4) are -40.36 dBm,

-39.92 dBm, -38.76 dBm and -39.99 dBm respectively. Similarly, optical power measured over a distance of 25 km for downlink channels (1, 2, 3 and 4) are -40 dBm, -39.9 dBm, -38.73 dBm and -39.94 dBm respectively. The differences between each channel power at required BER (0.01, 0.01, 0.03, and 0.05) dBm are called transmission power penalties. Whereas, analyzing the network for OOK uplink data we only consider the 25 km distance values in single feeder fiber. There will no B2B values. Optical power received at required BER for channels (1, 2 and 4) at a distance of 25 km are -31.88 dBm, -27.61 dBm and -28.89 dBm respectively.

Figure 5: Average BER of DPSK DL and OOK UL over 25 km

Figure 3: BER for multiplexed Downlink and Uplink both B2B and 25 km

All DPSK downlink and OOK uplink channels over a distance of 25 km are shown in Figure 4. It is evident that overall network performance is good. Conversely, for better representation of network, the preferable channels are channel-1 and channel-4. As these channels exhibit better results for both downlink and uplink scenarios as compared to the rest. The average power penalty for four downlink multiplexed channels is measured about 0.1 dBm after transmitting over 25 km without any signal amplifier. Figure 5 illustrates average BER for B2B and 25 km downlink and uplink scenarios.

Figure 6: Eye diagrams of DL DPSK channels

Figure 4 BER of downlink and uplink multiplexed channels for 25km

All four DPSK downlink channels eye diagrams are presented in Figure 6. Whereas Figure 7 is showing all feasible OOK uplink eye diagrams. These eye diagrams illustrate that error free transmission is achieved in full duplex on single feeder fiber architecture.
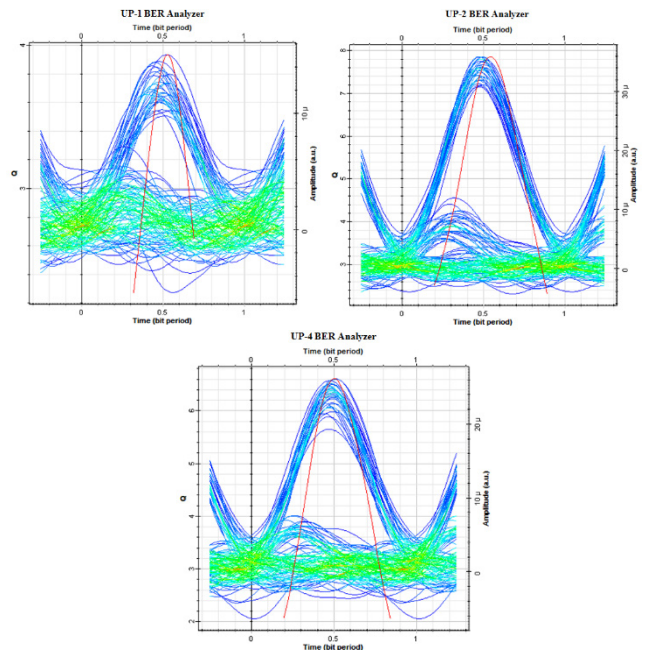
Figure 7: Eye diagram of OOK UL channels

5. Conclusion

We demonstrated 10 Gbps full duplex transmission scheme carried on single fiber network architecture. Our proposed system utilized DPSK format in NRZ shape for downlink path with data rate 10 Gbps/channel and re-modulated the downlink signal using OOK in RZ shape with the same data rate for uplink path. Results showed error free cost effective bi-directional transmission effectively achieved over a distance 25 km with low BER without any additional signal amplifier. Moreover it is also observed that the scheme presented enhanced receiver sensitivity and saved the capital (cost of second fiber for uplink and one external modulator).

References

[1] D. M. S. Sultan and M. T. Arefin ," GPON, the ltimate pertinent of next generation triple-play bandwidth resolution", J. Tel. Info. Techno. **2**: 53-60 (2011)
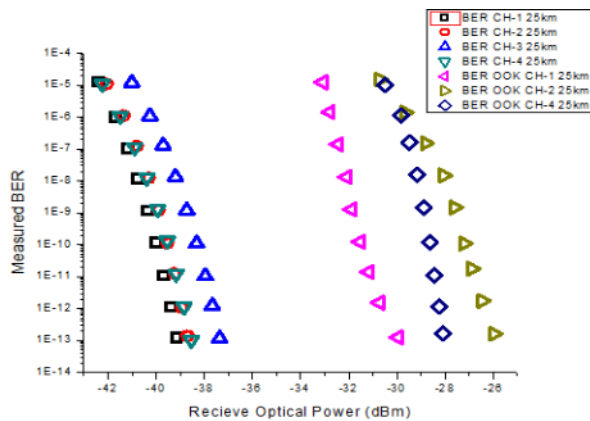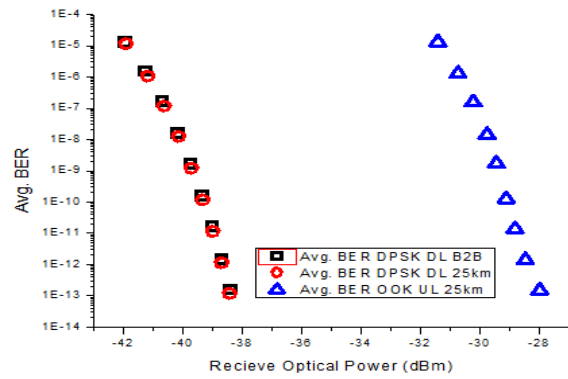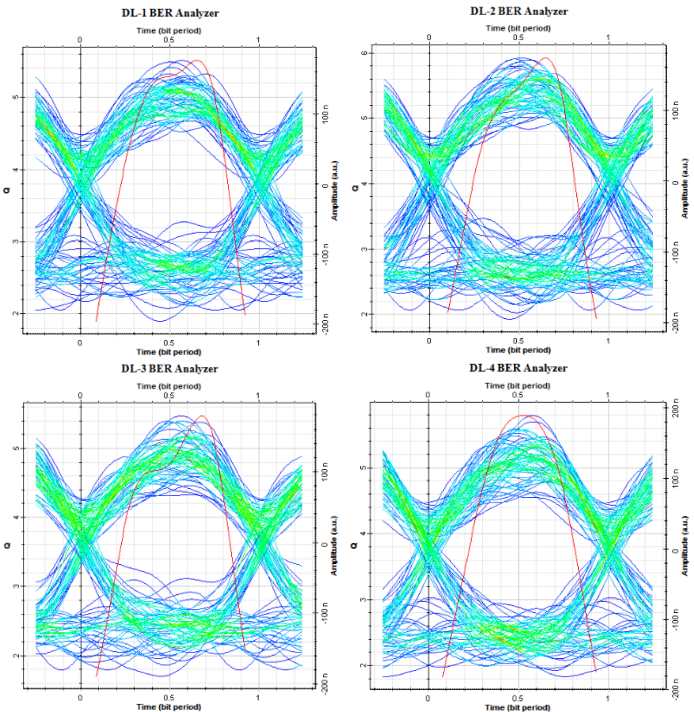
[2] J. Quan-xin, Y. Xiao-li, X. Xiang-jun, Y. Chong-xiu, and L. Bo, "A millimeter-wave WDM-ROF system based on super continuum technique", Optoelect. Letters, **7**: 440-442(2011).

[3] K. Prince, T. B. Gibbon, R. Rodes, E. Hviid, C. I. Mikkelsen, C. Neumeyr, M. Ortsiefer, E. Ronneberg, J. Rosskopf, P. Ohlen, E. In de Betou, B. Stoltz, E. Goobar, J. Olsson, R. Fletcher, C. Abbott, M. Rask, N. Plappert, G. Vollrath, and I. T. Monroy, "GigaWam next-generation WDM-PON enabling gigabit per-user data bandwidth," J. Lightwave Techno. **30**: 1444-1454 (2012).

[4] I. Cale, A. Salihovic, M. Ivekovic, "Gigabit Passive Optical Network – GPON", in Proceedings of the ITI 2007 29th International Conferece on Infomation Technology Interfaces, 679-684 (2007).

[5] A. M. Sitaram, Kadali. M. Swamy, A. R. Krishna, "Gigabit passive optical networks (GPON) the ultimate solution for large bandwidth", Int. J. Innov. Techno. Explor. Engg. **1**: (51-53) 2012.

[6] W. Zahaoqing," Research on the Application of GPON Technologies", IEEE International Conferences on Multimedia and Signal Processing, 61-63 (2011).

[7] Sumanpreet, S. Dewra, "A review on gigabit passive optical network (GPON)", Int. J. Adv. Res. Comp. Comm. Engg., **3**: 5844-5848 (2014).

[8] Y. Liu, G. Zhang, Q. Li, "WDM/TDM hybrid GPON technology", Symposium on Photonics and Optoelectronics (SOPO), 1-3 (2011).

[9] A. M. Khan, Z. Jie, Y. Khan, M. Idrees, Y. Zhao, S. Niazi, A. Husein, A. Munir, I. Ahmed and J. Liu, " A simple and cost-effective design for simultaneous transmission of point-topoint and broadcast services in WDM-PON", Int. J. Fut. Gen. Comm. Network. **6** (41-56) 2013.

[10] Y. Khan, X. Xin, A. Hussain, A. Latif, L. Bo, A. M. Khan, " A cost effective architecture for full duplex hybrid WDM/TDM-PON using dpsk downstream and colorless re-modulated upstream ook data", Adv. Info. Sci. Services Sciences., **4**: 28-35 (2013).

[11] M. I. Afridi, J. Zhang, Y. Khan, A. Ali, A. Hussain, Y. Zhao, S. Niazi, A. M. Khan, "A full duplex broadcasting enabled centralized light source WDM-PON architecture", J. Comput. Info. Sys., **8**: 8885-8890 (2012).

[12] C. H. Yeh, H. C. Chien and S. Chi, "Cost effective colorless rsoa-based WDM-PON with 2.5 gbit/s uplink signal", IEEE Optical Fiber Communication Conference, 1-3 (2008).

[13] A. Hussain, Y. Chong-xiu, X. Xiang-jun, Y. Quan-xin, L. Bo, A. Hussain, A. Latif, A. Munir, Y. Khan, and I. Afridi, "A novel duplex WDM-PON with DPSK modulated downstream and re-modulation of the downlink signal for OOK upstream", Optoelect. Letters, **8**: 134-137 (2012).

[14] A. Hussain, X. Xiang-jun, A. Latif , A. Hussain, Y. Chong-xiu, A. Munir, Y. Khan, and M. I. Afridi, "A novel symmetric 10 Gbit/s architecture with a single feeder fiber for WDM-PON based on chirp-managed laser", Optoelect. Letters, **8**: 468-472 (2012).

[15] T. Ul Islam, A. Husain, S.S. Arshraf, "10Gbps Bidirectional Transmission GPON Network Based on Single Fiber", IEEE International Conferences on Emerging Technologies (ICET), Peshawar Pakistan, (2015).

[16] L. Zhang, X. Hu, P. Cao, T. Wang, and Y. Su, "A bidirectional radio over fiber system with multiband-signal generation using one single-drive MZM", Optics Express, **19**: 5196-5201 (2011).

ARM based Bidirectional Visitor Counter and Automatic Room Light Controller using PIR sensors

Muhammad Umar Farooq*, Aamna Shakoor[1], Abu Bakar Siddique[2]

[1]*Electrical Engineering Department, University of Engineering and Technology Lahore, 54890, Pakistan*

[2] *Electrical Engineering Department, University of Engineering and Technology Lahore, 54890, Pakistan*

A B S T R A C T

With the advancement of technology intelligent devices are fast approaching the realm of necessity from the status of luxury. With limited energy resources, it is the need of time to revolutionize the traditional methods of counting visitors inside hotels, recreational places, meeting rooms and cinemas to control the electrical appliances. Moreover, the improved living standards demand developing circuits that would ease the complexity of life. Many systems have been developed to fill this technological gap but most of them are not applicable in real time scenarios due to their limitations. This paper describes the development and implementation of real time bidirectional visitor counter along with automatic room light controller. The proposed system keeps track of visitors visiting a room as well as takes over the control of the room lights. As a visitor enters the room, the count is incremented by one and the lights are switched on. While the count is decremented if a person leaves the room. Lights of the room are switched off only if there is no person inside. Though a number of systems have been developed in this field but most of them are not practically applicable due to outdated technology. In this paper, we have used state of the art components to develop a practically applicable system. Finally, the system was deployed and tested in real world situations to enumerate its efficiency.

1. Introduction

Most of the regions in the world are undergoing a wave of terrorism. Ongoing circumstances has made one's life completely uncertain. Both developing and developed countries are facing terrorists attacks on social places, not sparing even hotels, schools and care centers. Aftermath of such incidents is large number of causalities. Human deaths and injuries are estimated by trial and error method [1]. Visitor detection check is also vital for no-go and restricted areas. Moreover, in limited sitting places such as cinemas, conference and meeting rooms, it is necessary to keep track of total number of visitors. This requires a system capable of keeping count of and check on total number of visitors in a zone or a building.

Bidirectional Visitor Counter (BVC) is a system used to count the visitors entering and leaving a room. The word bidirectional signifies the count of both types i.e. entering and leaving. When a person enters the room the count is incremented and when a person leaves the room that count is decremented. Bidirectional counters are designed accordance with the real time demands. The design becomes tedious for single door systems where all the visitors are going in and coming out through a single channel.

The energy sources are going scarce. In developing countries the energy consumption rate is higher than the production rate. Therefore it is the need of time to save the energy as

* Electrical Engineering Department UET Lahore, +923030463541,
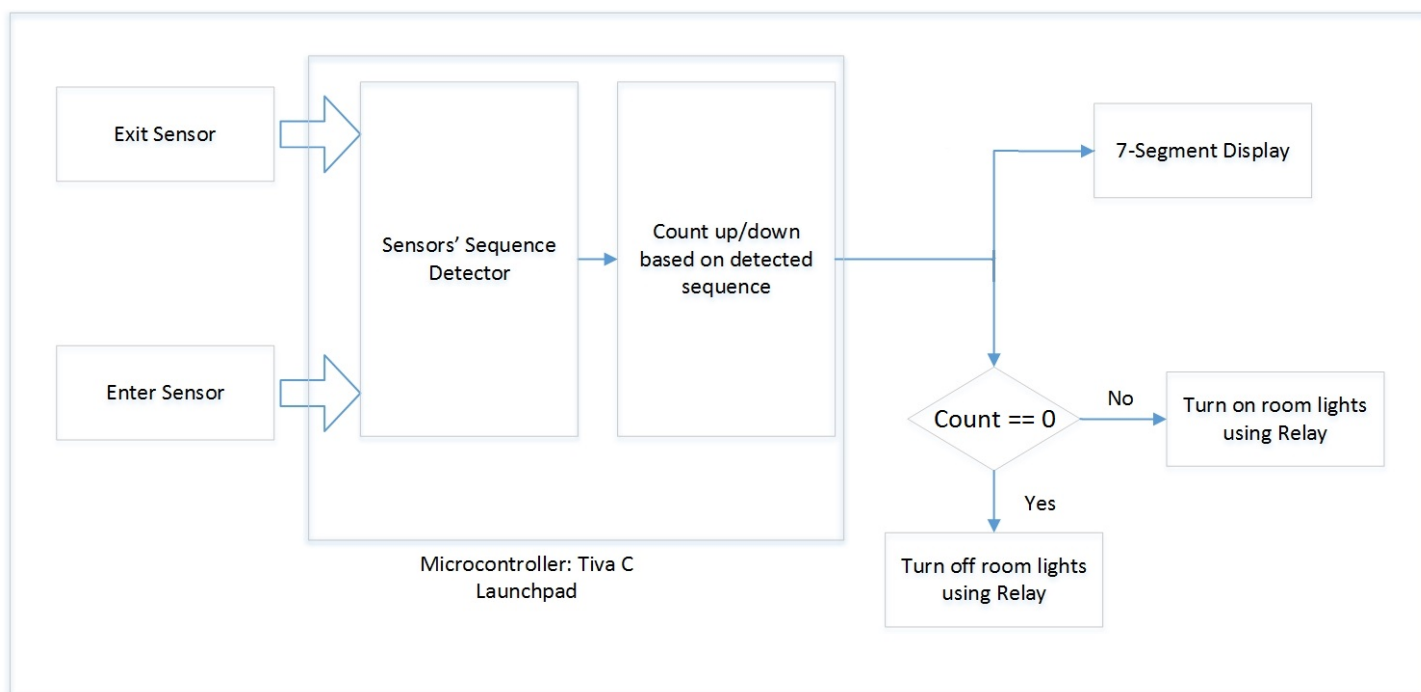mufarooq40@gmail.com

Figure 1: Architecture of Bidirectional Visitor Counter and Automatic Room Light Controller

appliances are manually operated. Most of the times, the electric lights and fans are left running even in the fully evacuated rooms. It demands a shift towards an automated system in order to save energy. This paper describes the development and real time implementation of a bidirectional visitor counter and Automatic Room Light Controller (ARLC). Room light controller works on top of the information gathered through BVC. As soon as the net accumulated counter value falls to zero, the lights of the room and the fans will be turned off to save electricity. The room is automatically re-energized when the count is incremented.

Contrasting to previously developed systems on conventional microcontrollers like PIC and Atmel and limited ranged Infra-Red sensors (IR Sensors), we have used state of the art technology. Though the work can be done by conventional microcontrollers, but with increasing computer technology, it is difficult to program most of those microcontrollers. Moreover, with advanced field of study, researchers and the students are interested in state of art microcontrollers rather than conventional ones. So, our system may be regarded as shift of a developed system from conventional to state of the art technology.

2. Literature Review

Before the advancement of information systems, counting of visitors passing through a location used to been done manually. The room appliances are still mostly controlled manually in most parts of the world that often leads to power wastage in case of personal negligence. With the innovation in technology, many electronic systems such as bidirectional visitors' counters and automatic appliance controllers have been developed to keep check of the visitors visiting a hall and controlling the lights of that room [2-8].

the visitors up and down using output from a IR sensor. These sensors consist of an IR transmitter/receiver (TX/RX) pair. The design of BVCs can be quite simple for two door systems. Where one door is dedicated for entering and the other for leaving. One sensor monitors for the visitors entering and the other one monitors the visitors leaving the room. This is the scenario for which many projects have been developed [2], [5], [8]. But the design becomes more challenging for single door systems where all the visitors are entering and leaving through the single channel. The conventional systems employ IR Transmitter receiver pair, each installed on opposing sides of the door [3]. In such systems, the sensor height, sensor alignment and power supply availability to both the devices offer many installation hurdles. The system can still fail to detect a kid if the installing height of sensors is a larger than the kids' height. Similarly, some visitors may also pass through channel without being detected if the height of the sensors is too low. Moreover, most of the existing systems are based on unreliable IR sensors with their limited range and poor detection with transparent or bright colored materials [11].

In comparison to the older systems, we have used practically applicable PIR sensors rather than ordinary IR sensors. Typical IR sensors used by earlier developers, have much limited range [11]. They can be used to successfully develop a model of sensing range of a few centimeters to inches. However, for practical application on several feet wide doors, PIR sensors are the best choice that we have used in our design. Moreover, a number of conventional microcontrollers were programmed through serial/parallel ports on PC which have been vanished from most of the present laptops and PCs used by a university student. It echoes to shift older technology on the state of the art

microcontrollers. That's why we used a latest microcontroller developed by Texas Instruments (TI).

3. Proposed System

The proposed system is designed using ARM cortex based microcontroller, a seven segment display and two PIR sensors. One of the sensors is installed just outside and the other one just inside the door. Microcontroller determines whether a visitor is coming in or going out by reading the output sequence of the two sensors. We will call the outside sensor Sensor-A and the inside sensor as Sensor-B throughout this paper. The output of the microcontroller derives a relay circuit that turns on the lights of the room when the counter is incremented from 0. All the lights and fans remain turn on until the count is again decremented to its initial value of zero. The flow of our proposed algorithm is shown in Figure 1.

4. Materials and Methods

4.1. Materials

Prior to moving to the working methodology of our system, the used materials are discussed briefly here. Following components has been used in our proposed system:

- Power Supply
- Tiva C Launchpad
- PIR proximity sensor
- HC-SR501
- Common Anode 7-segement display and driver circuit
- Single Relay Module

4.1.1. Power Supply

To provide power to all the components of proposed system, we developed a power supply unit. The first part of this unit is a transformer that steps down 220 V AC mains to 12 V AC. These low voltages are then rectified through a full-wave rectifier. The rectified output is then filtered through filter capacitors and regulated to 5 V DC using a 7805 linear regulator. This supply
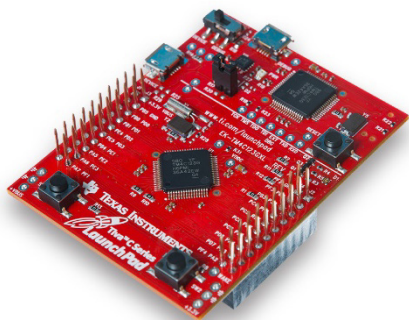

Figure 3: HC-SR501 PIR proximity sensor [9]

unit powers all the components including microcontroller, sensors, seven segment driver circuit and the relay module.

4.1.2. Tiva C Launchpad

In the design we have used ARM Cortex-M (TM4C1233H6PM microcontroller) based Tiva C Launchpad (by Texas Instruments) shown in Figure 2. Details of the microcontroller are given in [10]. The board requires 5 V regulated power supply on VBUS and GND pins. The power is provided through regulated supply of 5 V. Six GPIO ports are available on the board with nomenclature Port A, Port B, Port C, Port D, Port E and Port F. We make use of selected pins from port A, B, E and F. Port A and B are used to provide power and data to 7-segment display respectively. Port E is used to integrate PIR sensors' interrupts and single relay module. The status indicator LEDs are connected to port F. The microcontroller drives and reads the PIR sensors, the 7-segment display and trigger the relay switch.

4.1.3. PIR Proximity Sensor

For visitor detection, we have used two Passive Infra-Red (PIR) proximity motion sensor HC-SR501 as shown in Figure 3. Operating voltage range of sensor is from 4.5 V to 20 V and the power is provided through the supply unit described in first section. Delay time and block time of the sensors are adjustable. The sensing range of HC-SR501 is about 120 degrees up to the distance of seven meters [9]. Though the linear range is useful for most practical scenarios, we found out experimentally that the angle is too wide for satisfactory operation of visitor counting in real world scenarios. The solution of this problem is also discussed in order to improve efficiency. PIR sensors sense an object by comparing the heat emitted by the moving object and the background. So, such sensors must be installed only for stationary backgrounds and heat invariant environments to avoid false switching. Ambient temperature conditions for HC-SR501 is exactly in accordance with room temperature conditions of most of the regions including Asia and some of the European countries.

Figure 2: Tiva C Launchpad microcontroller TM4C1233H6PM [10]
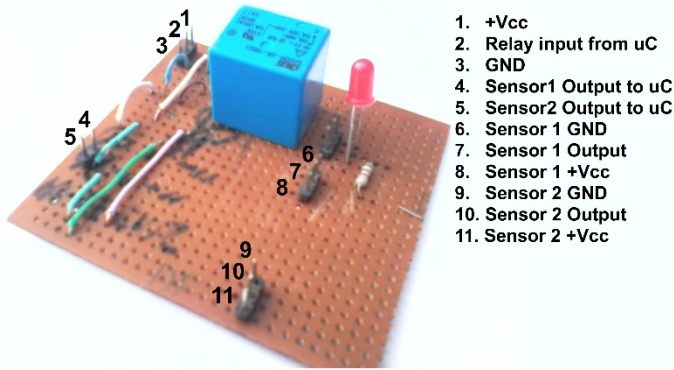
1. +Vcc
2. Relay input from uC
3. GND
4. Sensor1 Output to uC
5. Sensor2 Output to uC
6. Sensor 1 GND
7. Sensor 1 Output
8. Sensor 1 +Vcc
9. Sensor 2 GND
10. Sensor 2 Output
11. Sensor 2 +Vcc

Figure 4: Single Relay Module

Figure 5: Signal loss due to non-overlapping proximity area

4.1.4. Common Anode 7-Segment Display

To display the number of visitors inside a room, we have used a common anode 7-segment display. For this purpose, a driving circuit is designed using four NPN transistors. The driving circuit is powered from the same power supply.

4.1.5. Single Relay Module

This module controls the electric appliances. In common, the room appliances operate on 220 V. So, the single relay module turns on and off these appliances of the room in accordance with the output of bidirectional visitor counter. Single relay module is designed using 5 V DC-220 V AC relay (Figure 4). Relay is triggered by the signal asserted on GPIO pin of microcontroller. As soon as the count is incremented from zero, the relay module triggers and turns on the appliances. The relay moves back to its initial condition only when count falls to zero again.

4.2. Methodology

4.2.1. Working

When a visitor enters a room, it is detected sequentially first by sensor A and then by sensor B. The microcontroller recognizes that sequence and increments the occupancy counter. It can be problematic if there is non-overlapping proximity area of sensors (shown in Figure 5 as a typical case). As soon as anyone of the sensors senses a motion, the corresponding signal is asserted. This signal remains high for a specific time interval after the sensor output goes low. This signal gets away with the problems created by non-overlapping proximity area.

The working of our proposed system is shown in Figure 6. The dotted line shows the door and the Signal-A and Signal-B are
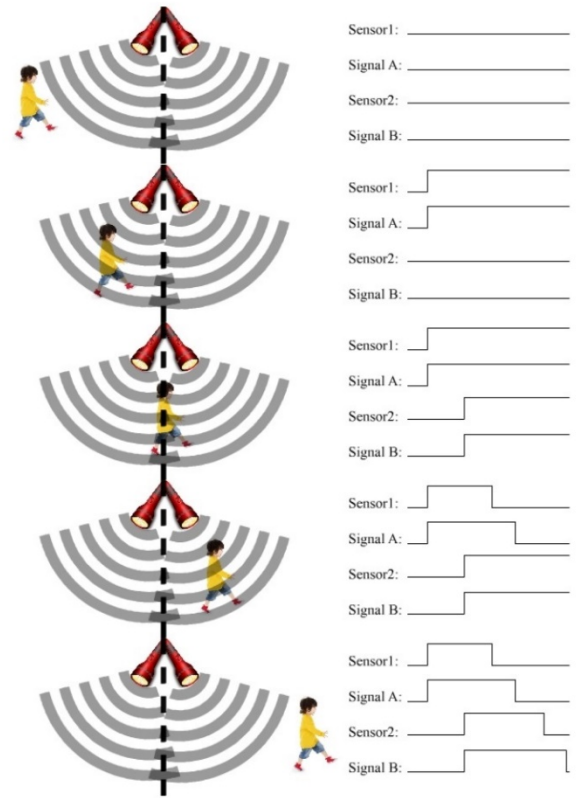

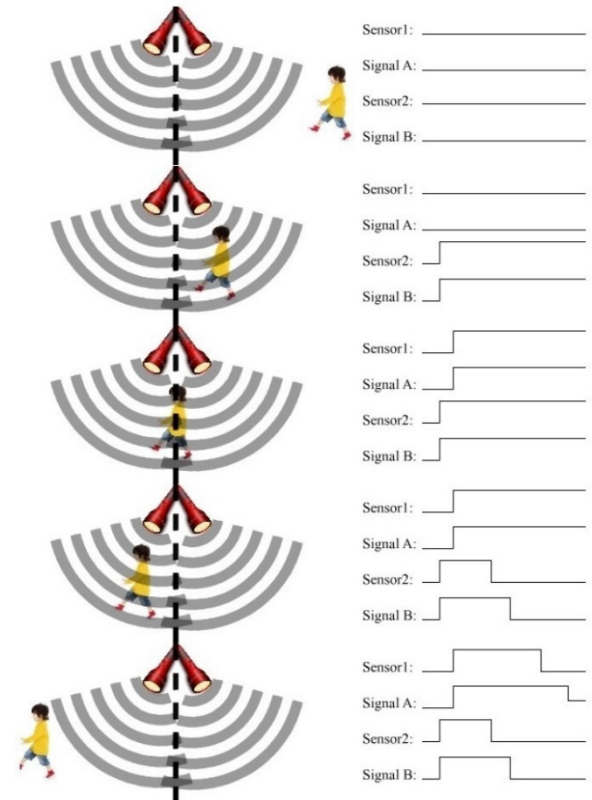Figure 6: Working methodology of our purposed system when a visitor enters

Figure 7: Working methodology of our purposed system when a visitor leaves

the corresponding signals asserted by Sensor A and Sensor B respectively. Same analogy is used for decrementing the occupancy count with only difference that the sensors sequence will be reversed as is shown in Figure 7.

4.2.2. Pseudo Code

```
Algorithm 1: Pseduo Code for uController
if sensor2 then
    system_timer_start ;
    if signalA then
        increment;
    else
        signalB = 1;
    end
end
if sensor1 then
    system_timer_start ;
    if signalB then
        deccrement;
    else
        signalA = 1;
    end
end
System_Timer_Handler :
system_timer_stop;
signalA = signalB = 0;
```

5. Testing and Results

The real time testing was done on main entrance of Department of Electrical Engineering, UET Lahore. The testing under controlled conditions produced 100 % accuracy. The wrong triggers were avoided by allowing just one visitor to be in the range of the sensors at a time. However testing in real time conditions produced about 60 % efficiency the cause of which was diagnosed to be the wide sensing angle of PIR sensors.

In order to increase the efficiency in this scenario it was required to optimally reduce this wide angle. We added an extra view restricting geometry in front of the sensors as depicted in Figure 8 . Due to this addition, we were able to reduce the angle range from 120 degrees to only 40 degrees. Testing this new design in real time improved the accuracy to 96 %.The error of 4 % was found when two persons passed
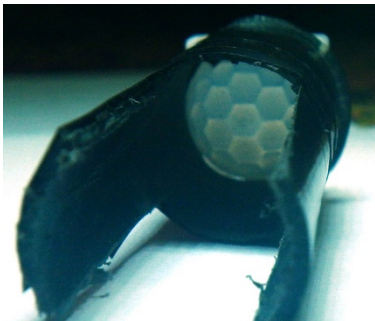

Figure 8: Geometry used to reduce wide angle

before the sensors exactly at the same time. It can be avoided by queueing on the entrances of highly recommended places. For second testing, a class room of the department was chosen. The whole system including BVC and ARLC was tested in this last phase. The system yielded 100 % efficiency by accurately counting the students entering and leaving the class room and turning on and off the lights accordingly.

6. Conclusion

Replacement of the outdated technology with latest one, have made us enable to develop a practically applicable BVC system that produced highly efficient results in practical scenarios. The system is an effective addition for security systems. It may be implemented at sensitive buildings and highly secret meeting rooms. Moreover, it relaxes the management burden in public recreation and limited seats places such as cinemas. In addition to visitor counter, automatic room light controller produces amazing efficiency to control the room appliances which is a desired product for energy deficient developing countries.

7. Future Work

The project can be expanded in various projections. For time being, we have controlled room lights in digital manner such that the lights are turned off automatically when no person is inside the room and turned on automatically when the count is incremented. We intend to control light intensity based on the number of people inside the room. It will be more power friendly in order to save energy. We will also embed with Internet of Things (IoT) technology and WLAN connectivity for observations on world wide web. Moreover, we have intended to develop an automated ticketing systems at cinemas and recreational places to reduce the further load of the management.

Conflict of Interest

The authors declare no conflict of interest.

Acknowledgment

The authors would like to thank Department of Electrical Engineering, UET Lahore for their support to fulfill the laboratory and equipment requirements for the completion of this project.

References

Journal articles:

[1] Edje E. Abel, Ureigho Roy Joel, "Information Systems: The pprospects of bi-directional counter system in the hotel industry", Found. Comp. Sci. FCS. **2**(9) (2015).

[2] Gaurav Waradkar, Hitesh Ramina, Vinay Maitry, Tejasvi Ansurkar, Asha Rawat, Parth Das, "Automated room light controller with visitor counter", Imper. J. Interdisc. Res., **2**(4): 777-780 (2016).

[3] A. Mathur, K. S. Nagl, "Microcontroller-based bidirectional visitor counter", Electronics for You, 78-81 (2007). [Online] Available: http://www.scribd.com/doc/49533576/BiDirectional-VisitorCounter, Accessed in June, 2016.

[4] Mohanaprakash, Sathya, Dhanabal, "Modern multipurpose security and power management system", Int. J. Engg. Res. Gen. Sci., **3**(2): (2015).

[5] K. Shah, P. Savaliya, M. Patel, "Automatic room light controller with bidirectional visitor counter", Int. J. ICT Res. Develop., **1**(4): (2015).

[6] Kimbley, R. Mehrotra, SA Khan, S.K. Pawar, "Automatic room light controller using microcontroller and visitor counter", Int. J. Res. Engg. Techno., **5**(3): (2016).

[7] A. Dey, S. Chakraborty, S. Islam, M. Pramanik, Md. AH Malick, "Design of controllable bidirectional visitor counter" , Int. J. Innov. Res. Elect Electro., Instru. Cont. Engg., **4**(5): 133-136 (2016).

[8] K.H. Majumdar, H. Biswas, H.A. Shaim, K.T. Ahmmed, "Automated Energy Saving and Safety System" in International Conference on Electrical Engineering and Information & Communication Technology (ICEEICT) 2014.

[9] Tiva TM4C1233H6PM Microcontroller, Datasheet [Online]. Available:. http://www.ti.com/lit/ds/symlink/tm4c1233h6pm.pdf, accessed in June, 2016.

[10] "Tiva C. Launchpad DataSheet" , [Online]. Available:. http://www.ti.com/lit/ds/symlink/tm4c1233h6pm.pdf, accessed in June, 2016.

[11] B. Saracoglu, *"A Guide to IR/PIR Sensor Set-Up and Testing"* , Michigan State University.

Representation of Clinical Information in Outpatient Oncology for Prognosis Using Regression

Jennifer Winikus[*1,2], Laura E. Brown[3]

[1]*Computer Science and Engineering, University at Buffalo, The State University of New York, 14260, USA*

[2]*Electrical and Computer Engineering, Michigan Technological University, 49931, USA*

[3]*Computer Science, Michigan Technological University, 49931, USA*

A R T I C L E I N F O	A B S T R A C T
	The determination of length of survival, or prognosis, is often viewed through statistical hazard models or with respect to a future reference time point in a classification approach (e.g., survival after 2 or 5 years). In this research, regression was used to determine a patient's prognosis. Also, multiple behavioral representations of clinical data, including difference trends and splines, are considered for predictor variables, which is different from demographic and tumor characteristics often used. With this approach the amount of clinical samples considered from the available patient data in the model in conjunction with the behavioral representation was explored. The models with the best prognostic performance had data representations that included limited clinical samples and some behavioral interpretations.

1. Introduction

This paper is an extension of work originally presented in 2016 at the IEEE International Conference on Electro Information Technology (EIT) [1]. This extends the prior work by focusing on the prediction of the length of survival through regression rather than with classification techniques. The link between the representation of the patient clinical data and the regression methods for prognosis will be explored. The results show that the data representation with the best prognostic performance may include limited clinical samples and also beharial interpretations of the data.

The American Cancer Society estimates for the year 2016 there will be 1,685,210 new cases of cancer diagnosed. With 1,630 individuals expected to lose their lives each day to cancer [2]. For those affected by cancer, the accurate length of survival prognosis is an important problem which needs to be addressed in order to provide patients and their families information about the effectiveness of treatments, end of life treatment, and/or palliative care.

There are many factors which may go into cancer prognosis prediction including: the type of cancer (some types of cancer are cure-able or go into long-term remission, and others have a low, five-year survival rate), severity of the cancer (stages), patient specific history and condition (comorbidities, state of health, etc.), and treatments. For any given representation, different methods may be used to predict patient prognosis. Many of the techniques consider binary survival, providing information on only if a patient will live to a certain point in time or not. Alternative prognosis methods include classification and regression, providing more information on the length of survival.

For this work, the representation of clinical data with an outpatient oncology data set is considered for prognosis. The clinical data for the patients, consisting of multi-modal non-uniform time-limited data, will be represented through samples taken at discrete time points and with two behavioral representations, difference trends and splines. The prognosis was predicted as length of survival (LOS) using linear and quadratic regression, Gaussian Process with constant basis, and Support Vector Regression (SVR) using radial bias function and linear kernels. The LOS predicted was compared with the actual LOS for each patient to evaluate the prediction models (presented in terms of absolute and relative error).

*Jennifer Winikus, 351 Davis Hall, Buffalo, NY 14260,
Tel: 716-645-4757
Email: jawiniku@mtu.edu

Related work concerning approaches for oncology representation and prognosis is presented in Section 2. The methods for representing the clinical data and experimental design are then presented in Sections 3 and 4. Finally, the results of the regression analysis are presented in Section 5.

2. Background

Machine learning has played a role in many different aspects of oncology including diagnosis, recurance, prognosis, image analysis, malignancy, and staging of tumors [3]. In these methods, the data used can include gene expressions, radiographic images, tissue biopsy sample data, predictors like sex, age, cancer stage, thickness and cancer stage traits such as positive nodes [4]. Cancer tumor staging is a common tool in the data as it considers the size of the tumor, the involvement of lymph nodes and if the cancer has spread [5].

For the clinical data observations, it is possible to treat them as as a time series. In this form there are several methods for representing or transforming the data available, e.g., Fourier analysis (DFT), wavelet analysis (DWT), piecewise aggregate approximation (PAA), etc [6]. Temporal abstraction approaches, which describe a behavior over a period of time (e.g. weight increasing while hemoglobin decreasing), have also been used to represent clinical data [7-8]. It is also possible to take the multiple variables to address the multiple sampling frequencies and types of observations that occur to reduce the values for each observation type to a single value for each period [9].

For the prediction of survival it is often considered from a statistical standpoint with life tables [10], or approaches like Kaplan-Meier or the Cox proportional hazard model [11]. These have the limitation of not providing information about the probability of death, rather only insight based on the population survival over time [12]. Other approaches have been extended to look at survival chances with respect to a point of time, however they are limited to a single point. That is, whether a patient will survive up to time X, where the time points generally considered are for 0.5, 1, 2, 3, and 5 years [13].

Diverse machine learning techniques have been used for predicting survival time including support vector machines [14], Bayesian Networks [15], k-nearest neighbor, and random forest [16]. In one study , the prediction is survivability of 5 years for patients with breast cancer with an accuracy of 89-94% reported using neural networks, decision trees, and logistic regression [17]. Multi-class classification provides more insight into survival time, than a binary classifier, with narrower windows of prognosis. Examples of multi-class approaches include using an ensemble method with 400 support vector machines of binary classifiers [13] or neural networks with four classes [18].

With the complexity of clinical data, classification can also be done based on training incorporating multiple experts. In the case of classification through this approach, temporal abstraction is used to simplify the data and different algorithms, including majority rule and SVM, are used to create consensus classification models [19].

3. Methods

The data used in this study was provided by a private outpatient oncology practice and made available to the researchers by EMOL Health of Clawson, MI.

3.1. Data Collection and LOS Reference Points

For each patient, routine clinical and laboratory tests (weight, WT, albumin, ALB, and hemoglobin, HGB) and treatment administration dates (chemotherapy, blood transfusions, and two erythropoietins) were collected for two years. The amount and duration of data collection varies between patients depending on the number of visits and survival time. The determination of age at time of death was confirmed with the Social Security Death Index.

Table 1 Data Set Characteristics

Properties	Data Set
Patients, *num.*	1311
Weight – lbs. (WT) obs., *num.*	10,653
Albumin – g/dL (ALB) obs., *num.*	5,547
Hemoglobin – g/dL (HGB) obs., *num.*	17,481
Treatments, *num.*	3,411
Age at death (yrs), *mean*	71.61
Age (yrs), *min/mean/max*	22 / 71 / 98
Obs./patient, *min/mean/max*	1 / 28 / 178
LOS from final obs. (days), *mean*	139

Outpatient clinical data is problematic due to the non-uniform sampling, e.g., time between clinic visits or laboratory tests is not uniform. Additionally, the type of clinical information collected may vary between visits and between patients, e.g., different blood tests may be ordered during each visit or not at all for a given patient. The non-uniformity can be observed in Figure 1 as each set of observations is for a different patient and presents a unique distributions of observations.

A prognosis is formed with respect to a reference time point. For example, predicting if a patient has a LOS of two years requires establishing a reference point from which to count the two years. We establish the three reference points, t, t^*_1, and t^*_2 as the basis of the LOS prediction. For each patient, the reference time point t is set when the first type of observation ceases being measured (see Figure 1C). This point was selected to minimize extrapolation errors and dealing with missing data. To avoid bias (t coincides with an observation), t^*_1 and t^*_2 are selected at random from a range about t, with $t^*_1 \in [t\text{-}15, t\text{+}5]$ selected from the range of 15 days further from death to 5 days closer to death and $t^*_2 \in [t\text{-}28, t\text{+}14]$.

The reference points t^* are used in forming the data representation. The evaluation of the LOS prediction is based on the reference points, t^*_1 and t^*_2

3.2. Data Representation

Three representations of the patient clinical observations are considered: clinical data sample values, difference trends, and splines. A fourth type of data representation that of numeric occurances is used for the counts of medical treatments which
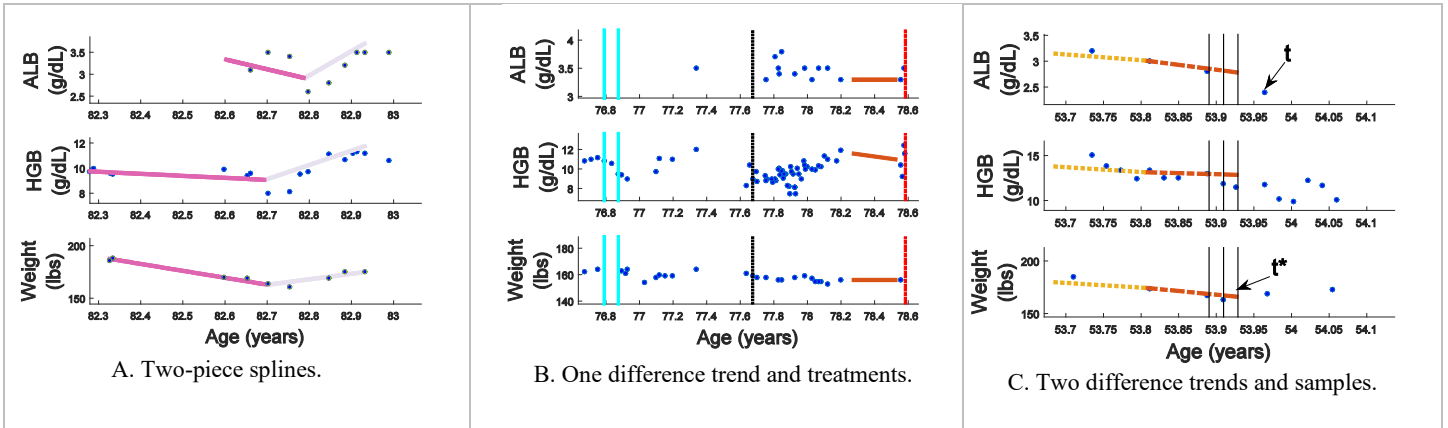
Figure 1 Sample patient data is illustrated with the clinical observations of ALB, HGB and weight (top, middle, and bottom axes). The vertical lines show administered treatments: solid (cyan) - erythropoietin, dashed (black) - blood transfusion, and dot-dash (red) - chemotherapy [1].

the patient experiences. In the data set, these counts include blood transfusion, two different erythropoietins, and chemotherapy. The numeric occurrences (number of treatments) are based in native units prior to standardization.

A patient's clinical values are estimated at uniform intervals for ALB, HGB, and WT at t^* then back at an interval of 7 or 14 days. An example is shown in Figure 1C, where vertical lines represent where the clinical data samples are to be estimated at time t^*, t^* - 7, and t^* - 14 (a sample spacing of 7 days). Cubic splines were utilized to obtain values at the sample times between clinical observations for input to predict LOS by evaluated the splines at the times that the samples were desired. These values are standardized as inputs to the model.

A difference trend (Diffs) describes the observed behavior as increasing, decreasing or stable via a difference between values for ALB, HGB, and WT. Two versions are considered. First, one difference values (1 Diffs) are calculated between values at t^* and 90 days earlier, t^*-90 (note, the values may be predicted, as a sample may not have been collected at this exact time interval); see Figure 1B. Alternatively, two trends (2 Diffs) are found, from t^* back 45 days, then from this point back an additional 45 days; also, shown in Figure 1C).

Finally, splines are used to describe the behavior of the observations. A two-piece second order spline is used to fit the entire observation period for ALB, HGB, and WT observations for a patient (unlike the difference trend which has a recent specified period of consideration); see Figure 1A. The splines' slope coefficient is discretized and used as input to predict LOS.

In summary, the predictors for prognosis include the number of treatments and the following options to consider in the evaluation: 0-5 patient clinical sample values; 1, 2, or no difference trends; and inclusion or not of spline coefficients.

3.3. Length of Survival (LOS) Prediction via Regression

The problem of regression is a supervised learning technique that aims to develop a model to map an input x to an output $f(x)$. The assigned output is a prediction of a continuous quantity or numerical value.

3.3.1 Linear and Quadratic Regression

In linear regression, the objective of determining the numerical result of $f(x)$ is found through a linear model,

$$f(x) = wx + w_0, \tag{1}$$

where x is the input and w is the weight that fits the model, that for a linear model is the slope. The parameter w_0 is the offset or bias parameter to adjust the fit. The parameters in this case are chosen based on the minimization of the error when fitting with the training set.

Similar to the linear regression, quadratic regression determines a numerical outcome but from a higher order model,

$$f(x) = w_2 x^2 + w_1 x + w_0. \tag{2}$$

3.3.2 Gaussian Process Regression

With a Gaussian Process (GP), the inputs are treated as a set of random variables and incorporated with a covariance function to determine a probabilistic outcome of the regression value [20]. The model is defined by the mean and the covariance functions. Given the K input pairs (x, y), the GP regression model summarizes, assuming a zero mean, to [21],

$$P(y|y_1, \ldots, y_K, C(x_i, x_j), \{x_1, \ldots, x_k\}) = \frac{1}{\sqrt{2\pi}\sigma} e^{-\left(\frac{(y-y_*)^2}{2\sigma^2}\right)}, \tag{3}$$

where,

$$y^* = k(x)^T C_K^{-1}(y_1, \ldots, y_K), \tag{4}$$

$$k(x) = \left(C(x_1, x), C(x_2, x), \ldots, C(x_K, x)\right), and \tag{5}$$

$$\sigma = C(x, x) - k(x)^T C_K^{-1} k(x), \tag{6}$$

such that C_K is the covariance matrix evaluated considering the K training set inputs and the current input x. The covariance matrix has the ability to incorporate a kernel or function to modify the functionality, often smoothing or bring periodicity to the behavior [21]. The correct covariance function can increase when it is in regions which are further away from previous regions of known values, and thus shrinks when near [22]. The constant basis will be used for the function in this analysis.

3.3.3 Support Vector Regression

Support vector regression (SVR) is a kernel based approach to determine the regression output. The regression is a set of linear functions,

$$f(x, \alpha) = (w \cdot x) + b, \tag{7}$$

that is aimed to have the error minimized through the loss function ε, and where α is the Lagrange multiplier. The support vectors are represented in the term $\boldsymbol{x}$ and during the fit process variables $\boldsymbol{w}$ and $\boldsymbol{b}$ are determined, such that $\boldsymbol{w}$ is the weight and $\boldsymbol{b}$ is the offset or bias. To allow for the spread in the values, a slack variable is used, ξ_i. The objective is then to minimize [23],

$$\Phi(\boldsymbol{w}, \xi^*, \xi) = \frac{1}{2}(\boldsymbol{w} \cdot \boldsymbol{w}) + C\left(\sum_{i=1}^{l} \xi_i^* + \sum_{i=1}^{l} \xi_i\right), \qquad (8)$$

when there are l samples. To support this boundary, the slack variable, ξ_i, must be greater then or equal to zero [23]. In the evaluation the constraint is used to relate the loss and slack variables to the function,

$$y_i - (\boldsymbol{w} \cdot x_i) - \boldsymbol{b} \leq \varepsilon + \xi_i, \ i = 1, \dots, l. \qquad (9)$$

The SVR approach can be extended to allow for the application of kernel which satisfy Mercer's Condition to be used. In our work, linear and radial basis function kernels will be used.

4. Experimental Design

There are multiple ways discussed to represent the patient observations: clinical data samples, difference trends, and splines. For example, the number of clinical data samples considered varies from zero to five. The number of difference trends included in the evaluation is zero to two. The spline information is either included or not. All input variables which are not discrete are standardized.

For the evaluation, multiple regression approaches will be used including linear and quadratic regression, GP, and SVR with radial bias function and linear kernels.

For SVR, the linear kernel will be used with the cost parameters from $C = \{0.1, 1, 10, 50, 100, 500\}$, in addition the radial basis function (RBF) kernel will consider $\sigma = \{0.1, 1, 2, 5, 10\}$. Each regression model is learned using Matlab 2015b.

In all evaluations, a 10-fold cross evaluation approach was used to train and test. The SVR parameters were selected through a nested cross validation approach. The performance was compared based on the absolute and relative error in the LOS determined for each model evaluated. Statistical p-values from a t-test were used to verify statistical differences or lack thereof in comparing different representation techniques within evaluation methods.

5. Results

The first part of the evaluation was conducted to examine the impact of different number of clinical sample values in the representation (0-5). The data representation also included both behavioral interpretations; namely 1 Diffs and splines. Table *2* shows the best performance was not with more samples but zero or one based on the lowest median relative error, for all but SVR with a linear kernel (although the difference in median relative error between 1, 2, 3, or 5 samples is small). The analysis of the p-values from the t-test showed that the increase in samples had no statistical benefit over less samples for the models. An exception is in the quadratic regression which had a p-value of 0.05 in comparing performance of 1 versus 3 samples. The same analysis was done using t^*_1 as the reference point, which lead to similar results and conclusions. Because the performance of the models with more samples are not statistically better, then the next part of the evaluation will include only one clinical sample value.

Table 2 Results on t^*_2 for data representations with 1 Diffs, splines, and different number of clinical sample values with 14d sample spacing.

Samples	Median Relative Error				
	SVR-Lin	SVR-RBF	Linear	Quad	GP
0	0.658	**0.778**	0.838	**1.011**	**0.860**
1	0.634	0.834	**0.800**	1.182	0.879
2	0.631	0.828	0.830	1.257	0.928
3	0.631	0.880	0.811	1.425	0.933
4	0.655	0.817	0.834	1.686	0.900
5	**0.630**	0.794	0.850	2.303	0.923

Table *3* presents results examining the performance benefit of the inclusion of the behavioral representations namely difference trends (Diffs) and splines. With two exceptions, SVR with the RBF kernel and the quadratic regression, the best performing models contained one behavioral representation. In the various modes of behavioral representation considered, the models did not have any statistical benefit, with p-values greater than 0.1 in most cases. One exception is in quadratic, the model with no splines and no Diffs showed a statistically significant improvement to the model with 2 Diffs and splines with a p-value of 0.014. Similar results were observeved for t^*_1.

The different regression methodologies show an ability to work with the diversity in the clinical data inputs of the samples to various degrees. The best performing methodology consistently is the SVR with the linear kernel followed by the linear regression approach. The RBF kernel version of the SVR did well with the data, just not as well as the linear kernel method, and the GP was not as successful with the fit but did not have the high degree of variance in the error that was seen with the quadratic regression.

Table 3 Results on t^*_2 with one clinical sample and different data representations involving the number of Diffs and inclusion of splines.

# Diffs	Splines	Median Relative Error				
		SVR-Lin	SVR-RBF	Linear	Quad	GP
0	0	0.636	**0.819**	0.881	**0.958**	0.874
0	1	0.649	0.844	**0.800**	1.064	**0.870**
1	0	**0.619**	0.834	0.885	0.98	0.874
1	1	0.634	0.834	0.803	1.182	0.879
2	0	0.720	0.868	0.866	0.979	0.878
2	1	0.665	0.877	0.8177	1.33	0.893

Table 4 Best performing regression models. Above the triple line is t^*_1 and below is t^*_2.

Evaluation Method	Data Representation Summary	Median Absolute Error (Days)	Median Relative Error
SVR-Linear	1 Sample, 7 day, 2 Diffs, Splines	32.48	**0.625**
SVR- RBF	0 Samples, 2 Diffs, Splines	31.48	0.640
Linear Regression	3 Samples, 7 day, 2 Diffs, Splines	51.19	0.765
Quad Regression	1 Sample 14 day, No Diffs, No Splines	53.05	0.800
Gaussian Proc.	0 Samples, 2 Diffs, Splines	52.81	0.822
SVR-Linear	1 Sample, 1 Diffs, No Splines	31.35	**0.619**
SVR- RBF	0 Samples, 1 Diffs, Splines	41.60	0.752
Linear Regression	1 Sample, 14 day, No Diffs, Splines	50.27	0.800
Quad Regression	0 Samples, No Diffs, Splines	56.05	0.889
Gaussian Proc.	1 Sample, 7 Day, No Diffs, Splines	53.37	0.852

The best performing models for each regression methodology is seen in Table 4. These models overall have the best performance with one behavioral representation included with either zero or one sample included. There are a couple cases that the performance was best with multiple behavioral representation included (both Diffs and Splines), and one case with more than one sample being beneficial based on the lower median relative errors.

In Table 4, the median absolute error was also reported. However, it may be a deceiving measure since for each patient the same amount of absolute error may hold more meaning to some cases then other (e.g., an error of 30 days for a patient surviving 40 days versus 180 days). Therefore, to help controll for each patient's LOS, the relative error has been reported and used to compare representations and methods. Overall, the best performance in the absolute error was also seen with the SVR methods using this representation approach.

6. Conclusion

The inclusion of more clinical sample values does not provide a statistically significant improvement in the prognostic performance, measured as a reduction in relative error, using regression methodologies. What does help improve the ability to determine a prognosis is the inclusion of behavioral representations and the selection of appropriate regression methods, like the SVR method used here. While regression and classification are not directly comparable, the original results of benefits from the behavioral representations have held true with prior work. There are several future directions for this work with respect to the data representation. For example, rather than use sampling with interpolation, an alternative would be to consider dimensionality reduction techniques to reduce the need for samples and behavioral representations.

Conflict of Interest

The authors declare no conflict of interest.

Acknowledgment

References

[1] J. Winikus and L. E. Brown, "Representation and incorporation of clinical information in outpatient oncology prognosis using Bayesian networks and Naïve Bayes," in IEEE International Conference on Electro Information Technology (EIT), 2016.

[2] American Cancer Society, "Cancer facts and figures 2016," 2016. [Online]. Available: http://www.cancer.org/acs/groups/content/@research/documents/document/acspc-047079.pdf.

[3] A. Vellido and P. J. Lisboa, "Neural networks and other machine learning methods in cancer research," in Comput. Amb. Intel., 964--971 (2007).

[4] B. Sierra and P. Larranaga, "Predicting survival in malignant skin melanoma using Bayesian networks," Artificial Intel. Medicine, **14**: 215-230 (1998).

[5] J. Hayward, S. A. Alvarez, C. Ruiz, M. Sullivan, J. Tseng and G. Whaen, "Machine learning of clinical performance in pancreatic cancer database," Artificial Intelligence in Medicine, **49**: 187-195 (2010).

[6] L. Karamitopoulos and G. Evangelidis, "Current trends in time series representation," in Proc. 11th Panhellenic Conference on Informatics, 2007.

[7] I. Batal, L. Sacchi, R. Bellazzi and M. Hauskrecht, "A temporal abstraction framework for classifying clinical temporal data," in AMIA Annual Symposium Proceedings, 2009.

[8] I. Batal, H. Valizadegan, G. F. Cooper and M. Hauskrecht, "A pattern mining approach for classifying multivariate temporal data," in IEEE Int Conf Bioinformatics Biomed, 2011.

[9] Y.-J. Tseng, X.-O. Ping, J.-D. Liang, P.-M. Yang, G.-T. Huang and F. Lai, "Multiple-time-series clinical data processing for classification with merging algorithm and statistical measures," IEEE J. Biomed. Health Informat., **19**(3): 1036-1043 (2015).

[10] D. R. Cox, "Regression models and life-tables," J. Royal Statistical Society. Series B (Methodological), **34**:187-220 (1972).

[11] P. Royston, "The lognormal distribution as a model for survival time in cancer, with an emphasis on prognostic factors," Statistica Neerlandica, **55**: 89-104 (2001).

[12] L. Ohno-Machado, "Modeling medical prognosis: survival analysis techniques," J. Biomed. Infomat. **34**: 428-439 (2001).

[13] S. Gupta, T. Tran, W. Luo, D. Phung, R. L. Kennedy, A. Broad, D. Campbell, D. Kipp, M. Singh, M. Khasraw, L. Matheson, D. M. Ashley and S. Venkaresh, "Machine-learning prediction of cancer survival: a retrospective study using electronic administrative records and a cancer registry," BMJ Open, **4**(3): (2014).

[14] W. Kim, K. S. Kim, J. E. Lee, D.-Y. Noh, S.-W. Kim, Y. S. Jung, M. Y. Park and R. W. Park, "Development of novel breast cancer recurrence prediction model using support vector machine," J. Breast Cancer, **15**: 230-238 (2012).

[15] O. Gevaert, F. D. Smet, D. Timmerman, Y. Moreau and B. D. Moor, "Predicting the prognosis of breast cancer by integrating clinical and microarray data with Bayesian networks," Bioinformatics, **22**(14): e184-e190 (2006).

[16] B. Gan, C.-H. Zheng and H.-q. Wang, "A survey of pattern classification-based methods for predicting survival time of lung cancer patients," in Bioinformatics and Biomedicine (BIBM), 2014 IEEE International Conference on, 2014.

[17] D. Delen, G. Walker and A. Kadam, "Predicting breast cancer survivability: a comparison of three data mining methods," Artific. Intel. Medi., **34**: 113-127 (2005).

[18] I. Anagnostopoulos, C. Anagnostopoulos, D. Vergados, A. Rouskas and G. Kormentzas, "The Wisconsin breast cancer problem: diagnosis and TTR/DFS time prognosis using probabilistic and generalised regression information classifiers," Oncology Reports, **15**: 975-981 (2006).

[19] H. Valizadegan, Q. Nguyen and M. Hauskrecht, "Learning classification models from multiple experts," J. Biomed. Informat., **46**(6): 1125-1135 (2013).

[20] C. E. Rasmussen and C. K. Williams, Guassian processes for machine learning, Cambridge: MIT Press, 2006.

[21] P. Baldi, Bioinformatics: The machine learning approach, Cambridge: MIT Press, 1998.

[22] Z. Liu, L. Wu and M. Hauskrecht, "Modeling clinical time series using gaussian process sequences," in SIAM international conference on data mining, 2013.

[23] V. N. Vapnik, The nature of statistical learning theory, 2 ed., Springer, 2000.

[24] E. Alpaydin, Introduction to machine learning, 2 ed., Cambridge: MIT Press, 2010.

Strong Authentication Protocol based on Java Crypto Chip as a Secure Element

Majid Mumtaz[*,1], Sead Muftic[2], Nazri bin Abdullah[3]

[1]Lecturer, COMSATS Institute of Information Technology, Quaid Avenue, Wah Cantt, 46000, Pakistan

[2]CEO, SETECS Inc. Rockville, MD 20852, USA

[3]PhD Student, ICT/Dept. of Communication Systems, Royal Institute of Technology (KTH) Stockholm, Sweden

ARTICLE INFO

ABSTRACT

Smart electronic devices and gadgets and their applications are becoming more and more popular. Most of those devices and their applications handle personal, financial, medical and other sensitive data that require security and privacy protection. In this paper we describe one aspect of such protection – user authentication protocol based on the use of X.509 certificates. The system uses Public Key Infrastructure (PKI), challenge/response protocol, mobile proxy servers, and Java cards with crypto capabilities used as a Secure Element. Innovative design of the protocol, its implementation, and evaluation results are described. In addition to end-user authentication, the described solution also supports the use of X.509 certificates for additional security services – confidentiality, integrity, and non-repudiation of transactions and data in an open network environment. The system uses Application Programming Interfaces (APIs) to access Java cards functions and credentials that can be used as add-ons to enhance any mobile application with security features and services.

1. Introduction: User Authentication

Authentication of users is one of the most important security services for any application in the Internet environment. It guarantees that applications and their resources are used only by legitimate and authorized users. In addition, it represents important prerequisite for many other security services, such as data confidentiality (for exchange of cryptographic keys), data integrity (protection of digital digests), access control, non–repudiation, and so on. Authentication as the security service is also used to verify identities of other components of an IT environment, such as applications, servers, user workstations, messages, documents, E-mail letters, and other digital objects.

Because of its importance in any IT environment, it is essential that authentication is always performed correctly and with high degree of trust in its protocol and the outcome.

The essential goal of an authentication protocol is to verify the identities of parties and components participating in some application or transaction. This goal is usually accomplished by validating some secret value associated with the claimed identity.

Alternative protocols include verification of some unique and intrinsic properties of individuals that provide their identities and participate in their validation.

This paper is focused on the authentication protocol specified in the National Institute of Standards and Technology (NIST) FIPS 196 standard [1]. The essence of that protocol is challenge/response procedure based on randomly generated number for each execution of the protocol, so that specific instance of the protocol and its results are non–repeatable. This approach prevents man-in-the-middle attack based on replay of protocol messages. Cryptographic protection of messages is based on public key cryptography, where both participants in the protocol – Identity Claimant and Identity Verifier, have a pair of asymmetric crypto keys and corresponding certificates. Using these credentials all messages of the protocol are cryptographically protected – digitally signed and enveloped, what guarantees successful verification of all messages and therefore successful completion of the protocol.

FIPS 196 standard does not specify specific details of the cryptographic protection of protocol messages. But, this aspect is complemented by another NIST standard – SP 800-63-1 [2]. This standard defines four levels of assurance, Levels 1 to 4, in terms of

*Corresponding Author Majid Mumtaz, CIIT Wah Campus Wah Cantt Pakistan, +92(0) 51-9314384 & mmumtaz@ciitwah.edu.pk

the strength of cryptographic algorithms, their parameters, authentication procedures, consequences of authentication errors, and misuse of credentials. Level 1 is the lowest assurance level, and Level 4 is the highest.

Brief description of the four assurance levels and their main characteristics is the following:

1.1 Assurance Level 1 – Low Assurance

At this level identity proofing is not required – simple user *login name* may be used for that purpose. Authentication mechanism is usually user *login password*, which is used as a shared secret with the Identity Verifier. Such authentication mechanism provides some assurance that the same Claimant who participated in previous transactions is accessing again the protected transaction or data. At Level 1, long-term shared authentication secrets (user password) are revealed to and shared with Verifiers.

The protocol relies on encryption of passwords for their transfer through a secure communication channel, usually SSL. This assurance level does not require cryptographic methods that block offline attacks by eavesdroppers. Authentication protocols that are implemented based on principles suggested for this level have several problems. The most important are: sharing of secret authentication credentials what gives the possibility of dishonest server administrators to impersonate users. Credentials stored at the servers are vulnerable and usually multiple credentials are used at different servers. The protocol that solves all these problems, described in section III.

1.2 Assurance Level 2 – Single Factor Remote Authentication

This level provides moderate assurance for authentication protocols. At this level identity proofing requirements are introduced, requiring presentation of identifying materials or information. For single factor authentication, Memorized Secret Tokens, Pre-Registered Knowledge Tokens, Look-up Secret Tokens, Out of Band Tokens, and Single Factor One-Time Password Devices are suggested. Successful authentication requires that the Claimant proves using a secure authentication protocol that he/she controls the token. In addition to Level 1 requirements, authentication assertions must be resistant to disclosure, redirection, capture, and substitution attacks. This implies that their cryptographic protection is needed. Certified and approved cryptographic techniques are required for protection of all assertions used at Level 2 and above.

Protocols implemented at this assurance level have reasonable good security, except that they are based on a single authentication factor. So, their assurance is not too high and these protocols are not suitable for highly sensitive applications and data.

1.3 Assurance Level 3 – Multi-Factor Remote Authentication

This level provides medium assurance in authentication protocol since at least two authentication factors are required. At this level identity proofing procedures require verification of identifiers. Authentication is based on proof of possession of the allowed types of tokens through a cryptographic protocol using strong cryptographic mechanisms that protect primary authentication tokens against compromise by all threats at Level 2 as well as Verifier impersonation attacks.

Authentication requires that the Claimant proves, using a secure authentication protocol, that he or she controls the token. The Claimant "unlocks" the token (the first factor) with a password or biometric (the second factor). Long-term shared authentication secrets are never revealed to any party except the Claimant and Verifiers.

Although authentication protocols at this assurance level are stronger than at Level 2, they still have weaknesses of shared secrets with Verifiers as well as multiplicity of such secrets with multiple Verifiers.

1.4 Assurance Level 4 – Multi Factor Remote Authentication

This level provides the highest degree of assurance in authentication protocols. At this assurance level in-person identity proofing is required what implies that identification data must be established by some trusted Registration Authority. The core requirement at this level is that only hardware cryptographic tokens must be used. The token is required to be a hardware cryptographic module validated at Federal Information Processing Standard (FIPS) 140-2 Level 2 or higher with at least FIPS 140-2 Level 3 physical security [3]. Level 4 token requirements can be met by using the PIV authentication certificate of a FIPS 201 compliant Personal Identity Verification (PIV) smart card [4].

The key characteristics and distinguished features of the strong authentication protocol described in this paper is that it provides the highest level of assurance at Level 4. In addition, another important feature of the solution is that, by suitable extensions of the FIPS 201 standard, the same cryptographic token (PIV card) can support other types of protocols at three other assurance levels. These features are available not only using Java smart cards with PC/Windows workstations, but also using Java crypto chips combined with smart phones. Therefore, the protocol is at Assurance Level 4 and it is available for PCs, for smart phones, and for other mobile devices and gadgets. In order to even prevent brute–force analysis using powerful computers by legal agencies, but without proper authorization, all data are randomized before encryption using ExOR with random 256 bit masks. This transformation makes analysis of encrypted data exponentially more difficult compared with data encrypted using standard crypto algorithms.

The remaining sections of the paper are organized as follows: in Section 2 related work and relevant alternative solutions are described and analyzed. In Section 3 all details of our protocol, its components and steps are described. Section 4 describes the management of security credentials as used in the protocol. Section 5 describes current implementation. Whereas Section 6 contains the results of evaluation and validation based on requirements of the Assurance Level 4. The last Section contains the conclusion and suggestions for further research and potential improvements.

2. Related Work and Standards

There are several research papers and standards dealing with strong authentication protocol using Java chips and mobile PKI. Although they address interesting problems, none of them describe a solution that is as comprehensive and also formally validated, as the protocol described in this paper.

Wireless Application Protocol (WAP) Forum was the first to specify Wireless PKI (WPKI) protocol for wireless environments [12]. In the WPKI protocol Web portal acts as a Gateway Server. It receives WAP client requests and transfers them to the Registration Authority (RA) and Certification Authority (CA)

servers. The WAP client uses direct URL instead of X.509 certificate exchange. The entity that wants to communicate securely with a WAP client needs first to download the certificate from given URL and then verify client's signature on the authentication token.

The paper [13] describes an approach based on the use of mobile phones and SIM (Subscriber Identity Module) chips. The proposed solution utilizes security features, user identities, and public/private key pairs available inside SIM Module. The solution is dependent on a telecom issuing and personalizing SIM chips during client's subscription, so security of user's data and transactions depends on third party. Therefore, this system requires user's trust on services and actions of the third parties and also lacks protection of consumers privacy.

Research results reported in [14] proposed the use of enhanced PKI credentials as security tokens for mobile phones. The system comprises several components: a PKINIT component (i.e. an enhanced version of Kerberos); a client component; PANDA component (i.e. a device powered by Zigbee protocol) for communication and sensing locations; Delegation Server component is used to manage certificates and private keys for signing certificates; Referee Server component represents protocol bridge between a server and a client. Mutual authentication is performed by the Delegation Server and it is based on PKI. Upon receiving proxy certificate and Delegation Server's public key, a client signs it by his/her own private key and sends it back to the Delegation Server. In response, the Server returns a challenge to the client. The client encrypts the challenge and returns it back to the Delegation Server. Delegation Server performs its verification with the assistance of the Referee Server. Upon success, PKINIT is activated to issue Service-Granting Ticket (SGT) to the client. Authors claimed that the protocol provides authentication, digital signatures, non-repudiation, and secure distribution of keys to the client. The solution is comprehensive but quite complex, it has quite high deployment cost as it has a number of resources required to support different services at different levels. Our system provides the same security services, but with simpler structure and in transparent fashion to end user's.

Research results in [15] suggest the use of certificates for mobile phones. The authors claim that their authentication protocol is not only based on PKI certificates, but that it also provides secure solution to mobile applications. In addition, they claim user confidence that their credentials are password protected and kept secret. They measure the strength and protocol latency of their solution using security threats. Authors compare their solution with well-known authentication solutions by using formal verification approach and claim that their solution is more efficient and has the lowest latency for mobile phones. But, such claim requires practical testing in an enterprise environment and also requires tamper-proof technology.

Trichina [16] proposed a PKI system for SIM-based mobile payments in Finland. This proprietary solution was deployed with the help of telecommunication operator for secure mobile payments. Mostly financial organizations located in Finland can utilize the system according to operator guidelines. Network operator is responsible for issuance of PKI-SIM cards to customers. FINEID SAT applet module inside the SIM card generates digital signature and corresponding public-key certificate for customers. The big challenge to such system is privacy and customer confidence, as it is based on trust in third party services. A number of challenges are highlighted by [17] for

such solutions especially when using online m-commerce applications.

Another PKI solution for mobile environments was proposed by Jeun and Kilsoo [18]. They first generate public/private key pair on a personal computer (PC) and manually transfer it into a mobile phone. Customers initiate PKI services by using SMS message requests to the server. In their system mobile devices rely completely on PC security, as PC generates public/private key pair and certificates on behalf of a customer. If PC is compromised, the complete customer's security is compromised. The solution has a number of challenges including insecure storage of public/private keys and their manual transfer to mobile phones.

Lee [19] proposed a WPKI based solution. In the solution an Elliptic Curve Digital Signature Algorithm (ECDSA) is utilized for key pair generation. He claimed that the generated certificate has reduced size as compared to the standard X.509 certificate. For validation of certificates, he uses Online Certificate Status Protocol (OCSP) instead of Certificate Revocation Lists (CRL). Although the solution is based on optimized protocols for certificate management, it has a number of limitations for mobile applications. A serious issue for every PKI-based solution is the protection of a private key. The best solution for tamper-proof storage and protection of private keys is to use either smart card chips or smart micro SD card chips. Compared with Lee's solution, our protocol use a tamper-proof technologies. In addition, its completeness, availability on multiple platforms, and compliance to standards have been proven using official validation and certification standards and methodologies.

3. Protocol Components and Steps

Two core components of our system are Strong Authentication Client and Strong Authentication Server. There are two implementations of the Client. One as Java *Web Start (JWS)* module, which is dynamically downloaded to and activated in the PC/Windows environment upon activation of the protocol. The other is a mobile application with versions for IOS and Android smart phones, called *m–Security*. Both versions are protected against malware and illegal code modification: JWS module is digitally signed, while for mobile applications software modules are encrypted before loading into mobile devices. For execution of such encrypted software modules special Java Class Loader is implemented as an extension of the standard Java Class Loader. Security Loader dynamically decrypts Java classes in the process of loading them into main memory before execution.

Strong Authentication Server comprises two servers: Web server and a classical network Strong Authentication server. Web server, when accessed through PC browser, dispatches JWS Strong Authentication module to the PC where client side functions of the protocol are performed. Network Strong Authentication server listens the socket and performs server side functions of the protocol. This server interacts with both, JWS client and also with m–Security client, during execution of the protocol.

The steps of the protocol are fully compliant with requirements for validation of HSPD-12 (PIV) products in order to be included in the GSA HSPD–12 Approved Products List [5]. These requirements are specified in the document [6]. All cryptographic operations are performed by the PIV smart card. The steps are the following:

Step 1: User either clicks on an icon for Cloud Login module or starts browser and visits security–enhanced application server. In both cases, login panel is displayed (Figure 2).

Step 2: User inserts PIV card into the smart card reader and enters his/her PIN using keyboard and simple smart card reader or using more secure smart card reader with the PIN pad.

Step 3: If PIN is correct, smart card will be activated and PIV authentication certificate is read form the card.

Step 4: Certificate is sent to the Strong Authentication Server, representing the first, identification message, in accordance with the FIPS 196 standard.

Step 5: Strong Authentication Server verifies user by verifying that

- User is registered in the IDMS and his/her status is correct (not suspended or terminated)
- Certificate is verified against CRL and through verification of the certificate chain to the top of the PKI
- The status of the smart card is verified against the database of valid PIV cards.

Step 6: If all verifications complete successfully, Strong Authentication Server generates random number, envelopes it using user's public key (extracted from the user's certificate) and sends it back to the user as the challenge together with its own certificate, in accordance with the FIPS 196 standard.

Step 7: Challenge is passed into user's PIV card, where it is decrypted using user's private key stored in the card, then enveloped using server's public key (extracted from its certificate), thus creating user's response.

Step 8: Response is returned to the Strong Authentication Server which opens the envelope using its private key and verifies user's response against its original challenge

Step 9: If the verification is successful, Strong Authentication Server contacts Policy Decision Point (PDP) Server to issue SAML/SSO ticket to the user

Step 10: SAML/SSO ticket is issued for the user and returned to the Strong Authentication Server, which sends it to the user together with a random session key, both protected using public key cryptography

Step 11: User stores SAML/SSO ticket into PIV card.

The final results of the authentication procedure are that

- User is authenticated with certainty, as the person in possession of the PIV card issued to that user
- User has SAML/SSO ticket in his/her smart card,
- PDP Server has the copy of the user's ticket,
- Shared secret session key is established between Strong Authentication Server and user's workstation.

4. Management of Security Credentials

The following security credentials are used in the protocol:

(1) user registration data, stored in an IDMS server and used in the form of the Distinguished Name object; (2) user X.509 certificate; (3) SAML/SSO ticket; and (4) PIV smart card. This implies that, in addition to Strong Authentication server, several other servers are used to manage those credentials. In particular, based on the list of four credentials, four such servers are used: (1) Identity Management System (IDMS) server managing user's

registration data and their identities; (2) Certificate Authority (CA) server managing X.509 certificates; (3) Policy Decision Point (PDP) server managing authorization policies and tokens; and (4) Card Management Server for issuing and managing PIV cards.

Various aspects of security management are based on an innovative concept of security proxies [7]. Those are "intermediate" servers, connecting users with various security and application servers. Based on such concept, Strong Authentication Server is designed and implemented as a proxy for other security servers. In that way, users can access and use various security services through a single "contact point". Besides flexibility for users, this approach has also advantages in terms of user security, privacy and anonymity. The details about servers, their data, services, protocols and security, are beyond the scope of this paper. Their use and services are described for completeness of this paper. The architecture of the system is shown in Figure 1:
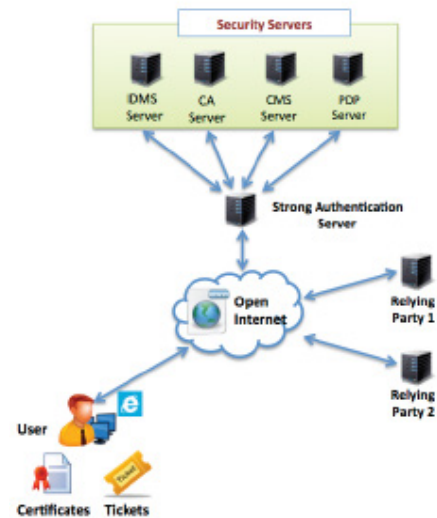

Figure 1: SA Server as Security Proxy

5. Current Implementation

The complete system is already implemented, tested, and certified. This section describes only its three main components: (1) PC/Windows based client; (2) mobile client (m–Security); and (3) Crypto Services Provider (CSP).
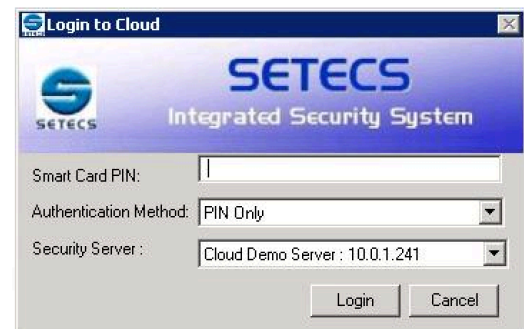

Figure 2: Login Panel of the JWS Client

5.1 PC/Windows JWS Client

As already described, this client is dynamically downloaded from the Web interface of the Strong Authentication Server into user's local PC/Windows workstation. Upon activation, it performs transparently all its functions. Users activate their PIV

card by entering PIN in the Login panel (Figure 2). If smart card reader with PIN pad is used, then PIN is entered using the reader. Upon activation of the card, the steps of the protocol, described in section 3, are performed and the client simply displays success message.

5.2 Mobile Security Client

Strong Authentication Client for mobile platforms, besides strong authentication protocol, it also includes all functions necessary to manage security credentials that are needed in the strong authentication protocol. These functions are accessed using Graphical User Interface (GUI) menu shown in Figure 3. The functions are organizes in a logical sequence of steps.

Figure 3: GUI of m–Security Application

Button *m–Identity* is used to register or update registration data. After that, the button *m–Applets* is used to download PIV and Security applets into JavaCard chip. During download, personal data are loaded into PIV applet, according to the PIV standard [8]. *m–Certificates* button generates in the chip two RSA keys, extracts public key, sends it in the form of PKCS#10 Certificate Request to the CA server, receives the PKCS#7 reply, and stores certificate in the PIV applet of the card. After that, the chip and the Client are ready to perform strong authentication, as already described. *m–Key Management* button is used to refresh session keys established during authentication procedure.

5.3 Crypto Services Provider

Both types of Clients, PC/Windows version and also mobile version, are using Crypto Services Provider (CSP) for all their cryptographic functions. CSP is the component of the security system that provides cryptographic services to both clients and also to all servers.

Several versions of the CSP have been designed and implemented. The details are described in [9]. That paper describes modules, APIs and validation procedure for the CSP, which is used by Strong Authentication clients described in this paper. Since all Strong Authentication Clients use crypto chips, some details of usage of the CSP, when Secure Element is a crypto chip, are here described.

With PCs standard Java cards are inserted into a smart card reader connected to the PC workstation. With mobile phones, there are two versions of embodiments of crypto chip. With one, the chip is embedded into microSD card, which is then inserted in the microSD slot in mobile phones that have such slot. For mobile phones that do not have microSD slot, external smart card reader

is used, attached to the phone. Standard Java card is inserted into the mobile smart card reader. This solution is shown in Figure 4.

The card is inserted into mobile smart card reader that has PIN pad and LCD display to handle PIN and card data. The reader has audio interface, so it may be used with all types of smart phones. The card and the reader are inserted into a phone on the top, but to save space of the paper, they are shown next to each other.

Figure 4: Mobile Smart Card Reader and PIV Smart Card

Extensive research has been already performed related to managing and using Universal Integrated Circuit Chips (UICC) directly in smart phones, when such chips become broadly available in smart phones [10].

6. Evaluation and Validation

This section briefly describes the approach and results of the evaluation procedure and formal validation procedure that have been performed for the described system.

The protocol has been evaluated against NIST requirements for authentication protocols at Level 4 [2]. Besides its core requirements that the protocol uses hardware token and two factors authentication, the standard requires:

Level 4 requires strong cryptographic authentication of all parties and data transferred between parties.

The protocol uses strong cryptographic algorithms (AES and RSA) with long crypto keys (256 bits for AES and 1024 for RSA). Both algorithms are implemented in hardware. All messages within the protocol are encrypted and digitally enveloped, so they are all strongly protected.

The token secret shall be protected from compromise through the malicious code threat.

In the system there are two token secrets: user's PIV card PIN and user's RSA private key. Both are stored in the card and cannot be read, only used. RSA private key is even generated in the card and never leaves the card. PIN is protected by its blocking after three unsuccessful verification attempts.

Long-term shared authentication secrets, if used, shall never be revealed to any party except the Claimant and CSP; however, session (temporary) shared secrets may be provided to Verifiers or Relying Parties by the CSP.

The system does not use shared secrets. Session keys are exchanged cryptographically signed and enveloped using public

key cryptography, so they are shared and can be used only with designated, legitimate Verifiers.

Strong, approved cryptographic techniques shall be used for all operations including the transfer of session data. All data shall be cryptographically authenticated.

The protocol uses AES (256 bits key) and RSA (1024 bits keys). Both algorithms are officially approved and validated [3]. Man-in-the-Middle (MitM) attacks are completely eliminated, as all messages are digitally enveloped by recipient's public key, so they can be opened only by the designated, legitimate recipients.

Level 4 assurance may be satisfied by client authenticated TLS (implemented in all modern browsers), with Claimants who have public key Hardware Cryptographic Tokens.

This requirement is out of scope of the protocol. It requires TLS based on client's certificate, so Web server of the Strong Authentication client must be configured to require client authentication in the TLS handshake process.

In addition to evaluation of the protocol for compliance with the NIST Assurance Level 4, the protocol has also been officially validated by the GSA, an agency of the US Federal Government. Validation was performed for the category "*PIV Authentication System*" of the GSA HSPD-12 Validation Program [11] and included in the official US Government HSPD–12 PIV Approved Products List [5].

7. Conclusion and Future directions

In this paper we have described our design and current implementation of the strong authentication solution for PC/Windows, mobile phones, smart gadgets, and other mobile devices. The prototype has been developed and evaluated according to industry compliance standards with lowest to highest authentication assurance levels. The designed solution provides transparent security, privacy and anonymity services to end user's.

As the next steps we are planning to integrate our system with different applications including vehicle tracking devices, health care appliances, and other embedded devices, especially Internet of Things [20]. In our future work we will integrate the solution with cloud-centric Internet of Things applications.

Another interesting area that we are already pursuing is use of the protocol for peer-to-peer authentication, without third parties. The innovative concept for validation of such transactions is blockchain. At the moment, there is a great need to provide strong authentication when accessing and using blockchain, but there are no even early solutions.

Finally, the third area of our research and development interest and our current activities is security of peer-to-peer transactions, also based on the use of the blockchain.

Conflict of Interest

The authors declare no conflict of interest.

Acknowledgment

References

[1] NIST, National Institute of Standards and Technology, "Entity Authentication using Public Key Cryptography", FIPS 196, http://www.nist.gov/manuscript-publication-search.cfm?pub_id=901429 [Retrieved March 2016]

[2] NIST, National Institute of Standards and Technology, "Electronic Authentication Guideline", NIST SP 800-63-1, http://csrc.nist.gov/publications/nistpubs/800-63-1/SP-800-63-1.pdf [Retrieved March 2016]

[3] NIST, National Institute of Standards and Technologies, "Validated 140-1 and FIPS 140-2 Cryptographic Modules", Item 1111, http://csrc.nist.gov/groups/STM/cmvp/documents/140-1/140val-all.htm [Retrieved March 2016]

[4] NIST, National Institute of Standards and Technologies, "FIPS 201 – Personal Identity Verification (PIV) of Federal Employees and Contractors", March 2006, http://nvlpubs.nist.gov/nistpubs/FIPS/NIST.FIPS.201-2.pdf [Retrieved June 2016]

[5] GSA, US Federal Government, "HSPD-12 Approved Products List", http://www.idmanagement.gov/approved-products-list [Retrieved June 2016]

[6] GSA/US Federal Government, "PIV Authentication System, Approval Procedure, v2.0.0", April 14, 2010, http://www.idmanagement.gov/ [Retrieved June 2016]

[7] N., bin Abdullah, "Internet Security and Privacy System based on the Concept of Trusted Proxies", Licentiate Report, Royal Institute of Technology, Stockholm, Sweden, 2015

[8] NIST, National Institute of Standards and Technologies, "Interfaces for Personal Identity Verification, Part 4: The PIV Transitional Interfaces & Data Model Specification", NIST SP 800-73-3, http://csrc.nist.gov/publications/PubsSPs.html#800-73 [Retrieved April 2016]

[9] S. Muftic, "Integrated Crypto Services Provider for Web and Mobile Applications", submitted to the IEEE Conference on Communications and Network Security, (2015).

[10] H. Zhao, "Secure Management of Multi–Application Mobile Platforms", Ph.D. dissertation, Royal Institute of Technology, Stockholm, Sweden, June 2013.

[11] GSA, US Federal Government, "FIPS 201 Evaluation Program", http://www.idmanagement.gov/about-fips-201-ep-program [Retrieved Jan 2016]

[12] "Wireless Application Protocol: Public Key Infrastructure Definition", WAP Forum. April 24, 2001.

[13] D. v. Thanh, T. Jonvik, B. Feng, D. v. Thuan, I, Jorstad, "Ubisafe: Simple Strong Authentication for Internet Applications using Mobile Phones", Proceedings of the IEEE "GlobeComm" (2008).

[14] K. Saravana, T. Vaisbnavi, "Rabin Public Key Cryptosystem for Mobile Authentication", Proceedings of the IEEE International Conference On Advances In Engineering, Science And Management, (2012).

[15] K. W. Park, S. S. Lim, K. H. Park, "Computationally Efficient PKI-based Single Sign-On Protocol (PKASSO) for Mobile Devices", IEEE Trans. Comp., **57**(6): (2008).

[16] E. Trichina, K. Hypponen, M. Hassinen. ″SIM-enabled Open Mobile Payment System Based on Nation-wide PKI″, ISSE 2007 Securing Electronic Business Processes, 355-366 (2007).

[17] S. Vishwakarma, P. Kumar Samant, A. Sharma, "Attacks in a PKI-Based Architecture for M-Commerce" IEEE International Conference on Computational Intelligence & Communication Technology, 52-56 (2015).

[18] Chun, I. Jeun and Kilsoo, ″Mobile-PKI Service Model for Ubiquitous Environment″ Comm. Comp. Info. Sci. **12**: 118-124 (2008).

[19] Y. Lee, J. Lee and J. Song, ″Design and implementation of wireless PKI technology suitable for mobile phone in mobile-commerce″, Comp. Comm., **30**(4): 893-903 (2006).

[20] R. Gupta, R. Garg, "Mobile Applications modeling and security handling Cloud-centric Internet of Things", Second International Conference on Advances in Computing and Communication Engineering, 285-290 (2015).

FenceBook a Geofencing based Advertisements Application Using Android

Owais Qayum[*], Tahreem Sohail

Electronics Engineering Department, University of Engineering and Technology, Peshawar, 25000, Pakistan

A R T I C L E I N F O	A B S T R A C T
	Geo-fencing (geofencing) is a great feature in a software program that uses Global Positioning System (GPS) or radio frequency identification (RFID) to define the geographical boundaries feature. Actually geofence is a virtual barrier. Geofencing is an innovative technology, an online marketplace for proactive contextual services that allows users to easily find interesting services, can easily subscribe to it and to allow providers offer their services for a variety of applications such as electronic toll collection, contextual advertising or tourist information systems, even without additional infrastructure. The main objective of this research was to understand how the use of spatial data can improve advertising performance for customers. Tracking systems and monitoring, based on global navigation services by satellite, and include geofencing function, could also contribute to the exact location of an institution or company and increase sales and business perspective efficiently. Instead of large billboards they can now advertise on smartphones which is economically and accurately tested. Therefore, we have developed a concept for a market that offers geofence, which can be applied by all and increase the use and integration of proactive services based on location in everyday life.

1. Introduction

The location-based services (LBS) have recently undergone a massive shift in popularity. While the first generation of LBS has not attracted much attention in recent years, the markets will create a wide range of LBS demanding second-generation applications, for example, in the areas of tourism information, navigation, asset tracking, mobile games and mobile marketing, to name just a few. Those above the LBS were under full control over the mobile network of the user operator. As a result, most of these principle LBS do not meet the requirements of users in terms of whether they are limited to rudimentary functions built with less creativity, or was use too expensive or both, see [1], [2]. This is in contrast to current LBS based on a value chain focused on the user where the position of the user is given by the GPS-enabled mobile phone and transmitted to the respective service provider over the network 3G data service either on request or an update- Strategy to meet the needs of users.

The emergence of GPS receivers on the mobile devices has now made it much possible for the first time that proactive monitoring

LBS's has permanently involved the user(s) with the option of just triggering an action of default position event execution. In many situations in our daily lives, proactive LBS's that are more affordable than the reactants, in which the user have to specifically request for the data based on the location. There are several types of GPS position location point events that can be tested. For example, if the user is in the vicinity of a point of interest (POI) or to user. In the recent past, the concept of *geofencing*, which represents a subset of LBSs, and which sometimes are also called *Zone-based LBSs* [3], is gaining momentum. Geofences helps in describing the geographic area (i.e. geographic barrier) a POI, for example, in terms of a circle or a polygon, and combine the area with location events and actions. Typical location events are entering and leaving the geographic region enclosed by the geofence or staying inside or outside for a certain amount of time.

Examples for the actions associated with a geofence or geofences are the presentation of information, an audible notification (music file) when another user sojourns nearby, or the download of a multimedia presentation.

Still, users have to face serious problems in finding the desired

---

[*]Owais Qayyum, Near GMS Amangarh Nowshera, Pakistan, +923359734397, Qayum.insaane@gmail.com

services or having to install many different applications for the same type of LBS's. On the other hand, providers often do not have the knowledge or resources needed since the efficiency of the evaluation of spatial events is quite complex [4], [5]. Our approach solves these problems by providing a common language to describe *geofence services* GFS's by introducing an application "Fencebook".

Figure 1: Overview of Geofencing

In the near future, it is expected that for a given local region, for example, a street, a city or a suburb of a city, there will be a multitude of geofencing, which are offered by many vendors to serve application areas as mentioned above. In these multi-vendor environments, some providers may limit their services Geofence a local region, while others interact on a national or even global basis, making the efficient distribution of essential geofences. Our concept will help to minimize the amount of data transferred by only the transfer of the relevant geographic data and current between users and providers. In this paper, the concept of Geofencing is grown by giving a formal definition of geofencing and its characteristics and demonstrating its usefulness in different application scenarios. Furthermore, the paper presents the idea of a geofence market, where suppliers are able to offer their geofences and users can search for and subscribe to geofences interested and relevant to your current local region. Moreover, this approach is compatible specifying provider, hosting, and representing their GFS's without putting additional infrastructure, providing a common language to describe our market GFS's and to register, find and recover services. Therefore, a market of this kind can be seen as an intermediary between supply and demand of geofencing; suppliers can export the GFS's market, while users can search conveniently in one place and import.

2. Methodology

In many markets, companies need to invest in advertising to raise awareness of new products, prices and special offers (see informative advertising). Until recently, advertising strategies are primarily for the companies to adapt the traditional media and

mass audiences. Today, companies can take advantage of new opportunities to offer specific ads targeted market segments, such as

1. Mobile coupons and sophisticated forms of advertising based on location, including geofencing and geoconquesting.
2. The use of such advertising techniques greatly increases the possibility of targeted advertising and discrimination.
3. Price in real markets, not all consumers are equally valuable for companies. While some consumers may have a relative preference for the product (hard segment) of a company other consumers may have a relative preference to competing products (weak segment). Therefore, companies in these markets need to choose the intensity of advertising and price that fits every market segment.

Objective:
The objective of this paper will be cleared by explaining the flow chart and algorithmic description.

2.1. Algorithmic:

The algorithm on the basis of which we created our application and the number of customers were almost of the same rate as per our calculations:

$$Z = [N^{r.p/y} * y]/p$$

Where,

$\quad$ Z = No of Expected Customers
$\quad$ r = Radius of Geofence (km)
$\quad$ p = Total No of People
$\quad$ N = No of advertisements
$\quad$ y = Time consumed

So the total number of customers who will be receiving the notification of advertisement completely depend on the No of ads, the time consumed, total no of people in that geofence and the radius of the geofence. We named this algorithm as "*owais's algorithm*" Let's take an example, lets no of to be displayed are two so there are two categories of ads now (one sports related and one business related), the time consumed is 120 seconds and the radius of the geofence is 500m. Total number of people living inside the geofence are lets say 3000. So number of customers be *231.707* which are almost the same with respect to our survey.

2.2. Flowchart:

a. ***Query Operating System for General Location and Accuracy:*** First of all, the current location of the user/customer will be checked and recorded.

b. ***Send Location and Accuracy to Server:*** After that the location of the customer will be sent to the database where it will be compared with the Latitude and longitude values of the geofence.

c. ***Receive Set of Nearest geofences:*** The location's latitude and longitude values will be compared will all

the nearest geofences.

d. ***Receive Location Update Event from Operating System***: Geographic coordinates are continuously updating and when ever a user/customer enters a geofence the coordinates are automatically compared with the geofence.

e. ***Query Operating System for General Location and Accuracy:*** Its like the first step the locations are stored and compared continuously in to the data base.

f. ***Compare New Location to Set of Nearest geofences:*** The process will be repeated again and the extracted coordinates will be compared with the nearest geofences.

g. ***Is new location near geofence***: If there is any new location near geofence then the process will go further, else the process will be repeated again from step (c).

h. ***Obtain location at higher resolution***: If there is new location near the geofence then a high resolution means the zoomed version of the location will be obtained.

i. ***Is New(HR) Location near Geofence:*** Then the application will check for the new location (in the zoomed Version) near the geofence if there is no such Location then the process will be repeated again from step (c), otherwise the application will go further.

j. ***Is Location in Geofence Not Previously Entered:*** As the user/customer enters the geofence, a question will arise that is the location in the geofence previously entered or not?

If yes, then (K) will be implemented else (M) will be implemented.

k. ***Mark Geofence as entered:*** if the geofence is not previously entered so a function will be called.

l. ***Send Message to Server Indicating Geofence Entry:*** So if the user is not entered before the specific geofence, the message(ad) related to that geofence would be sent to the Server which will indicate the Entry of the user.
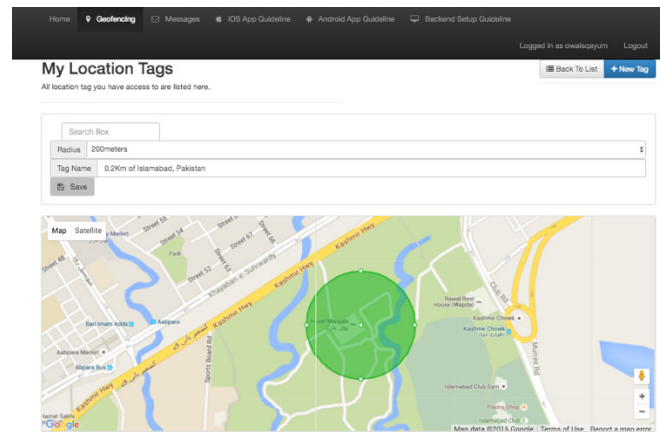
The m, n, o, p is behaving exactly the same just in the opposite direction of the geofence entry. In this case it's the exiting from the geofence.

This paper shows that how geofencing play its role and the results also shows that it is extremely beneficial. First of all, the shop keeper or retailer will signup to the account and would set the desired location on map. After that he will be asked to set the radius as well. By clicking the "New tag" one would be prompted to set the desired geofence. Tag name would be generated automatically with respect to the location. Now its time to define a specific message for the created geofence, so that when the customer enters the location or leave the location they are been notified. The message will be based on the choice of the retailer either he wants to display the ad by entering the geofence or exiting the geofence.
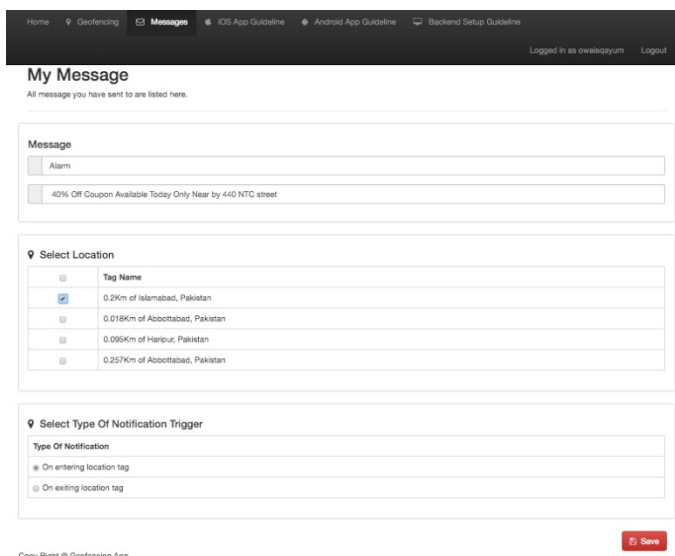

Figure 2: Block Diagram

Figure 3: Adding Geo Tag

Figure 4: Advertisement for the created geofence

After following these simple steps, the ad will finally appear on the Android or IOS phone as the customer enters the geofence. Retailer can also turn the geofence status on and off any time She/he want's.
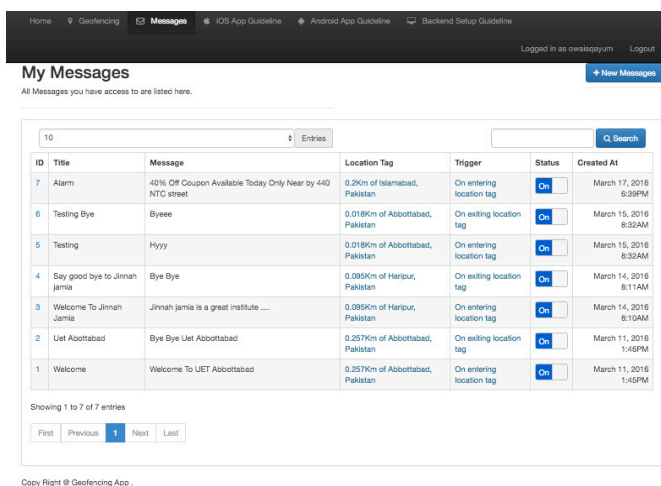

Figure 5: Setting the Geofence

Finally, when the customer enters the geofence, he will be notified and the ad will also display even when the customer is not using his phone.

So after discussing the complete methodology lets see what are the astonishing results achieved by testing the application locally.

3. Results and Discussion

The paper explains the result obtained in a really comprehensive way. The facts elaborate the future worth of Geofencing. After analyzing the application for a specific period of time its been concluded that the advertisements through geofencing were 35% more beneficial than the random methods of advertising. This means that if this application is implemented on a very large scale, it can turn around the world of advertisements and can change the complete shape of advertisements system.
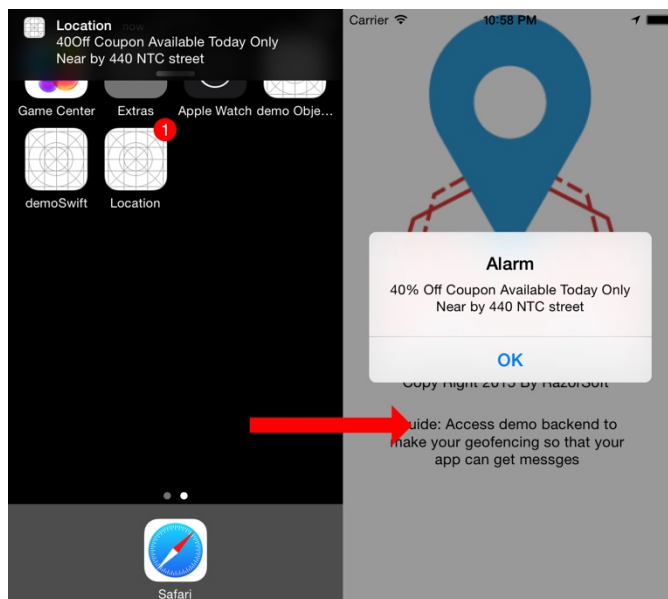
Figure 6: Live View of the App

Table 1: Analysis of Local Stores Advertisements flow

App	Shop A	Shop B	Shop C	Total
Max No of adds sent	23412	65873	841603	930888
Geofences	# of adds to Shop A	# of adds to Shop B	# of adds to Shop C	Size of Geofence
Geofence 1	734	734	935	2403
Geofence 2	734	745	916	2395
Geofence 3	734	760	953	2447
Geofence 4	734	739	930	2403
Geofence 5	12376	7001	987	20364
Geofence 6	749	45639	9134	55522
Geofence 7	745	799	12931	14475
Geofence 8	768	981	31835	33584
Geofence 9	784	713	73812	75309
Geofence 10	734	734	83571	85039
Geofence 11	36704	81274	53986	71964
Geofence 12	790	3000	93752	97362
Geofence 13	734	7435	32187	40356
Geofence 14	1200	9371	91467	92038
Geofence 15	734	96817	97630	99181

Graph 1: Growth in No of Advertisements Per week
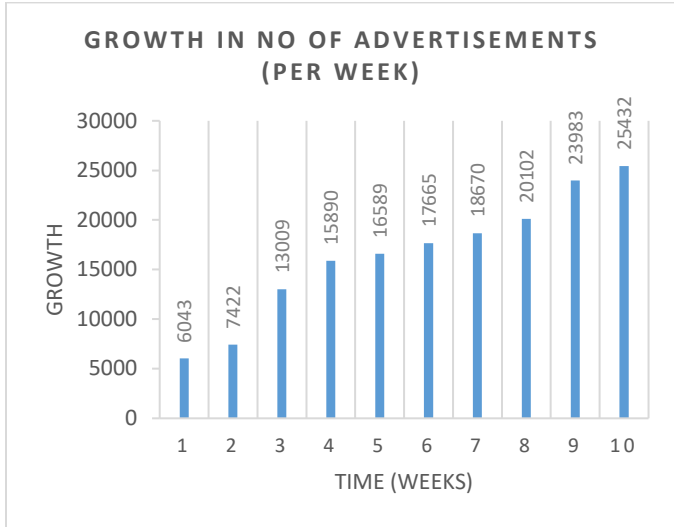
As the application is not live yet there is some troubleshooting to be done but after analyzing "Fencebook" for two and half months on a local platform, it is been analyzed that the use of internet is increased specially in Android phones[6],[7] and hence it is the main factor why people are switching towards LBS (Location based Services). These are the total no of advertisements with respect to the total weeks "Fencebook" was locally live. So this graphical overview is more expalined by table 2, table 3 and graph 3. As we can see in table 2 the comapirason is also made with the other methods just to comapre geofencing with other methods. Further comparison is with Billboards and Television advertisements. In conclusion of the comparison the following results were observed.

Table 2: Comparison with other methods

No of orders	Through Billboards	Through Television	Through Geofencing
week 1	3012	3798	6043
week 2	3112	3809	7422
week 3	4312	4321	13009
week 4	2342	4504	15890
week 5	4312	4355	16589

As we can see from table 2 the weekly comparison of all the methods of advertisements, geofencing is found to be the best among all. After five weeks the customers of geofencing almost increased to triple means 300% better then that of billboards advertisements. The advertisements with other methods like bill boards is are not further effective because its not economical and its also not noticeable even by the person living in the next street. Also the increase was not just measured in the number of customers but also in the number of shops who adopted the advertisement technique of geofencing. This can be shown in table 3. During analyzing all this data, it is also analyzed that no

of shops and stores exponentially started using the services and results were remarkable.

Table 3: Increase of shops/stores connectivity

No of weeks	No of shops
week 1	20 shops were advertising
week 2	50 shops were advertising
week 3	120 shops were advertising
week 4	200 shops were advertising
week 5	270 shops were advertising
week 6	360 shops were advertising
week 7	426 shops were advertising
week 8	675 shops were advertising

The above table can be easily elaborated with the help of a Graph. **Graph 2** shows how the number of shops increased exponentially.

Graph 2: Increase of shops/stores connectivity
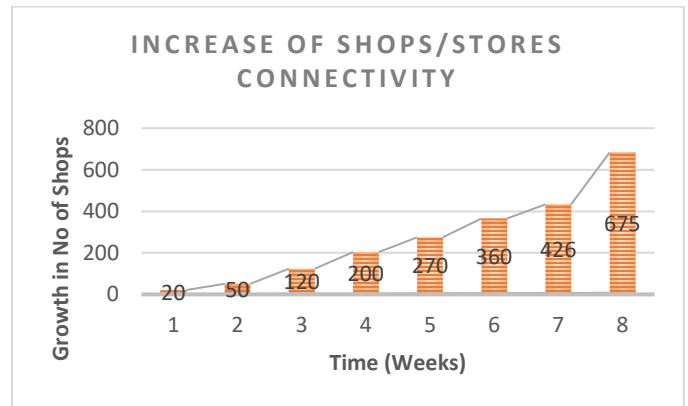
After week eight we stop permissions for other shops due to the lack of Server Space [8] and in the tenth week we finally shut the whole system down.

4. Previous work

Shilony in 1977 presented an idea about geofencing (LBS). Let Suppose a person name Adam shall consider two companies, A and B, the launch of a new product for consumers who can buy from a company only if they receive an advertising message. Advertising creates awareness (and also the price ratios). The set of potential buyers is composed of two different segments of the same size, half of consumers have a relative preference for product A, while the remaining consumers have a relative preference for the product B. The non-use of any buy the brand most preferred is exogenously given by $\gamma > 0$, place in an interpretation, this means that consumers can buy without cost society in his neighborhood, but it involves a shipping cost if they go to the farthest society. This structure of demand (the Shilony 1977) [9] suggests that, although companies may have an

advantage over its competitors, all informed (consumers) may, ultimately, be induced to change. With targeted advertising [10] and price discrimination, each company's strategy is to choose an intensity of advertising and difference to meet the strong and weak segments of the market price. Investing in advertising, companies so endogenous market segment captive customers (i.e. partially shown), selective (i.e. fully informed), and uninformed. To motivate our model, consider the following example from advertising based on the location through geofencing / geoconquesting, which has become a major player in the world of advertising and marketing theme. Suppose two companies, McDonalds (Mc) and Burger King (BK), is running an awareness of mobile advertising campaign of a new menu item. Both about the position of consumers are fully informed (for example, if a consumer is close to allowing them to send ads Mc or BK shop or store) and have access to advertising based on location *Location based ads* (LBA) [11] instruments with different offers (pricing) for customers in different locations. For example, consider a potential customer standing in front of the door of BK. BK can send the customer an offer advertising in question. The consumer can also be traced from the Mc in the district, which can, in turn, will send an advertisement with a special offer (discounts or other rewards). If the latest announcement is quite convincing, Mc able to attract the consumer to travel to more remote sales (incurring the cost). The practice of reaching consumers about competitor has recently been marked geoconquesting strategy. Today, geoconquesting ads are often used in markets where there is a small window of thought before buying (e.g. retail, restaurants, hotels, travel), as well as companies that sell goods (e.g. cars). The model described in this document fits well with advertising policies and prices that are currently possible using mobile devices, such as LBA and mobile coupons. This type of advertising strategies / prices has already been used by brands such as Starbucks, Burger King, Taco Bell, Tasti-D-Lite, Macy's, and Pepsi. For example, the CEO of PlaceIQ startup based in New York recently said PlaceIQ can be used to attract potential customers away from the position of a competitor. With this technology, Lexus could identify users of mobile phones in an Audi dealership and will serve as a mobile ad to direct them to the nearest Lexus dealer.

In the previous examples, consumers' physical location is a key determinant of firms' advertising strategies. However, our stylized model is also suitable for analyzing other forms of targeting advertising strategies in which the geographical element is not intrinsically present. For example, in the case of contextual advertising through search engines, firms may use conquesting ads by targeting them to consumers with an intrinsic preference for the rival firm. In this important work for understanding the decisions advertising companies for their segments strengths and weakness of market information is available. An important contribution is a clear description of market characteristics required for both advertising results, i.e. the most intense advertising on strong market of a company and its weak market balance when companies can make informative advertising revolt. And 'it demonstrated that the relative attractiveness of market weakness and the level of advertising costs are key determinants of equilibrium. When the appeal of the weakest segment is down, advertising regardless of the costs, the standard result in literature prevails: It's always best for each company to announce more

about his poor man in his strongest segment segment. When the weak market is sufficiently attractive, the two equilibrium outcomes are possible: Every company prefers to promote more intensely on its weakest segment when advertising costs are low enough; the opposite occurs when advertising costs are high. This result allows us to provide a theoretical basis for the increasingly popular advertising geoconquesting strategic strategies: Advertising with less intensity in their strong market, every company invites his opponent to play less aggressive in that market.

It 'also concerned that changes depending on the specific advertising decisions and balancing benefits when companies move from a world of a uniform price discrimination [12]. In particular, the result of an increase weakness of the advertising market arises only in equilibrium with price discrimination. With a uniform price, every company always prefer to promote more intensively on its strong market. Finally, our report also shows that price discrimination through targeted advertising can increase your business profits.

Our analysis is more closely related to Iyer et al. (2005). He Characterize a distinct market in a Varian (1980) [13] of type set-up: The market is segmented so exogenous between captive consumers and comparison shoppers. When companies decided to advertise a specific segment of informing the entire segment. The authors showed that all consumers remain poorly informed without advertising, advertising companies more and more for their preference to high segment shoppers. Thus, companies avoid the Bertrand strategic competition in this weak market (see Tirole 1988) [14]. Finally, Iyer et al. (2005), with respect to targeted advertising company decisions under uniform price against price discrimination. In their setting, price discrimination does not affect the advertising intensity targeted to each market segment; it also does not affect the firm's profits. Therefore, our work is complementary Iyer et al. (2005), studying targeted advertising and pricing structure with a different question. Thus, new knowledge can be obtained about the advertising strategies of companies and the impact of price discrimination on strategies and advertising profits of the firm. An important difference between our work and Iyer et al. (2005) is in the behavior of loyal customers (those with a strong preference for a brand). While Iyer et al. (2005) assume that the faithful consumers are increasingly buying their favorite brand (regardless of brand competition on prices), it first assumes that consumers in a particular market segment prefer the sign corresponding to a certain amount but are willing to consider buying rival brand, provided that the price difference is favorable. This hypothesis is consistent with the empirical results show that consumers may switch brands for cost reasons (see, for example, Keaveney 1995 Bolton and Lemon 1999) [15]. namurthi Krishna and Raj (1991) [16] found that consumers are less sensitive faithful to the price that consumers in the choice non loyal decision, but still react to price changes Second, in our set-up, firms' advertising decisions endogenously segment the market into captive (partially informed) consumers and selective (fully informed) consumers.In light of this, we find that in markets where consumers are uninformed without advertising, the equilibrium outcome may produce more advertising to weak markets. Our explanation is strategic, given the demand formulation à la Shilony (1977), the firms' ability to engage in price discrimination, and the interplay between

advertising costs and the attractiveness of the weak market segment.

Finally, this paper is related to the literature on competitive price discrimination with customer recognition (e.g., Chen 1997, Villas-Boas 1999, Fudenberg and Tirole 2000, and Esteves 2010). In these models the market generally exhibits best-response asymmetry (Corts 1998): The strong market segment of one firm is the weak market segment of the competitor. A common finding in such models (with symmetric firms and fully informed consumers) is that firms charge lower prices to customers in weak markets. Also, compared with uniform pricing, equilibrium profits fall with price discrimination.

5. Comparative Analysis

After comparing our work with previous researchers we concluded that out work is somehow relative to Iyer's work. Yes, there are some differences. There is very basic and important differences between Iyer's and ours work, that makes our research and development more sophisticated and better than Iyer's one and that is cost, speed and amount of targeted customers. In Iyer's research he divided the information to specific segments of area, as our covers the whole geofence who can not only acess in that geofence but after subscribing to that specific geofence can also comeback every single time they need that service. The table 1, table 3 and graph 1, graph 2 indicates the success rate quite loudly.

6. Conclusion

In this paper a new concept is proposed for the future marketplace in order to distribute GFSs according to a generic service format that will allow the users to easily find and subscribe to services. On the other hand, service providers can specify arbitrary GFSs without much effort or the need for own infrastructure. After analyzing the results, it is clear that geofencing is the future of advertisements and there is a huge potential in it.

The prototype implementation demonstrates the feasibility of a generic service format as proposed in this paper and that GFSs can easily be realized with current standard hardware and cellular network connections.

Using this feature the growth of customers is always rapid as shown in table 1, table 2, table 3 and graph 1, graph 2. So overall using geofencing technique using the algorithm we used in Fencebook its possible for almost every business to attract customers in quite a large number.

Future Work: The future work will be concentrated on implementing *Fencebook* as an improved marketplace test bed for providing many prototype GFS to even more users to gain data on the usability, performance and scalability of our approach. Afterwards we will focus on developing and extending our generic service format. A graphical editor which allows to visually place geofences on a map for creating GFS descriptions can further increase the ease of service provisioning thus bringing up a lot of new services. We will be focusing on Customer and retailer's communication and the feedback system, which will highly motivate the accuracy and efficiency of the application.

More over an online order system will be introduced so that the customers can easily order the items of there desires. There will also be an option for the customer for choosing the desired category for the notifications they want to receive and also the option of turning the notifications on and off.

Acknowledgment

References:

[1] P. Bellavista, A. Küpper, S. Helal. "Location-based services: Back to the future." IEEE Pervasive Computing **7(**2): 85-89 (2008).

[2] A. Cupper, G. Treu, C. Linnhoff-Popien. "TraX: a device-centric middleware framework for location-based services." IEEE Communications Magazine **44**(9): 114-120 (2006).

[3] A. Küpper, G. Treu. "From Location to Position Management: User Tracking for Location-based Services." In KiVS Kurzbeiträge und Workshop, 81-88 (2005).

[4] "Towards the observation of spatial events in distributed location-aware systems," in Proc. 22nd International Conference on Distributed Computing Systems Workshops, 581–582.

[5] A. Küpper, G. Treu. "Efficient proximity and separation detection among mobile targets for supporting location-based community services." ACM SIGMOBILE Mobile Computing and Communications Review **10**(3): 1-12 (2006).

[6] "Android Took 36% Smartphone Share in Q1: Gartner," Online Available: http://www.eweek.com/c/a/Mobile-and-Wireless/Android-Took-36-Smartphone-Share-in-Q1-Gartner-375805

[7] Apple. Apples App Store Marks Historic 50 Billionth Download. http://www.apple.com/pr/library/2013/05/16Apples-App-Store-Marks-Historic-50- Billionth-Download.html.

[8] M. S. Banik, S. Radhakrishnan, C.N. Sekharan. "Multicast routing with delay and delay variation constraints for collaborative applications on overlay networks." IEEE Transactions on Parallel and Distributed Systems **18**(3): 421-431 (2007).

[9] L.J. Mirman, I. Zilcha. "Characterizing optimal policies in a one-sector model of economic growth under uncertainty." Journal of Economic Theory **14**(2): 389-401 (1977).

[10] G.V. Lioudakis, E.A. Koutsoloukas, N.L. Dellas, N. Tselikas, S. Kapellaki, G.N. Prezerakos, D.I. Kaklamani, I.S. Venieris. "A middleware architecture for privacy protection." Computer Networks **51**(16): 4679-4696 (2007).

[11] R. Jain, A. Puri, R. Sengupta. "Geographical routing using partial information for wireless ad hoc networks." IEEE Personal communications **8**(1): 48-57 (2001).

[12] A. Küpper, G. Treu. "From Location to Position Management: User Tracking for Location-based Services." In KiVS Kurzbeiträge und Workshop, 81-88 (2005).

[13] H.R. Varian, "Redistributive taxation as social insurance." Journal of public Economics **14**(1): 49-68 (1980).

[14] J. Laffont, J. Tirole. "The dynamics of incentive contracts." *Econometrica:* Journal of the Econometric Society, 1153-1175 (1988).

[15] R.N. Bolton, K.N. Lemon. "A dynamic model of customers' usage of services: Usage as an antecedent and consequence of satisfaction." Journal of marketing research, 171-186 (1999).

[16] R. Diaz, I. Maria, F.J.R. Cataluña. "Antecedents of the importance of price in purchase decisions." Revista de Administração de Empresas **51**(4): 370-381 (2011).

Stand-alone Inverter: Reviews, Models and Tests the exist system in Term of the Power Quality, and Suggestions to Design it

Ali Algaddafi[*]

Institute of Energy and Sustainable Development, De Montfort University, Leicester, LE1 9BH, UK.

A B S T R A C T

Developments in power electronics have enabled the widespread application of Pulse Width Modulation (PWM) inverters, notably for obtaining electricity from renewable systems. This paper critical review the previous studies in designing stand-alone inverter and modelling the inverter with two control loops to improve and provide a high-quality power of a stand-alone inverter. Multi-loop control techniques for a stand-alone inverter are utilised as the first loop is a capacitor current control to provide active damping and improve transient and steady state inverter performance. The capacitor current control is cheaper than inductor current control, where a small current sensing resistor is used. The second loop is the output voltage control that is used to improve the system performance and also control the output voltage. The power quality of the off-grid system is measured experimentally and compared with the grid power, showing power quality of off-grid system to be better than that of the grid. The suggestions and key findings to design the stand-alone inverter are given based in the reviewing of previous publications and from the literature's point of view.

1. Introduction

This paper is an extension of work originally presented in 2016 International Conference on Electronics, Information, and Communications (ICEIC) [1]. In the stand-alone inverter, the control approach is required to have a fast transient response with a good dynamic performance to improve the overall efficiency and minimized the Total Harmonic Distortion (THD) of the output voltage and current to comply with IEEE 519-2014 standard.

The output voltage in a stand-alone inverter is required to be pure sinusoidal with minimum the THD [2]. Many control strategies may be used, such as repetitive control, dead-beat control and sliding mode control. The dead-beat control is sensitive to parameter variations and also is complex to use [3]. The repetitive control [3-5] can achieve low THD output of current in a few fundamental cycles; however, the dynamic performance of the inverter remains imperfect. The sliding mode control has been proved quite useful against uncertainty [3, 6, 7]. However, the well-known chattering problem should be considered in analog or digital realization of the control algorithm [2], requiring careful selection of the switching surface. Furthermore, multiple feedback loop control was proposed in [8]. It is easy to use in theory, given

comprehensive analysis for the various controller parameters. An internal current loop in the stand-alone inverter to improve the response speed and the steady state performance of inverter were presented as in [1, 9-12]. There are various current controllers for stand-alone inverter such as one cycle control [13, 14], hysteresis current control [12, 15-22]. However, the hysteresis current control suffers from the variation of the switching frequency which leads to the switching stress and causes a high THD for the output voltage and current. The capacitor current control is proposed as an internal control loop to avoid a DC offset on the AC side of the output voltage since the proposed inverter is transformer-less.

This paper critically reviews the recent publications of the stand-alone inverter and proposed two control loops to improve the THD of the output voltage and current. The effectiveness of the control system in modelling was validated by matching the experimental results. This paper is organized as follows: section two discusses the critical review previous studies of the stand-alone inverter. Section three models a control of a stand-alone inverter. While the experimentation works and validation are verified in section four. Section five presents the key findings and suggestions to design stand-alone inverter with recent important applications. The final section is drawn conclusions and future works.

[*]Corresponding: Ali Algaddafi, IESD, De Montfort University, Leicester, UK,
LE1 9BH, +447448295307, alisirte@yahoo.com

2. Critical Review Previous Studies of the Stand-Alone Inverter

Multiple feedback loop control techniques for single-phase voltage source was presented in [8]. The internal control is a capacitor current and the output loop is a voltage control loop. This technique improves the performance and capable of producing nearly perfect sinusoidal load voltage. However, the results are difficult to interpret and procedure to design a controller may not be explained, even though a linearized small signal dynamic model is developed. Also, a Fast Fourier Transform (FFT) algorithm analysis may not be taken into account.

Designing of a standalone PV system with battery storage was presented by Abdel-Salem et al. [23]. Although, the security of electricity was estimated by compromising storage batteries to cover night time, Also FFT analysis and THD of the output voltage was determined in both cases with filter and without a filter, but the THD is high. It would be useful if the THD reduced to be less than 3<% for the current and 5 <% for the voltage to meet IEEE 519-2014 standard requirements.

Sometimes, the power is required to be high for a stand-alone system, hence stand-alone multiple inverters are used. A small signal analysis for parallel connected inverters in the stand-alone system was presented by Coelho, et al.[24]. Although the control approach of the inverters depends on the frequency and voltage droop, which depends on the local variable measurements there are some limitations which have been neglected as follows: the THD of the output current and voltage does not take into account. And also, the stand-alone inverter was assumed as a source voltage and the harmonic components have been ignored. Furthermore, from the waveform of the output current that presented in [24], it is clear that the THD of the output current is significantly high, which is required more investigation by using FFT analysis and evaluated by measuring the THD and thereafter it should be compared with IEEE 519-2014 standard.

In recent, the Sensor-less five levels packed U-cell inverter operating as stand-alone alone and grid connected system was presented by Vahedi et al. [25] Although this system may operate as stand-alone or grid connected system and THD of the output voltage and current is reduced the system is a complex and costly. Perhaps the main disadvantage of paper of Vahedi et al. was used two control loops with six switches. Hence the two control loops are used as proposed in [25] with full bridge inverter that would be less cost and reduce the complexity, which makes the system cheaper than the system proposed by Vahedi et al.

A sensor-less parabolic current control approach in the inductor of stand-alone inverter was proposed by Zhang, et al. [12]. Fig 1 shows stand-alone inverter with output voltage compensator loop as an outer loop while the internal parabolic current loop control is the inner loop. A Hall effect current sensor will take the time to respond if the digital analog converter is implemented. However, the analog circuit with a Hall effect current sensor in inductor was implemented to increase the response speed by using an operation amplifier as shown in fig 2, where the parabolic current is generated by T*=RoCo.

But the inductor current is more expensive and may not reduce the output voltage ripple, hence the capacitor current in the output capacitor was used as proposed by Algaddafi et al.[26].
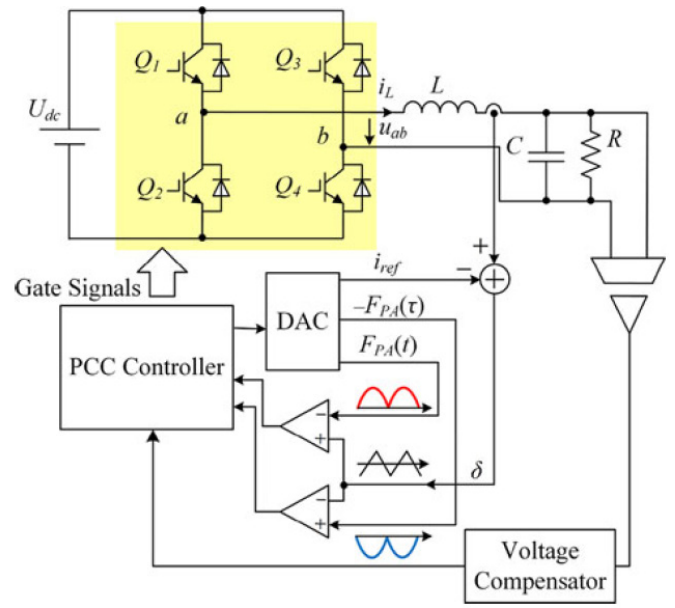

Figure.1. Diagram of a stand-alone inverter with internal parabolic current loop and external voltage loop
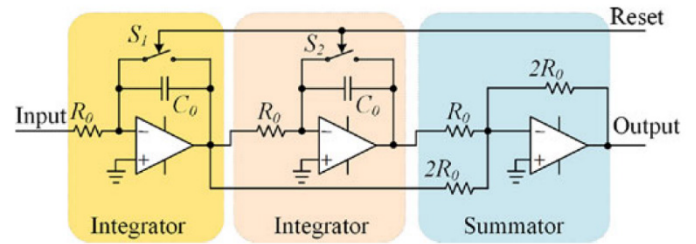

Figure.2. Parabolic carrier waveform generator

3. Model the Proposed Stand-Alone Inverter with Two Loop controllers

3.1. Inverter model

The procedure to select a stand-alone Photovoltaic (PV) system presented in [3]. Specifying and integrating PV components for a RES will include voltage and power choices to be made, stored, the PV modules themselves, with a vital link being the charge controller. This could be a DC-DC converter or DC-AC inverter [7]. In this section, the stand-alone inverter is considered. A single phase stand–alone inverter is shown as in fig.3, consisting of the DC voltage source, inverter full bridge, controlled by a Sinusoidal Pulse Width Modulation (SPWM) generator, the output voltage of DC/AC inverter needs a filter to attenuate switching harmonic components, thus, the LC filter is used. The mathematical model of a single-phase inverter with LC filter is given by applying KVL and KCL in [3, 27, 28] as follows:

$$\frac{dV_c}{dt} = \frac{1}{c}i_L + \frac{1}{c}i_o \qquad (1)$$

$$\frac{di_L}{dt} = \frac{1}{L}V_{inv} - \frac{1}{L}V_c - \frac{R}{L}i_L \qquad (2)$$

At no load the transfer function between the output voltage and the input voltage can be given where the output voltage Vo is equal to the voltage on capacitor Vc:

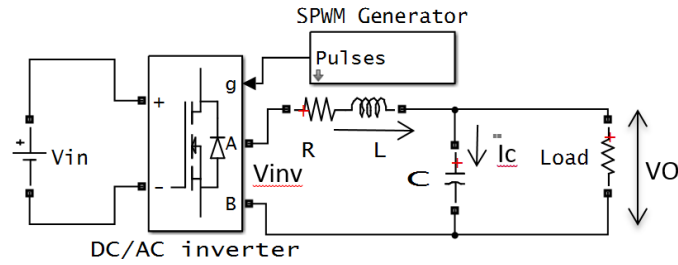$$\frac{V_o}{V_{inv}} = \frac{1}{LCs^2 + RCs + 1} \qquad (3)$$

Figure.3. Power circuit of stand-alone inverter

3.2. Design optimal control of a stand-alone inverter

The capacitor current is controlled by an inner loop as shown in fig.4 where the inductor with parasitic resistance is used.
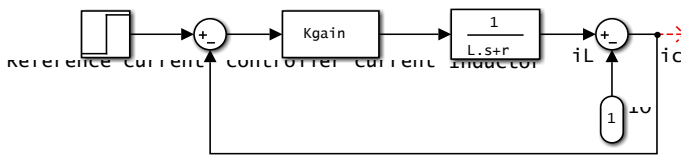

Figure.4. Block diagram of capacitor current controller

In this paper, two loop controllers are proposed to control the output voltage. The first loop is a capacitor current controller and the second loop is the output voltage of the stand-alone inverter controller as depicted in fig.5.
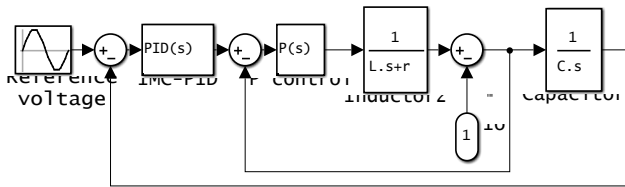
Figure.5. Full block diagram of stand-alone inverter

The parameters of the numerical model of the stand-alone inverter are selected based on [6], with an ideal of the full bridge assumed also the effect of grid current is neglected.
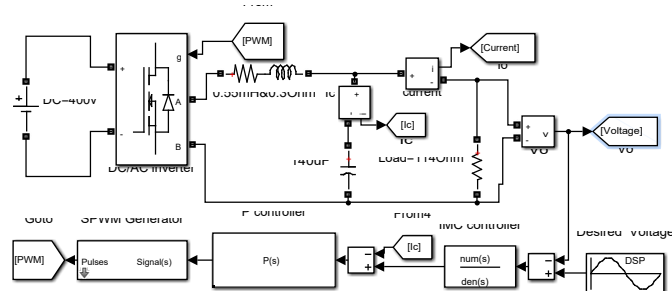
Figure.6. Circuit diagram of stand-alone inverter with proposed controller

3.3. Simulation Results

To evaluate the performance of the proposed controller of a stand-alone inverter, the output voltage and current were measured as in fig.7. It is clear that the stand-alone inverter works at unity power factor. The load is selected to be114 Ω to compare with experimental results.
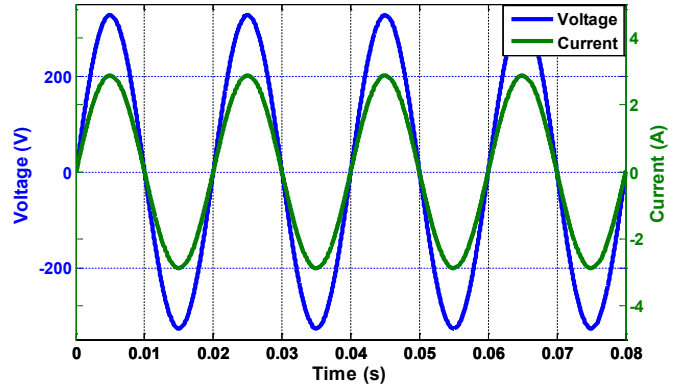
Figure.7. Output voltage and current of stand-alone inverter

The THD of output current was analysed in the frequency domain. The spectral analysis is shown in fig.8. The THD of the output is minimal and complied with IEEE-standard analyses of the output voltage of stand-alone inverter
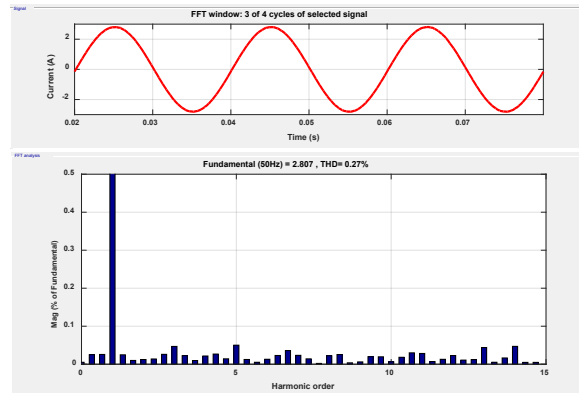
Figure.8. Output current of stand-alone inverter and its FFT analysis

The main issues of the stand-alone inverter are a fluctuation of the input voltage and variation of the load. In this paper, the variations of the load are only considered. A unit step with an ideal breaker is used to connect and disconnect the load, and a resistive load is varied to investigate the response of the system.
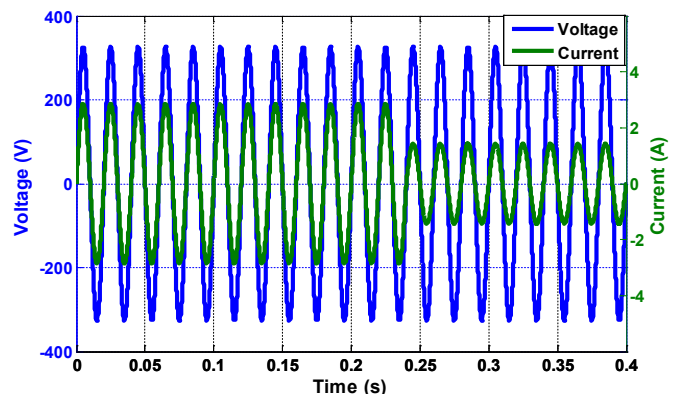
Figure.9. The response of stand-alone inverter to reduce the load

At 0.24s the unit step is selected to trip, therefore, the output current will decrease to half as shown in fig 9. The response of the stand-alone inverter is very fast and smooth to reduce the load. In fig.10 the output current responds to increases in the load and the output voltage may not be affected. This validates the robustness of the controller.
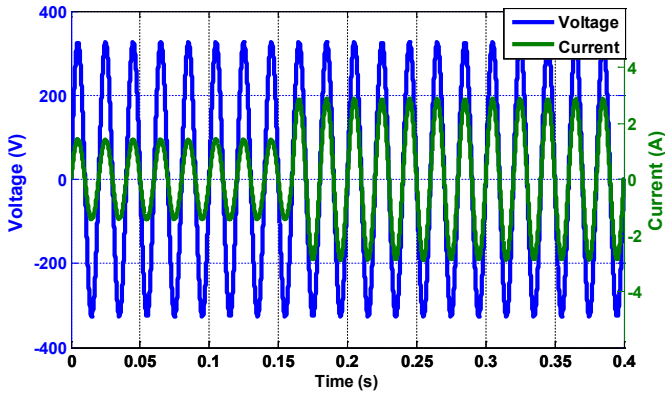

Figure.10. Smooth response of stand-alone inverter to increase the load

It is clear that the proposed controller of a stand-alone inverter has very smooth and fast response to variations of the load when the resistive load increases or decreases.

4. Experimentation works and Validation

4.1. Configuration of Sunny Island SI6.0H inverters as off-grid system

The Sunny Island (SI 6.0H) inverter is taken as out working example, which is a bidirectional converter. It can be operated on the island (off grid) where it forms a stand-alone system providing active and reactive power and on-grid modes. This section will test the power quality of the off-grid system and understanding the performance of SI 6.0H inverter and to compare with the power quality of the utility network. The power quality should meet the IEEE 519-2014 standard [29]. In this experiment, the SI 6.0H inverter with battery storage was used to supply the variable resistive loads.

4.2. Testing power quality of off-grid and utility network

Experimental work was conducted to test the power quality in the laboratory. The two resistors, each resistor is 228 Ω, were used. Those resistors were connected in parallel to give 114 Ω. The SI 6.0H inverter was configured in an off-grid mode and used to supply resistive loads. The output voltage and current of SI 6.0H inverter are analyzed where it supplied the resistive loads. The THD of the output voltage and current are measured by using a Power Analyzer and also the waveform components are analyzed by using FFT analysis. The FFT is used to evaluate the performance of a stand-alone inverter, as presented in [30]. The Same resistive loads are supplied from the grid and the same procedures are carried out in order to compare the acquired results of power quality of the grid with the off-grid system.

4.3. Experimental Results

In the stand-alone inverter, the output voltage and frequency should be fixed (do not change such as 230 V, 50Hz). The SI 6.0H inverter was set up as an off-grid system with battery storage.
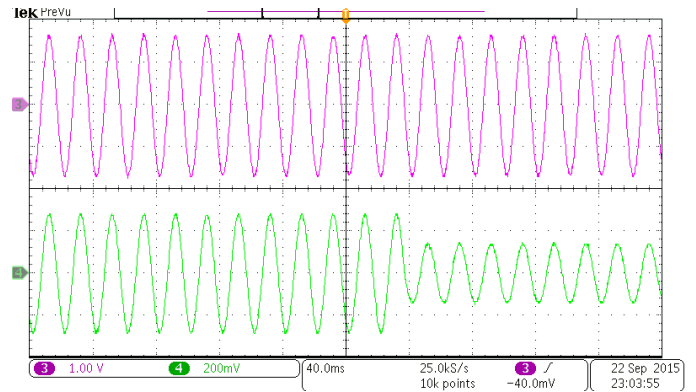

Figure.11. Test response of sunny island inverter to step down of the resistive load, trace 3 output voltage [200V/Div.] and trace 4 current loads [10A/Div.]

The oscilloscope is triggered to observe the response of the output current and voltage to variations of the resistive load. It is clear that the output voltage does not affect by variation of the load, while the current varies according to the variation of resistive loads. Moreover, when the load increases the current has small distortion for a short period of time as shown in fig 11 and fig. 12.
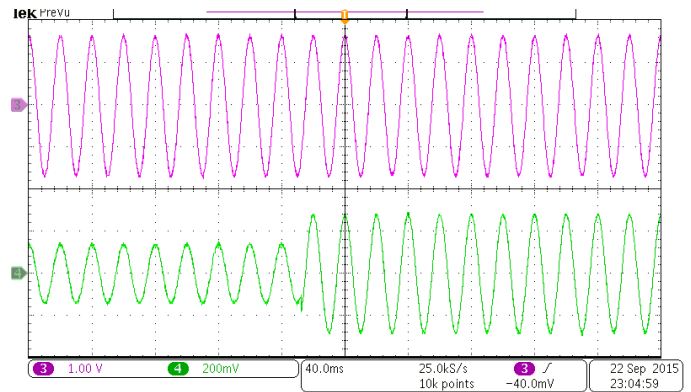

Figure.12. Step up the resistive load of off-grid sunny island and its response, trace 3 output voltage [200V/Div.] and trace 4 current loads [10A/Div.]

Therefore, the spectral analysis of the output current and voltage of SI 6.0H inverter is analysed as shown in fig.13 and fig .14, respectively.
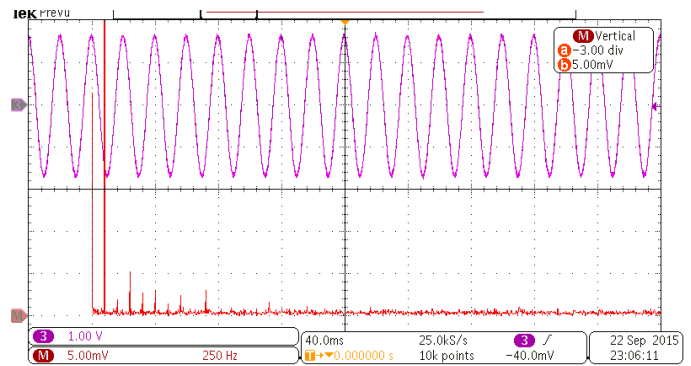

Figure.13. The output voltage of off-grid system and its FFT analysis [200V/Div.] and THD=1.6%

The grid is used to supply the same resistive load. The voltage and current on the resistive load were measured as shown in fig.15. From the waveforms of network voltage and load current, it is clear that the network utility has high harmonic components such as the

third harmonic. Therefore, those waveforms are analysed and measured by using power analysed to evaluate the power quality of the network
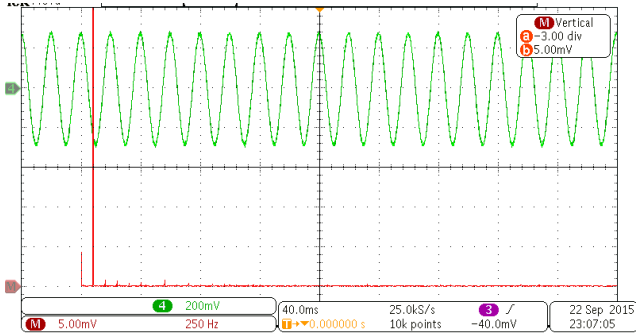

Figure.14. The waveform of output current [10A/Div.] of the off-grid system and its FFT where the THD=1. 123%
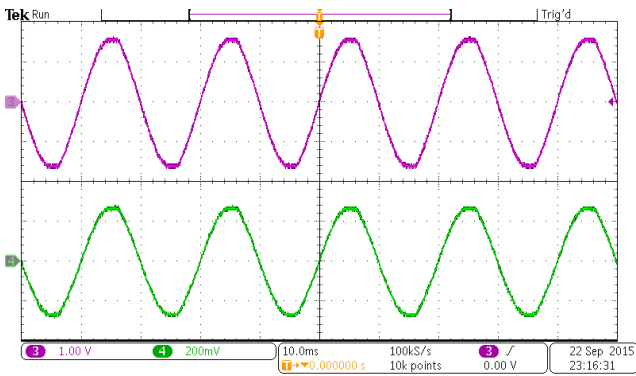

Figure.15. Trace 3 is the network voltage [200V/Div.] and trace 4 is the load current [10V/Div.]

Fig 16 shows the grid voltage and its spectrum. It is interesting to compare this waveform with the waveform of the output voltage of SI 6.0H inverter. The third, fifth and seventh harmonic of the grid voltage is higher than the output voltage of SI 6.0H inverter.

The THD of the output current of SI 6.0H inverter is less than the THD of the network when we compare between fig. 14 and fig.17. This is due to the different loads connected to the network, such as inductive load and resistive load are supplied from the network and those produce the harmonic components in the network. In addition, the line impedance and the renewable energy such as solar energy causes a distortion in the network.
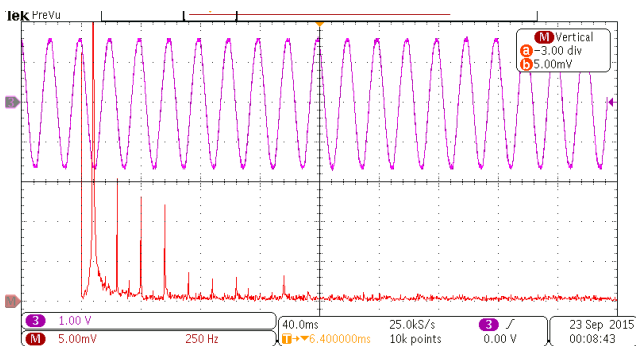
Figure.16. The Output voltage of the network and its FFT analysis[200V/Div.] and THD=2.5%
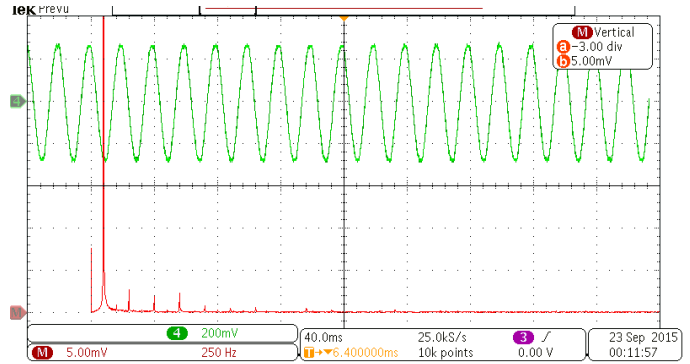
Figure.17. The waveform of current when it is supplied by a network [10A/Div.] and it's spectrum analyser where the THD=1. 5%

4.4. Limitations of Stand-Alone System

The ripple current in DC side of inverter is the main problem. This ripple current reduces the battery lifespan or fuel cell life as can be seen in fig.18. This problem has been discussed in depth in [31].
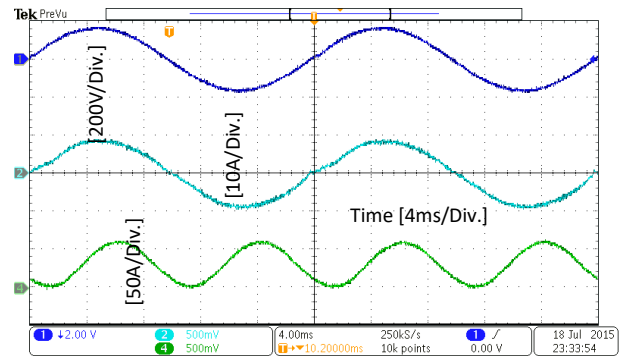

Figure.18. Trace 1 is the grid voltage, trace 2 is the current injected into the battery from the solar system, and trace 4 is the ripple current injected into the storage battery that has DC and AC components
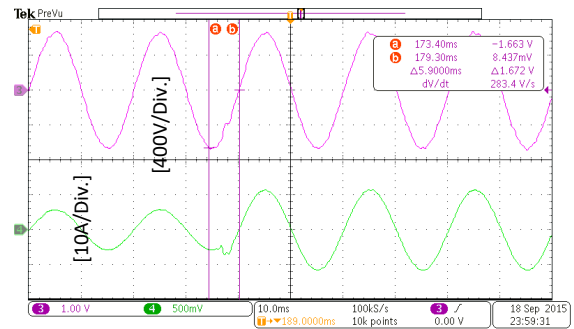

Figure.19. Response of the output current of the Mini-Grid in trace 4 and voltage in trace 3

The main issues of the stand-alone inverter relate to the input voltage fluctuation and load variation, with Munsell [32] recently presenting the potential challenges for networks as follows:

1- Growth of distributed energy sources

2- Changes in the customer preferences

3- Expansion of energy market services

4- Increasing regulation

Due to the above, grid reliability remains as critical as ever, which underscores it as a subject for future research.

5. Further Investigations to Reduce the Ripple Current and Suggestions

5.1. Reducing Current Ripple at Battery Side

Reducing input current ripple in a fuel cell system with load inverter was proposed by Changrong and Jih-Sheng to increase fuel cell lifespan [33]. The active control technique was incorporated with a current control loop to reduce this ripple even though; the harmonic analysis of the output current to evaluate the performance may not be considered. Also, the system has a four stage, which causes a complexity. The virtual resistor with an LC filter for PWM inverter was used to damp the transient oscillations by Dahono et al.[34]. Nevertheless, the virtual resistor gives nice waveforms for the output voltage and current, there are limitations as follow: the DC voltage source was assumed a constant and no ripple; although the THD of the output voltage was reduced, the value of the inductor is slightly large; FFT analysis may not take into account to evaluate the performance of the system and the output load was assumed to be source current. In fact, the virtual resistor is very good idea to reduce the losses. This requires an additional control load such as capacitor current loop as presented in [1]. Attempt for improving the battery life of the stand-alone solar system was presented by Das and Agarwal [35]. Despite this system can be used with solar PV, ultracapacitor bank, fuel cell and has a good dynamic response, but there are limitations which are:

- The system is complex because of the used bi-directional DC-DC converter, for battery DC-DC regulated for PV panel and inverter to the converter from DC-AC voltage.
- In the DC link, there is a ripple current which may not take into account. Also, the ripple current that goes the battery or flows from battery do not demonstrate or present since the title of this study was enhancing battery life.
- Also, this system was used for three phase inverter, which could be different with single phase inverter.

The AC mini-grid that presented in [1] is less stage of power. Hence, the losses are low and efficiency is high.

5.2. The Key Findings and Suggestions

To design the stand-alone inverter, the following procedures are required:

- Determine the value of the output power that is required to be delivered from the stand-alone inverter.
- Determine the power quality of the output voltage and current
- Based on the required power, the various elements of an inverter that include the switches and the LC filter will be selected.
- Based on the power quality, the LC filter will be characterised and the control approach will be implemented.
- From point of view, the two loops of the control system should be used as presented in [1] to improve the overall system despite the cost and a little complex control system.

- After designing the stand-alone inverter, it should be tested by the nonlinear load such as full-wave rectifier circuits that has to exaggerate the THD even further and thereafter the THD of the output current and voltage should be evaluated and compared with IEEE 519-2014 standard.

5.3. Applications of Stand-Alone Inverter

The inverter is a critical component used to convert Direct Current (DC) power output from the solar panels or batteries into Alternative Current (AC) for AC appliances. There are many applications for stand-alone inverter such as the PV solar system to pump the water in remote areas as shown in the figure below [36].

Figure.20. PV Water Pumping Beer Tssawa

Therefore, the solar water pump inverter is widely used for many applications such as irrigation system, livestock watering, or in remote areas with battery backup that are suitable for the solar home system, rural and village electrification. In general, stand-alone inverter or off-grid power systems operate independently of the grid and are most often used in isolated areas, where the stand-alone inverter provides a more affordable and reliable source of electricity.

5.4. Impact of global warming

Effect global warnings in the earth were summarized by Boso as follows [37]:

1. The world is the glaciers and polarise will be gradually melted, which will cause a problem for 100 million people because they live within 91.44 centimetres of sea water level.

2. Some animal will gradually extinct, such as polar bears.

3. A tropical climate will spread the diseases due to more moisture.

4. Hurricanes, tornados, heavy rains and floods will expect increase due to heavy moisture and circulation of the air.

5. Tropical countries may severe of droughts which will affect and damage agriculture and also cause problems for fresh water.

However, this study was suggested that the use renewable energy instead fossil fuels can mitigate some of the global warms issues, which was assumed as the first step to solving this problem.

Conclusion

This paper presents the power quality of an off-grid (SI 6.0H inverter) system and power quality of the national grid in the UK. The off-grid system has less distortion of waveforms than the grid. The numerical model of a stand-alone inverter is modelled with two loops. The inner loop is a capacitor current control and the outer loop is the output voltage controller. The inner loop does not change the tracking features of the closed-loop system; it does not only improve the performance of linear load but also improving the performance of the nonlinear loads. The output waveform of model inverter and analysis are presented in this paper. The power quality is improved and gives an excellent response to the variations of the load. The simulation results match the experimental results. In critical load or devices that require a pure power, such as magnetic resonance imaging- medical devices, the off-grid system is suitable to protect those devices from abnormal voltage and frequency. The recent publications of stand-alone inverter were critically reviewed and the key findings with suggestions were given to improve the overall system. Future work will be analysed the impact of fluctuation of the input voltage of a stand-alone inverter. In addition, the stand-alone inverter will be tested by the nonlinear load such as full-wave rectifier circuits and thereafter the THD of the output current and voltage will be assessed.

Conflict of Interest

The authors declare no conflict of interest.

Acknowledgment

References

[1]   A. Algaddafi, N. Brown, R. Gammon, S. A. Altuwayjiri, and M. Alghamdi, "Improving off-grid PV system power quality, and comparing with grid power quality," IEEE in 2016 International Conference on Electronics, Information, and Communications (ICEIC), 1-6(2016).

[2]   T.-S. Lee, S. Chiang, and J.-M. Chang, "H∞ loop-shaping controller designs for the single-phase UPS inverters," IEEE Transactions on Power Electronics, **16**: 473-481 (2001).

[3]   D. Wenfang, H. Qun, and X. Yingnian, "Study on IMC-PID control for single-phase voltage-source inverters," IEEE 6th International in Power Electronics and Motion Control Conference, 1514-1518 (2009).

[4]   K. Zhou, K.-S. Low, Y. Wang, F.-L. Luo, B. Zhang, and Y. Wang, "Zero-phase odd-harmonic repetitive controller for a single-phase PWM inverter," IEEE Transactions on Power Electronics, **21**:193-201 (2006).

[5]   K. Zhang, L. Peng, J. Xiong, and J. Chen, "State-feedback-with-integral Control plus Repetitive Control for PWM Inverters," IEEE in Proceedings of the Chinese Society of Electrical Engineering, 56-62 (2006).

[6]   N. Mohan, T. M. Undeland, and W. P. Robbins, Power Electronics: Converters, Applications, and Design: John Wiley & Sons, 2003.

[7]   R.-J. Wai, W.-H. Wang, and C.-Y. Lin, "High-performance stand-alone photovoltaic generation system," IEEE Transactions on Industrial Electronics, **55**: 240-250 (2008).

[8]   N. M. Abdel-Rahim and J. E. Quaicoe, "Analysis and design of a multiple feedback loop control strategy for single-phase voltage-source UPS inverters," IEEE Transactions on Power Electronics, **11**: 532-541 (1996).

[9]   G. Wang and Y. W. Li, "Parabolic PWM for current control of voltage-source converters (VSCs)," IEEE Transactions on Industrial Electronics, **57**: 3491-3496 (2010).

[10] L. Zhang, B. Gu, J. Dominic, B. Chen, C. Zheng, and J.-S. Lai, "A dead-time compensation method for parabolic current control with improved current tracking and enhanced stability range," IEEE Transactions on Power Electronics, **30**: 3892-3902 (2015).

[11] L. Zhang, J. Dominic, B. Gu, B. Chen, C. Zheng, and J.-S. Lai, "Implementation of parabolic current control for dual-carrier PWM," IEEE in 2015 Applied Power Electronics Conference and Exposition (APEC), 1487-1492 (2015).

[12] L. Zhang, R. Born, B. Gu, B. Chen, C. Zheng, X. Zhao, et al., "A Sensorless Implementation of the Parabolic Current Control for Single-Phase Stand-Alone Inverters," IEEE Transactions on Power Electronics, **31**: 3913-3921 (2016).

[13] K. M. Smedley and S. Cuk, "One-cycle control of switching converters," IEEE transactions on power electronics, **10**: 625-633 (1995).

[14] K. M. Smedley, L. Zhou, and C. Qiao, "Unified constant-frequency integration control of active power filters-steady-state and dynamics," IEEE Transactions on Power Electronics, **16**: 428-436 (2001).

[15] T. A. Froeschle, "Current controlled two-state modulation," ed: Google Patents, (1984).

[16] L. Malesani and P. Tenti, "A novel hysteresis control method for current-controlled voltage-source PWM inverters with constant modulation frequency," IEEE Transactions on Industry Applications, **26**: 88-92 (1990).

[17] L. Malesani, L. Rossetto, and A. Zuccato, "Digital adaptive hysteresis current control with clocked commutations and wide operating range," IEEE transactions on industry applications, **32**:316-325 (1996).

[18] R. Gupta, "Generalized frequency domain formulation of the switching frequency for hysteresis current controlled VSI used for load compensation," IEEE Transactions on Power Electronics, **27**: 2526-2535 (2012).

[19] Z. Yao and L. Xiao, "Two-switch dual-buck grid-connected inverter with hysteresis current control," IEEE Transactions on Power Electronics, **27**: 3310-3318 (2012).

[20] H. Mao, X. Yang, Z. Chen, and Z. Wang, "A hysteresis current controller for single-phase three-level voltage source inverters," IEEE Transactions on Power Electronics, **27**: 3330-3339 (2012).

[21] Q. Yao and D. G. Holmes, "A simple, novel method for variable-hysteresis-band current control of a three phase inverter with constant switching frequency," IEEE in Industry Applications Society Annual Meeting, 1993., Conference Record of the 1993, 1122-1129 (1993).

[22] S. Buso, S. Fasolo, L. Malesani, and P. Mattavelli, "A dead-beat adaptive hysteresis current control," IEEE Transactions on industry applications, **36**: 1174-1180 (2000).

[23] M. Abdel-Salam, A. Ahmed, A. El-kousy, K. Sayed, M. Amery, M. Swify, et al., "On the design and operation of a standalone residential PV system in Egypt," 2013 International Conference on Clean Electrical Power (ICCEP), 659-664 (2013).

[24] E. A. A. Coelho, P. C. Cortizo, and P. F. D. Garcia, "Small-signal stability for parallel-connected inverters in stand-alone AC supply systems," IEEE Transactions on Industry Applications, **38**: 533-542 (2002).

[25] H. Vahedi, P. A. Labb, x00E, and K. Al-Haddad, "Sensor-Less Five-Level Packed U-Cell (PUC5) Inverter Operating in Stand-Alone and Grid-Connected Modes," IEEE Transactions on Industrial Informatics, **12**: 361-370 (2016).

[26] A. Algaddafi, N. Brown, G. Rupert, and J. Al-Shahrani, "Modelling a Stand-Alone Inverter and Comparing the Power Quality of the National Grid with Off-Grid System," IEIE Transactions on Smart Processing and Computing, **5**: 35-42 (2016).

[27] J. F. Sultani, "Modelling, Design and Implementation of DQ Control in Single-Phase Grid-Connected Inverters for Photovoltaic Systems used in Domestic Dwellings," De Montfort University, (2013).

[28] M. Monfared, S. Golestan, and J. M. Guerrero, "Analysis, design, and experimental verification of a synchronous reference frame voltage control for single-phase inverters," IEEE Transactions on industrial Electronics, **61**: 258-269 (2014).

[29] Anon., IEEE Recommended Practice and Requirements for Harmonic Control in Electric Power Systems - Redline, available at: http://ieeexplore.ieee.org/xpl/articleDetails.jsp?arnumber=6826459&filter= AND(p_Publication_Number:6826457[accessed:01/01/2015], 1-213 (2014).

[30] D. O. Neacsu, Power-switching converters: medium and high power: CRC press, (2014).

[31] A. Algaddafi, J. Alshahrani, S. Hussain, K. Elnaddab, E. Diryak, and I. Daho, "Comparing The Impact of the Off-Grid System and On-Grid System On a Realistic Load." Proceeding in 32nd European Photovoltaic Solar Energy Conference and Exhibition, Munich, German, (2016).

[32] M. Munsell, "9 Projects Defining the Next-Generation Electricity System, available at: http://www.greentechmedia.com/articles/read/9-projects-defining-the-next-generation-electricity-system?utm_content=bufferfe6de&utm_medium=social&utm_source=facebook.com&utm_campaign=buffer [accessed:24/03/2016].

[33] L. Changrong and L. Jih-Sheng, "Low Frequency Current Ripple Reduction Technique with Active Control in a Fuel Cell Power System with Inverter Load," IEEE Transactions on Power Electronics, **22**: 1429-1436 (2007).

[34] P. A. Dahono, Y. R. Bahar, Y. Sato, and T. Kataoka, "Damping of transient oscillations on the output LC filter of PWM inverters by using a virtual resistor," IEEE in 4th International Conference on Proceedings Power Electronics and Drive Systems, 403-407 (2001).

[35] M. Das and V. Agarwal, "A novel control strategy for stand-alone solar PV systems with enhanced battery life," IEEE in Applied Power Electronics Conference and Exposition (APEC), 2014 Twenty-Ninth Annual IEEE, 2880-2887 (2014).

[36] M. Ekhlat, I. Salah, and N. Kreama, "Energy efficiency and renewable energy. Libya–National Study," General Electric Company of Libya (GECOL), (2007).

[37] B. K. Bose, "Global Warming: Energy, Environmental Pollution, and the Impact of Power Electronics," IEEE Industrial Electronics Magazine, **4**: 6-17 (2010).

A Comparative Study For Color Systems Used In The DCT-DWT Watermarking Algorithm

Khalid A. Al-Afandy[*], El-Sayed M. EL-Rabaie[1], Fathi E. Abd El-Samie[1], Osama S. Faragallah[2], Ahmed ELmhalaway[2], A. M. Shehata[2]

[1]Faculty of Electronic Engineering, Electronic and Communication Department, Menoufia University, Egypt

[2] Faculty of Electronic Engineering, Computer Engineering and Science Department, Menoufia University, Egypt

A R T I C L E   I N F O

A B S T R A C T

This paper presents a comparative study of using different color systems on watermarking algorithms. This comparison aim is to determining the robustness and the stability of the color systems used in the watermarking scheme. The watermarking algorithm that is used in this paper is a hybrid scheme using the Discrete Wavelet Transform (DWT) in the Discrete Cosine Transform (DCT) domain. The DCT-DWT watermarking algorithm is applied using three color systems, the RGB (Red, Green and Blue) color system, the HSV (Hue, Saturation and Value) color system and the YIQ color system. The comparison is based on visualization to detect any degradation in the watermarked image, the Peak Signal-to-Noise Ratio (PSNR) of the watermarked image, the Normalized Correlation (NC) of the extracted watermark after extraction, the embedding algorithm CPU time, and applying different types of attacks and then calculating the PSNR and the NC.

1. Introduction

Information technology such as digital data and multimedia can be easily duplicated, manipulated, and distributed in this time, so it's very important to have a copyright protection to save owners copyrights. There are many protection techniques, one of them is watermarking. Watermarking technology is the process of hiding an image called watermark or label into original digital data (image, video or audio) [1,2]. Watermarking schemes can be classified into two categories; spatial domain and transform domain [3]. There are several schemes of transform domain watermarking technology. One of these schemes is the Discrete Wavelet Transform (DWT) [1,3]. It is based on dividing an image into four non-overlapping bands. These bands are calculated in different frequencies; approximation sub-band (low frequency LL), horizontal sub-band (high frequency LH), vertical sub-band (high frequency HL), and diagonal sub-band (high frequency HH) [1,3]. Other used scheme of transform domain is the Discrete Cosine Transform (DCT) [5]. This transform is used to convert spatial domain image into discrete transform domain [6]. The watermarking scheme based on transform the color image to 2D

DCT for each color channel, embedding watermark into the DCT frequency, then the inverse DCT given watermarked image [5,6]. Hybrid schemes are used in watermarking schemes. One of them is DCT-DWT [7]. It is based on dividing the color image into 2D matrices. The DCT domain is extracted by applying the DCT for each 2-D matrix. Embedding watermark is done on the sub-band LL by utilize the DWT to divide the DCT domain into four sub-bands for each 2-D matrix [7-9].

Colors are an important communication tool for human; it is used for communication with outside environments [10]. Using colors in image processing improve the image data for better human understanding [10]. So it's important to represent colors as mathematical formulas. There are different color formats that can represent the image color information; they are called the color systems. One of these color systems is the RGB color system. It is an additive color system based on tri-chromatic theory, easy to implement and very common but non-linear with visual perception [11]. Other color system is the HSV (Hue, Saturation and Value) color system. It is a linear transform from the RGB color system. It is very easy to select a desire hue and modifying it by adjusting its saturation and value [11]. Another color system is the YIQ color system. It is an analogue space of NTSC (National Television Standard Committee) system and used for color TV [10]. It is

*Corresponding Author: Khalid Al-Afandy, Heliopolis, Cairo, Egypt,
Khalid_yuosif@yahoo.com

separate the RGB color system into a Luminance Y, and two chrominance information I,Q, it is useful in compression application [11].

The main aim of this paper is to apply the DCT-DWT watermarking algorithm using the RGB, the HSV and the YIQ color systems. A comparative study is done to determine the stability and the robustness of these three color systems after applying the watermarking algorithm.

The rest of this paper is organized as follows. Section 2 gives a description of the watermarking schemes. The color systems are shown in section 3. Section 4 shows the comparative topics. The simulation results are illustrated in section 5. Section 6 presents the conclusion followed by the most relevant references.

2. Watermarking Schemes

2.1. Discrete Wavelet Transform (DWT)

Wavelet transform is an information processing method; it has been widely used in many fields including image processing. The DWT divide an image into four non-overlapping bands. These bands are calculated in different frequencies [1]. Figure 1 shows the four sub-bands; approximation sub-band c_i (low frequency LL), horizontal sub-band (high frequency LH) ch_i, vertical sub-band (high frequency HL) cv_i, and diagonal sub-band (high frequency HH) cd_i. Figure 2 show the low pass and high pass analysis filter h[-m], g[-m] while the corresponding low pass and high pass synthesis filter are h[m] and g[m]; c_i and d_i are the low and high band output coefficient at level i [1,3].

The DWT analysis is given by:

$$ci+1[m,n] = (ci(m,n)*h[-m])\downarrow2 \qquad (1)$$

$$di+1[m,n] = (ci(m,n)*g[-m])\downarrow2 \qquad (2)$$

So the DWT synthesis is given by

$$Ci+1[m,n] = [(ci(m,n)\uparrow2)*h[m]) + [(di(m,n)\uparrow2)*g[m])] \qquad (3)$$

Where * denotes convolution and $\uparrow\downarrow$ denotes down sampling and up sampling by factor of 2.

LL	LH
HL	HH
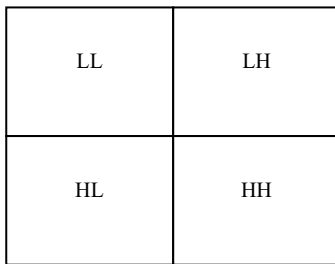
Figure 1. The DWT sub-bands [3].

2.2. Discrete Cosine Transform (DCT)

Discrete Cosine Transform (DCT) is a standout amongst the most well-known orthogonal change strategies utilized as a part of picture preparing. High vitality compaction property of the DCT is the reason. In watermarking, this property helps in choosing the area in image to insert the watermark with the most robustness [4]. The DCT divides aircraft carrier signal into three frequencies bands namely low, middle, and heights frequency bands. It is a frequency orbit watermarking scheme as the watermark is

embedded into one of these three bands, carrier signal pixel are not modified directly [5].
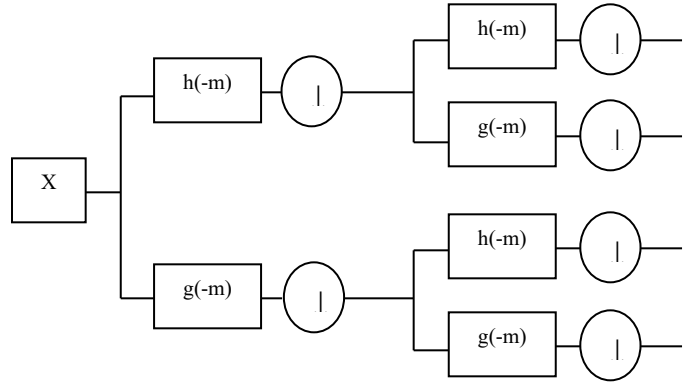

Figure 2. The two dimensional decomposition using DWT [3].

Two dimension discrete cosine transform 2D-DCT is defined as [6]

$$F(jk) = a(j)a(k) \sum_{m=0}^{M-1} \sum_{n=0}^{N-1} f(m,n) \cos\left[\frac{(2m+1)j\pi}{2M}\right] \cos\left[\frac{(2n+1)k\pi}{2N}\right] \quad (4)$$

Inverse transform 2D-IDCT is defined as [6]

$$f(mn) = \sum_{j=0}^{M-1} \sum_{k=0}^{N-1} a(j)a(k)F(jk) \cos\left[\frac{(2m+1)j\pi}{2M}\right] \cos\left[\frac{(2n+1)k\pi}{2N}\right] \quad (5)$$

Where M,N are image dimension,

$$0 \leq j \leq M\text{-}1,\ 0 \leq k \leq N\text{-}1,$$

$$a(j) = \begin{cases} \frac{1}{\sqrt{M}}, & j = 0 \\ \sqrt{\frac{2}{M}}, & 1 \leq j \leq M-1 \end{cases},$$

and

$$a(k) = \begin{cases} \frac{1}{\sqrt{N}}, & k = 0 \\ \sqrt{\frac{2}{N}}, & 1 \leq k \leq N-1 \end{cases}$$

2.3. The Hybrid Scheme DCT-DWT

The hybrid scheme DCT-DWT is based on utilized the DWT to divide the DCT domain into four sub-bands [7]. The color image is divided into three 2D matrices (depending on used color system). The DCT domain is extracted by applying the DCT for each 2D matrix. Embedding watermark is done on the sub-band LL by utilize the DWT to divide the DCT domain into four sub-bands for each 2D matrix [7-9].

3. Color System

3.1. The RGB (Red, Green and Blue) Color System

The RGB color system is an additive color system based on tri-chromatic theory, easy to implement, and very common, but non-linear with visual perception. It may be visualized as a cube with the three axis's corresponding to red, green and blue, this cube bottom corner when Red=Green=Blue=0 and opposite top corner when Red=Green=Blue=255. The RGB color system is frequently used in most computer applications [11]. In computer applications

the RGB color image represented as a three dimensional array with dimension M×N×3, where M×N is image axis X,Y and 3 is the three color channel Red, Green and Blue respectively [10]. Figure 3 show the RGB color model [10].
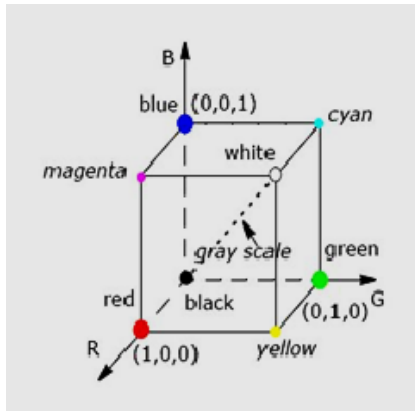

Figure 3. The RGB color model [10].

3.2. The HSV Color System

The HSV color system is a linear transform from the RGB color system. It is very easy to select a desire hue and modifying it by adjusting its saturation and value. It is defined as a position on a circular plane around the value axis. Hue is the angle from a nominal point around the circle to the color. Saturation is the radius from the central value axis to the color. Figure 4 show the HSV color model [10]. Conversion from the RGB color system to HSV color system as [11]:

Find the maximum and minimum values from the RGB triplet

$$\max = \max(R, G, B) \tag{6}$$

$$\min = \min(R, G, B) \tag{7}$$

If max=min then the image is monochrome (not color) because it is no Hue

The Saturation (S) is
$$S = \frac{\max - \min}{\max} \tag{8}$$

The Value (V) is
$$V = \max \tag{9}$$

$$R' = \frac{\max - R}{\max - \min} \tag{10}$$

$$G' = \frac{\max - G}{\max - \min} \tag{11}$$

$$B' = \frac{\max - B}{\max - \min} \tag{12}$$

If R=max
$$H = 60 \times (B' - G') \tag{13}$$

If G=max
$$H = 60 \times (2 + R' - B') \tag{14}$$

If B=max
$$H = 60 \times (4 + G' - R') \tag{15}$$

If H>=360
$$H = H - 360 \tag{16}$$

If H<0
$$H = H + 360 \tag{17}$$
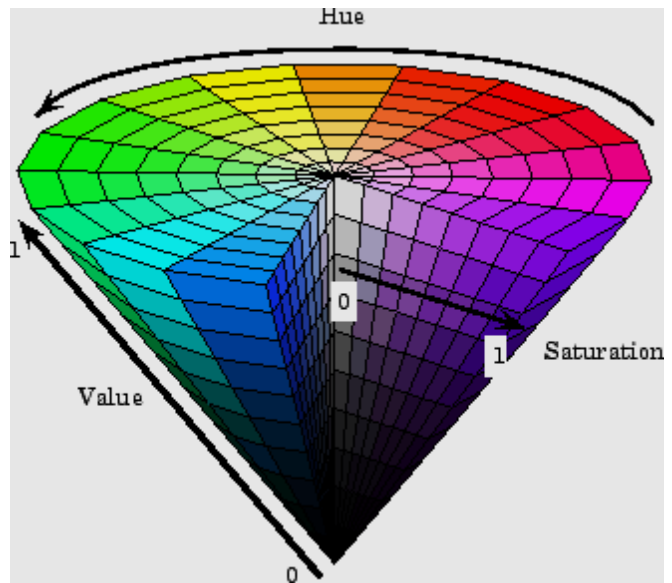
Figure 4. The HSV color model [10].

3.3. The YIQ Color System

The YIQ color system is an analogue space of the NTSC system that used for the American color TV. It separates the RGB color system into a Luminance Y, and two chrominance information I, Q. It is useful in compression application [11]. The YIQ system was designed to utilize sensitivity in luminance changes than hue or saturation changes. Figure 5 show the YIQ color system model [10]. The relation between the YIQ color system and the RGB color system as [11]:

From RGB to YIQ

$$\begin{bmatrix} Y \\ I \\ Q \end{bmatrix} = \begin{bmatrix} 0.299 & 0.587 & 0.114 \\ 0.586 & -0.275 & -0.321 \\ 0.212 & -0.528 & 0.311 \end{bmatrix} \begin{bmatrix} R \\ G \\ B \end{bmatrix} \tag{18}$$

From YIQ to RGB

$$\begin{bmatrix} R \\ G \\ B \end{bmatrix} = \begin{bmatrix} 0.30 & 0.60 & 0.21 \\ 0.59 & -0.28 & -0.52 \\ 0.11 & -0.32 & 0.31 \end{bmatrix} \begin{bmatrix} Y \\ I \\ Q \end{bmatrix} \tag{19}$$
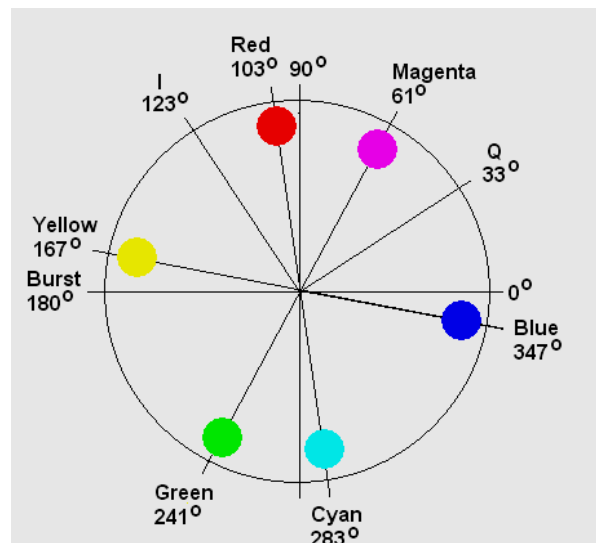

Figure 5. The YIQ color model [10].

4. The Comparative Topics

The aim of this paper is to present a comparative study of three different color systems used in watermarking scheme algorithms. The comparison is based on applying the DWT-DCT watermarking scheme algorithm for color images (host and watermark) using the RGB color system, the HSV color system and the YIQ color system. The DCT-DWT watermarking scheme is based on separation for each of the host and watermark color image into three 2-D matrices according to the used color system. The DCT domain is extracted by applying the DCT on each 2-D matrix extracted from color image. The DWT is utilized to divide the DCT domain for each 2-D matrix into four non-overlapping bands. The watermark is embedded into the LL sub-band [7-9]. A comparison is done between the three color systems RGB, HSV and YIQ. The comparison is based on visual detection, the PSNR, the NC, the embedding algorithm CPU time, and applying attacks to determine the robustness of color systems.

5. Simulation Results

All tests were performed using an Intel® core™i5 CPU M450 @2.4GHz with 6GB Memory and running Windows 7 64-bit operating system and using MATLAB 8. The images used are RGB colored JPEG images with size 512×512, and bit depth 24 host image Rokayya with resolution 72×72 dpi and watermark cats with resolution 180×180 dpi as shown in Figure 6. There are five main tests to determine the performance of a color system used in watermarking scheme algorithm. Visually test to determine the invisibility of watermark in the watermarked image and any degradation in colors compared to original image, the embedding algorithm CPU time, the Peak Signal-to-Noise Ratio (PSNR) of the watermarked image, the Normalized Correlation (NC) for the extracted watermark are calculated, and applying attacks on the watermarked image then extracting the watermark and calculating the PSNR and the NC again after attacks. PSNR can be calculated by [5]

$$MSE = \frac{1}{M \times N} \sum_{x=0,y=0}^{M-1,N-1} (A_w(x,y) - A(x,y))^2 \qquad (20)$$

$$PSNR\ (DB) = 10 \log_{10} \frac{255^2}{MSE} \qquad (21)$$

where A is original image, A_w is watermarked image and M, N size of original and watermarked image. NC calculate given by [5]

$$NC = \frac{W^* . W}{\|W^*\| . \|W\|} \qquad (22)$$

Where W is original watermark and W* is extract watermark

(a)   (b)

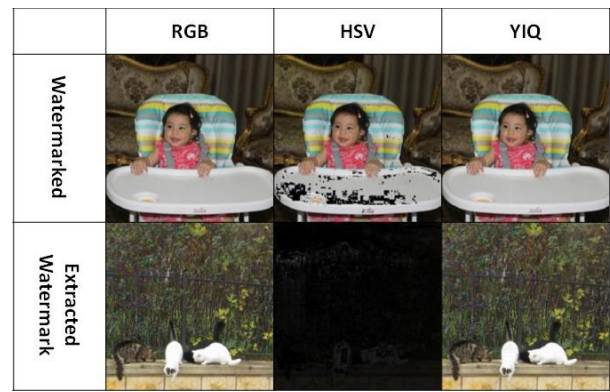Figure 6. (a) The host Image Rokayya, (b) The watermark image cats.

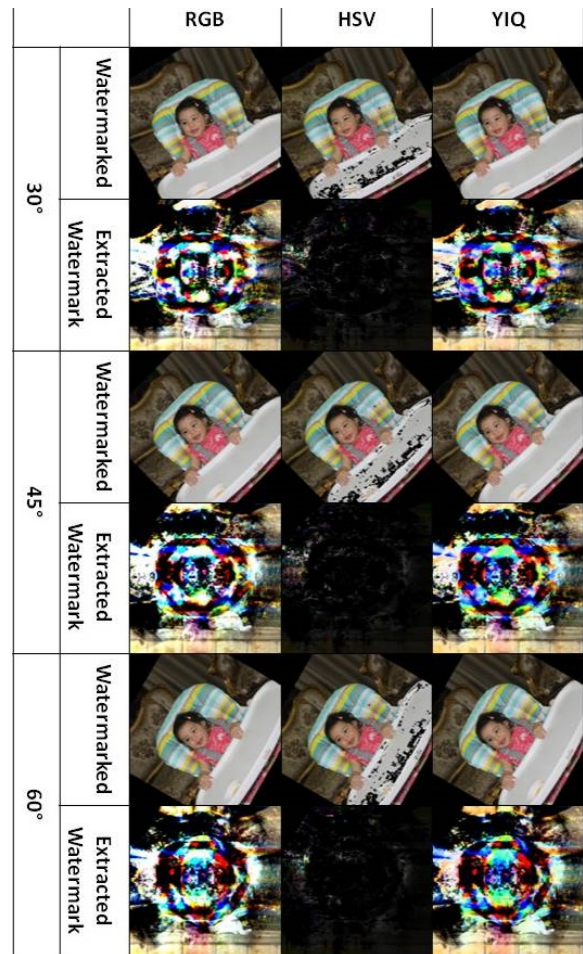Figure 7 Visualization tests without any attacks.

Figure 8 Visualization tests after rotation attacks 30°, 45°, and 60°.

Visualization comparison results without attacks are shown in figure 7. Figure 8 shows the rotate attacks (30°, 45° and 60°). Gaussian noise attacks are shown in figure 9 with variance parameters (0.01, 0.05 and 0.1). Figure 10 shows the blur attacks (motion, disk and average). The JPEG compression attacks are shown in figure 11 (20%, 40% and 60%). Figure 12 shows the resize to 256×256 attacks then resize to 512×512. The crop attacks are shown in figure 13. The evaluation matrices results (PSNR and NC) without attacks and embedding algorithm CPU time for the comparison are shown in table1 and figure 14. Table 2 and figure 15 show the evaluation matrices results (PSNR and NC) after attacks.
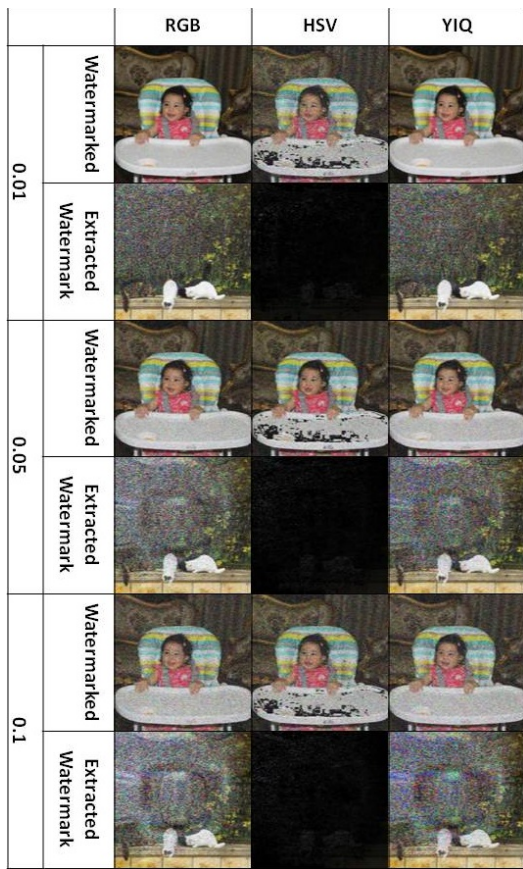
Figure 9 Visualization tests after Gaussian noise attacks with variance parameters 0.01, 0.05, 0.1.
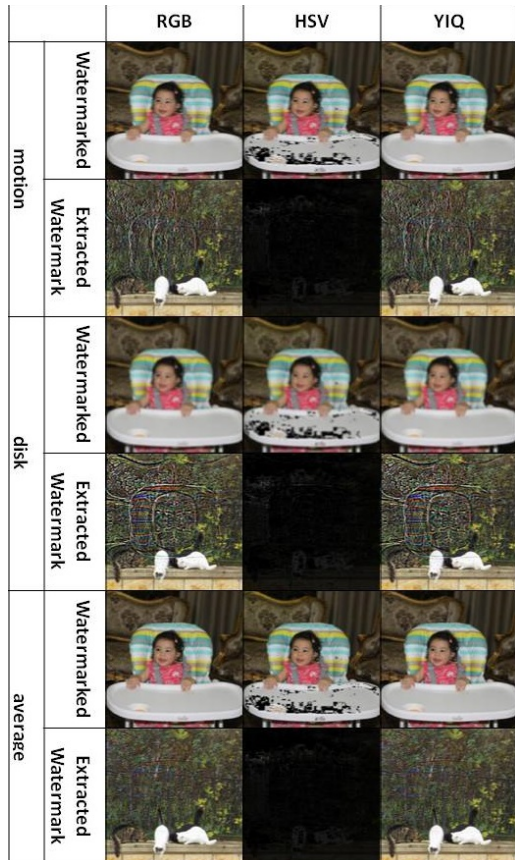

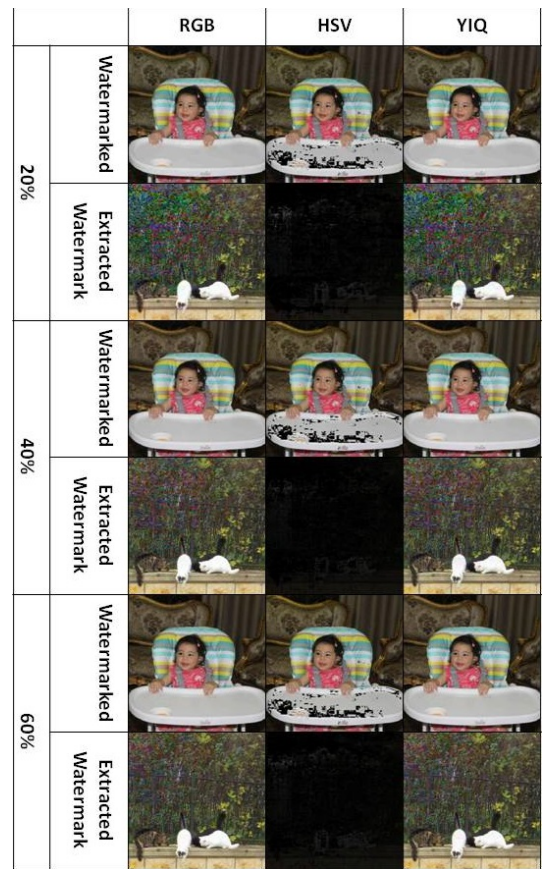Figure 10 Visualization tests after blur attacks (motion, disk, and average).

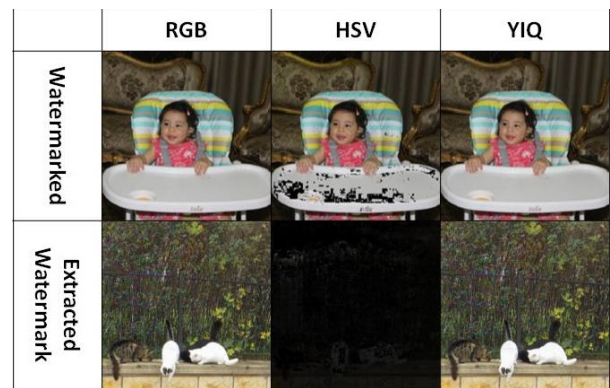Figure 11 Visualization tests after JPEG compression attacks 20%, 40%, and 60%.

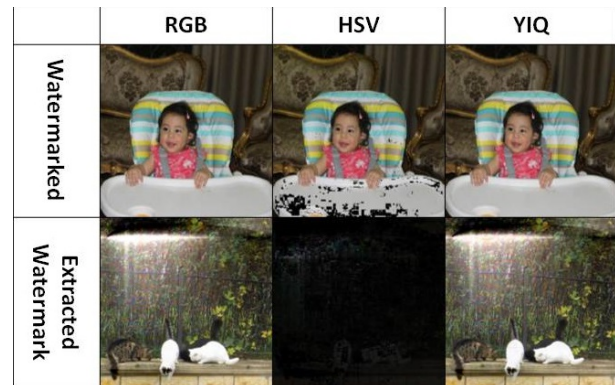Figure 12 Visualization tests after resize to 256×256 then resize to 512×512 attacks.

Figure 13 Visualization tests after crop attacks.

Table 1. The PSNR for watermarked image, the NC for extracted watermark without attacks and the CPU time for embedding algorithm.

Without attack	RGB	HSV	YIQ
PSNR red	33.9764	16.6698	33.9764
PSNR green	35.2180	16.6828	35.2180
PSNR blue	34.6320	16.6906	34.6320
NC red	0.9587	0.5927	0.9585
NC green	0.9646	0.5554	0.9644
NC blue	0.9377	0.4997	0.9373
CPU time (Sec)	1.5444	1.7004	1.95
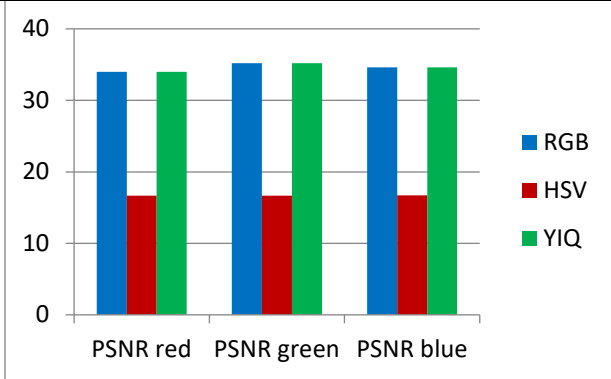
(a) The PSNR for watermarked images.
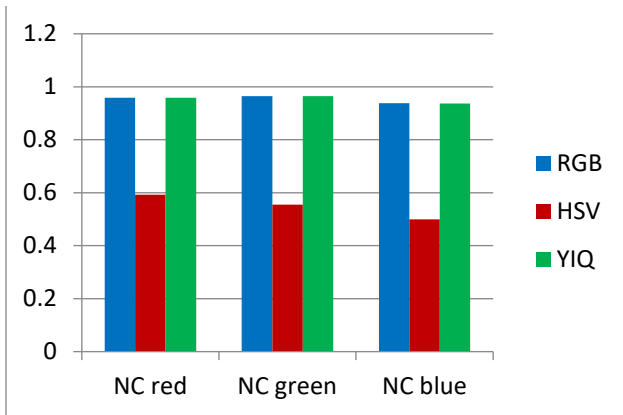
(b) The NC for extracted watermark.
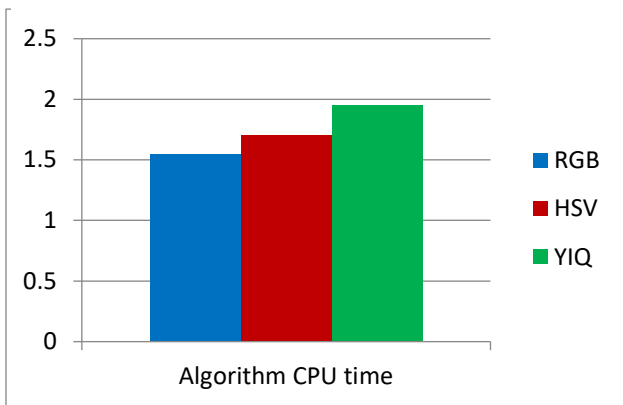
(c) Algorithm CPU time.

Figure 14. The evaluation matrices comparison based on the PSNR for watermarked image, the NC for extracted watermark without attacks and the CPU time for embedding algorithm.
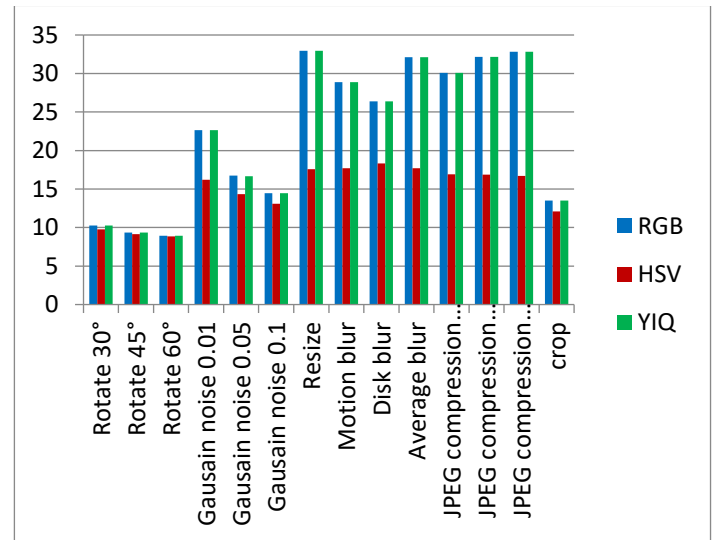
Table 2. The PSNR for watermarked image, and the NC for extracted watermark after attacks.

After attack		RGB	HSV	YIQ
Rotate 30°	PSNR red	10.8712	10.2095	10.8712
	PSNR green	10.7056	10.1637	10.7056
	PSNR blue	10.2787	9.7696	10.2787
	NC red	0.4134	0.1261	0.4385
	NC green	0.3737	0.1128	0.4029
	NC blue	0.3110	0.0758	0.3429
Rotate 45°	PSNR red	10.0475	9.7151	10.0475
	PSNR green	9.7717	9.5316	9.7717
	PSNR blue	9.3565	9.1425	9.3565
	NC red	0.4349	0.1309	0.4709
	NC green	0.3691	0.1242	0.4000
	NC blue	0.2992	0.0773	0.3192
Rotate 60°	PSNR red	9.6386	9.4558	9.6386
	PSNR green	9.4120	9.3174	9.4120
	PSNR blue	8.9305	8.8420	8.9305
	NC red	0.4347	0.1782	0.4660
	NC green	0.3594	0.1484	0.3848
	NC blue	0.3049	0.1052	0.3219
Gaussian noise 0.01	PSNR red	22.5692	16.1464	22.5873
	PSNR green	22.6814	16.1505	22.6942
	PSNR blue	22.6411	16.1870	22.6542
	NC red	0.6281	0.3893	0.6381
	NC green	0.5946	0.3712	0.6014
	NC blue	0.5402	0.3044	0.5505
Gaussian noise 0.05	PSNR red	16.6907	15.2738	16.6774
	PSNR green	16.6384	14.2272	16.6643
	PSNR blue	16.7434	14.3356	16.7488
	NC red	0.4637	0.1376	0.5034
	NC green	0.4144	0.1350	0.4472
	NC blue	0.3507	0.1189	0.3807
Gaussian noise 0.1	PSNR red	14.4521	13.0484	16.4830
	PSNR green	14.3016	12.9226	14.3182
	PSNR blue	14.4515	13.0859	14.4692
	NC red	0.4015	0.1027	0.4555
	NC green	0.3481	0.1054	0.3887
	NC blue	0.2765	0.0936	0.3104
Resize	PSNR red	32.6509	17.5709	32.6509
	PSNR green	33.2573	17.5776	33.2573
	PSNR blue	32.9487	17.5823	32.9487
	NC red	0.9318	0.6209	0.9316
	NC green	0.9333	0.584	0.9329
	NC blue	0.9050	0.5326	0.9045
Motion blur	PSNR red	28.9065	17.6938	28.9065
	PSNR green	28.7466	17.6686	28.7466
	PSNR blue	28.8790	17.6937	28.879
	NC red	0.8434	0.5767	0.8438
	NC green	0.8284	0.5423	0.8291
	NC blue	0.8024	0.4743	0.8038
Disk blur	PSNR red	26.1620	18.2997	26.1620
	PSNR green	26.3194	18.3153	26.3194
	PSNR blue	26.3862	18.3299	26.3862
	NC red	0.7696	0.5386	0.7702
	NC green	0.7600	0.5101	0.7620
	NC blue	0.7346	0.4336	0.7374

|				
Average blur	PSNR red	31.9021	17.6811	31.9021
	PSNR green	32.4367	17.6901	32.4367
	PSNR blue	32.1206	17.6905	32.1206
	NC red	0.9250	0.6214	0.9247
	NC green	0.9269	0.5835	0.9265
	NC blue	0.8990	0.5307	0.8984
JPEG compression	PSNR red	30.8030	16.9024	30.8030
	PSNR green	31.8857	16.9348	31.8857
	PSNR blue	30.1031	16.8905	30.1031
	NC red	0.8804	0.5430	0.8792
	NC green	0.8892	0.5023	0.8883
	NC blue	0.8225	0.4338	0.8209
JPEG compression	PSNR red	32.0421	16.8709	32.0421
	PSNR green	33.8185	16.9056	33.8185
	PSNR blue	32.1418	16.8881	32.1418
	NC red	0.9186	0.6038	0.9181
	NC green	0.9319	0.5630	0.9311
	NC blue	0.8809	0.4939	0.8797
JPEG compression	PSNR red	32.5064	16.6962	32.5064
	PSNR green	33.9616	16.7221	33.9616
	PSNR blue	32.8417	16.7128	32.8417
	NC red	0.9345	0.5899	0.9341
	NC green	0.9423	0.5560	0.9417
	NC blue	0.9036	0.4939	0.9025
Crop	PSNR red	13.2283	11.8709	13.2283
	PSNR green	13.6797	12.1924	13.6797
	PSNR blue	13.5194	12.0834	13.5194
	NC red	0.6993	0.4286	0.6991
	NC green	0.7009	0.3664	0.7056
	NC blue	0.6567	0.3253	0.6645
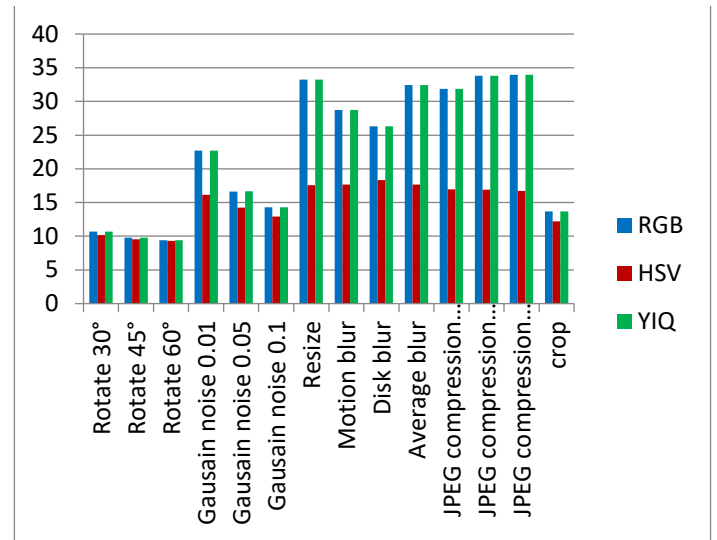
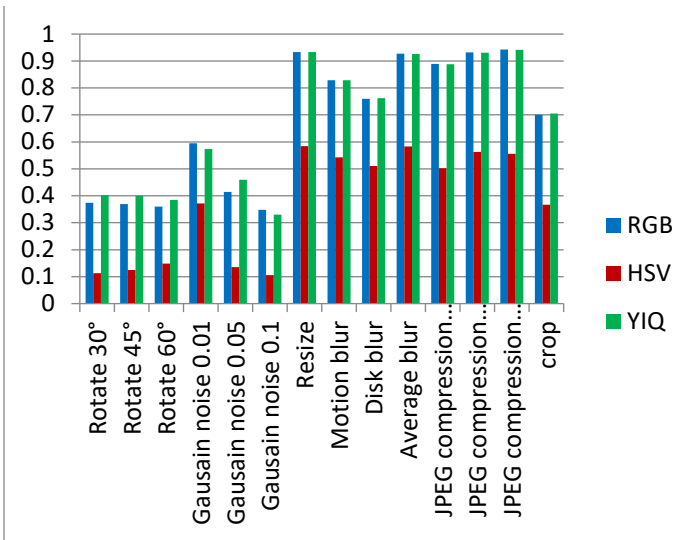(b) The PSNR for watermarked images for green channels after attacks.

(c) The PSNR for watermarked images for blue channels after attacks.
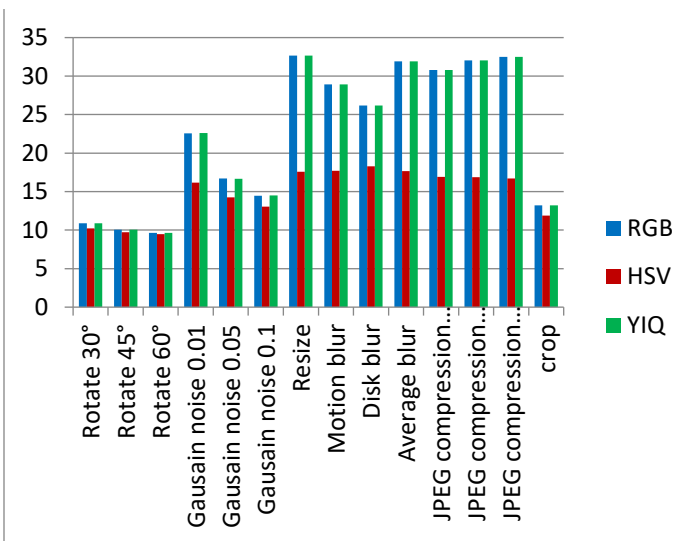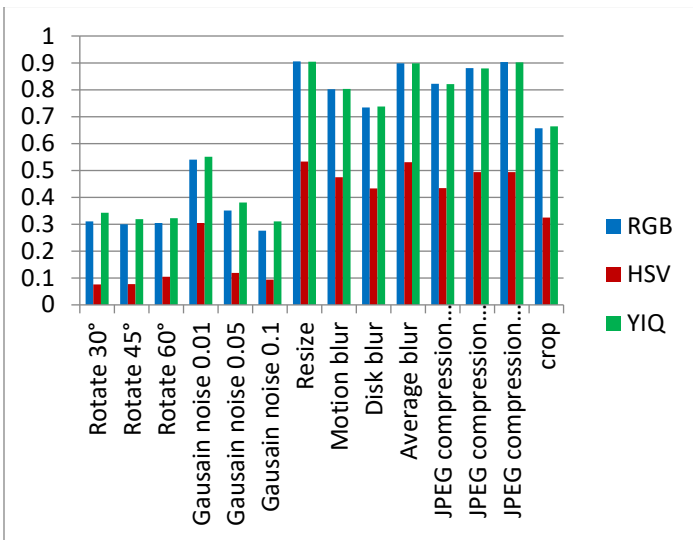

(a) The PSNR for watermarked images for red channels after attacks.
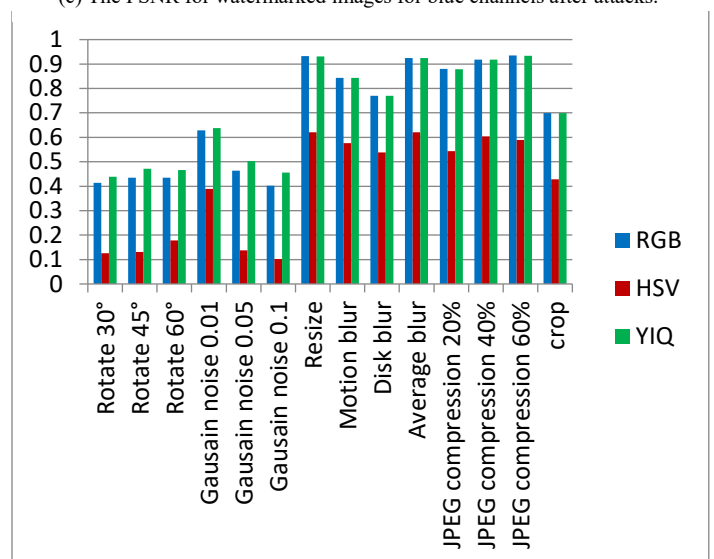
(d) The NC for extracted watermark for red channel after attacks.

(e) The NC for extracted watermark for green channel after attacks.

(f) The NC for extracted watermark for blue channel after attacks.

Figure 15. The evaluation matrices comparison based on the PSNR for watermarked image, and the NC for extracted watermark after attacks.

As shown from visualization test, experimental results and evaluation figures with and without attacks, results illustrate that; there is a degradation in colors for the watermarked images and the extracted watermark is not good for using the HSV color system, where there are no degradation in colors for the watermarked images and the extracted watermarks are good for using the RGB and the YIQ color systems. The PSNR and the NC values without and after attacks for the HSV color system are less than the RGB and the YIQ color systems. The PSNR and the NC values without attacks for the RGB color system are little higher than the YIQ color system. The PSNR and the NC values after some attacks for the YIQ color system are little higher than the RGB color system and similar after other attacks. The Embedding algorithm CPU time show that the RGB color system is the faster and the slower is the YIQ color system but the difference is fractions of second so that the three color systems are approximately similar in embedding algorithm CPU time.

The HSV color system is worse than the RGB and the YIQ color systems and weak against attacks. The RGB color system and the YIQ color system are approximately similar and robust against attacks.

6. Conclusion

This paper presents a comparison between three different color systems; the RGB color system, the HSV color system, and the YIQ color system in watermarking algorithms. This comparison is to determine the stability and the robustness of color systems that used for applying the watermarking schemes. The watermarking algorithm that is used in this paper is the hybrid scheme DCT-DWT. This comparison illustrates that the HSV color system is the weakest when compared to the RGB and the YIQ color systems and is not robust against attacks. The RGB color system and YIQ color system are approximately similar and robust against attacks. The YIQ color system is a little robust against attacks when compared to the RGB color system. The embedding algorithm CPU time using the RGB color system is a little faster than the HSV and the YIQ color systems; the difference is a fraction of second. The results reveal the superiority of using the RGB and the YIQ color systems over the HSV color system.

References

[1] Giri, Kaiser J., Mushtaq Ahmad Peer, and P. Nagabhushan, "A robust color image watermarking scheme using discrete wavelet transformation", International Journal of Image, Graphics and Signal Processing (IJIGSP), **7**(1): 47-52 (2014).

[2] Saini, Mandeep Singh, B. Venkata Kranthi, and Gursharanjeet Singh Kalra, "Comparative analysis of digital image watermarking techniques in frequency domain using MATLAB SIMULINK", International Journal of Engineering Research and Applications (IJERA), **2**(4): 2248-9622 (2012).

[3] Ganjir, Neha, and Nivedita Singh, "Bi-orthogonal wavelet transform based 3-D image watermarking on colour image", International Journal of Computer Science and Mobile Computing, **3**(8): 451-456 (2014).

[4] Kekre, Dr HB, Dr Tanuja Sarode, and Shachi Natu, "Hybrid watermarking of colour images using DCT-Wavelet, DCT and SVD", International Journal of Advances in Engineering and Technology, **6**(2): 769-779 (2013).

[5] Jiansheng, Mei, Li Sukang, and Tan Xiaomei, "A digital watermarking algorithm based on DCT and DWT", International Symposium on Web Information Systems and Applications (WISA'09), **9**(1): 104-107 (2009).

[6] Saini, Lalit Kumar, and Vishal Shrivastava., "Analysis of attacks on hybrid DWT-DCT algorithm for digital image watermarking with MATLAB", International Journal of Computer Science Trends and Technology (IJCST), **2**(3): 123-126 (2014).

[7] Mukherjee, Pameli, and Saurabh Mitra., "A review on copy-move forgery detection techniques based on DCT and DWT", International Journal of Computer Science and Mobile Computing, **4**(3): 702-708 (2015).

[8] Benoraira, Ali, Khier Benmahammed, and Noureddine Boucenna., "Blind image watermarking technique based on differential embedding in DWT and DCT domains", EURASIP Journal on Advances in Signal Processing, **2015**(1): 1-11 (2015).

[9] Kaur, Ramandeep, and Jatinder Kumar., "Integrated DCT, DWT and modified SVD based digital image watermarking", International Journal of Computer Science and Mobile Computing, **4**(5): 1002-1011 (2015).

[10] Noor A. Ibraheem, Mokhtar M. Hasan, Rafiqul Z. Khan and Pramod K. Mishra, "Understanding color models: a review", ARPN Journal of Science and Technology, **2**(3): 265-275 (2012).

[11] Adrian Ford, and Alan Roberts, Colour Space Conversions, Westminster University, London, 1-31 (1998).

Biosynthesis of Gold Nanoparticles by Fenugreek (Trigonella Foenum-Graecum) Extract

Ahmed Fragoon*,1, Lamiaa Frah2, Amal Mamoun2

1PHD, Department of Biomedical Engineering, Sudan University of Science and Technology, 11111, Sudan

2BSC, Department of Biomedical Engineering, Sudan University of Science and Technology, 11111, Sudan

A B S T R A C T

In this work fenugreek(Trigonella Foenum Graecum) extract was used to synthesis gold nanoparticles by simple and safe method .In aqueous solution of chloroaurate ions, fenugreek extract was used as reducing agent and gum Arabic as stabilizer by one synthetic route which is microwave irradiation .The nanoparticles were characterized and investigated by ultraviolet-visible (UV-Vis) spectrophotometry, transmission electron microscopy (TEM), energy-dispersive X-ray (EDX) spectroscopy, X-ray diffraction (XRD)and Fourier transform infrared spectroscopy(FTIR). The size and shape of the nanoparticles were found to be very sensitive to the quantity of the extract. And the shape of gold nanoparticles was found to be multiform; the EDX spectrum show high peaks of gold that indicate the pure nature of gold nanoparticles in chemical composition.

1. Introduction

This paper is an extension of work originally presented in 2015 International Conference on Computing, Control, Networking, Electronics and Embedded Systems Engineering (ICCNEEE) [1]. Nanotechnology, nanoscience, nanostructure, nanoparticles are now of the most widely used words in scientific literature. Nanoscale materials are very attractive for possible machine, which will be able to travel through the human body and repair damaged tissues or supercomputers which small enough to fit in shirt pocket. However, nanostructure materials have potentials application in many other areas, such as biological detection, controlled drug delivery, low-threshold laser, optical filters, and also sensors, among others [2-3].

In fact, metal nanoparticles have been used a long time ago e.g. Damascus steel which used to make sword and Glass Lycurgus Cup which has unique color. Even though, nanoparticles have been used a long time ago, but nobody realized that it reached nanoparticles scale[4-7], One of the most interesting aspects of metal nanoparticles is that their optical properties depend strongly upon the particle size and shape ,Bulk Au looks yellowish in

reflected light, but thin Au films look blue in transmission. This characteristic blue color steadily changes to orange, through several tones of purple and red, as the particle size is reduced down to ~3 nm. These effects are the result of changes in the so-called surface Plasmon resonance [8], the frequency at which conduction electrons oscillate in response to the alternating electric field of incident electromagnetic radiation. However, only metals with free electrons (essentially Au, Ag, Cu, and the alkali metals) possess Plasmon resonances in the visible spectrum, which give rise to such intense colors. Elongated nanoparticles (ellipsoids and nanorods) display two distinct Plasmon bands related to transverse and longitudinal electron oscillations. The longitudinal oscillation is very sensitive to the aspect ratio of the particles [9-10].

Most commonly studied metal nanoparticles include gold, silver, titanium oxide and iron nanoparticles. Among these, gold being inert and relatively less cytotoxic is extensively used for various applications [11].

Gold nanoparticle chemistry and physics has emerged as a broad new subdiscipline in the domain of colloids and surfaces. The unusual optical properties of small gold particles, their size dependent electrochemistry, and their high chemical stability

*Corresponding Author: Ahmed Fragoon, Khartoum, Sudan, +249991784173,
lamiaafarh1992@gmail.com, ahmedfragoon@sustech.edu

have made them the model system of choice for exploring a wide range of phenomena including self-assembly, biolabeling, catalysis, electron-transfer theories, phase transfer, DNA melting and assays, and crystal growth [12].

Among the use of living organisms for nanoparticle synthesis, plants have found application particularly in metal nanoparticle synthesis. Use of plants for synthesis of nanoparticles could be advantageous over other environmentally benign biological processes as this eliminates the elaborate process of maintaining cell cultures. Biosynthetic processes for nanoparticles would be more useful if nanoparticles were produced extracellularly using plants or their extracts and in a controlled manner according to their size, dispersity and shape. Plant use can also be suitably scaled up for large-scale synthesis of nanoparticles [13].

Fenugreek (Trigonella foenum-graecum) belongs to the family fabaceae. Fenugreek is used both as a herb (the leaves) an as a spice (the seed), has been used for long time as a hematopoietic and antioxidant agent in traditional therapeutics, in Sudan the seeds have many uses especially in folk medicine. Whole seeds are swallowed as antiacid and against dysentery and stomach disturbances [14-15].

Fenugreek have been shown it contain high levels of antioxidants in which may be due partly to the presence of flavonoids and polyphenols. In this paper, we present a detailed study of the biosynthesis of GNPs by the reaction of fenugreek extract with aqueous gold ions. We hypothesized that the effective utilization the various phytochemicals present in fenugreek and their antioxidant activities will provide simple, clean, nontoxic and environmentally being bioreduction process of gold salts into their corresponding nanoparticles.In additional, the obtained GNPs were further stabilized by gum Arabic, another plant source glycol protein[16].

The emphasis is on controlling the size and shape of the GNPs by varying the experimental conditions in the synthesis and thereby modulates the optical properties of the nanoparticles. Up to now, many efforts have been made to fabricate anisotropic gold nanostructures with various shapes [17]. Although some chemicals methods for the preparation of GNPs with pre-chosen size by changing the concentration of gold ions and stabilizer [18], or by seed mediated growth [19], they may utilize toxic chemicals either in the form of reducing agents or as stabilizing agents. However, a few works have reported on the biosynthesis of nanostructures with novel and controllable size or desirable shape. Here, we show that size control can be achieved by simple variation in the quantity of the fenugreek extract in the reaction medium. In this process, we use a household microwave oven as a heating apparatus to synthesize gold colloids. Microwave chemistry, which reviewed in detail in the areas of organic reactions [19] and analytical chemistry [20], synthesized nanoparticles were characterized by various methods, such as transmission electron microscopy (TEM), energy-dispersive X-ray (EDX), ultraviolet-visible (UV–Vis) and X-ray diffraction (XRD) [21].

2. Experimental Details

2.1 Materials

The fenugreek seed and the gum arabic powder were purchased from a local herbal shop in the Sudan. Hydrogen tetrachloroaurate tetrahydrate ($HAuCl_4.3H_2O$) purchased from Labline Co. Ltd. (Sudan) and used without further purification.

2.2 Instrumentations

2.2.1. UV–Vis Absorption Spectroscopy
Optical absorption spectra of the fenugreek seed ,extract reduced GNPs were recorded using a UV-1800 UV–Vis-spectrophotometer (Shimadzu, Japan) with 2 ml of GNPs solution in a 1 cm optical path cuvette.

2.2.2. Transmission Electron Microscopy
The morphology and size of the GNPs were analyzed using the TEM images obtained with transmission electron microscope JEM 2100 200 kV (JEOL, Japan).

2.2.3. Energy Dispersive X-Ray Spectroscopy
The chemical composition and element composition maps of GNPs were analyzed using EDX plot obtained with Energy Dispersive X-Ray Spectroscopy.

2.2.4 X-ray Powder Diffraction
The phase identification and crystal structures of GNPs were characterized using the XRD plot obtained with X-ray Powder Diffraction labx XRD 6000(Shimadzu, Japan). The GNPs solution were converted to dry by centrifuged (6000 rpm for 50 min) and dried under sun.

2.2.5. Fourier transforms infrared spectroscopy
The infrared spectrum of absorption, emission, photoconductivity or Raman scattering of GNPs were analyzed using FTIR plot obtained with Fourier transform infrared spectroscopy FTIR-8400S (Shimadzu, Japan).

2.3 Preparation of fenugreek Seeds Extract

Weighted 8g from fenugreek seed then washed with sterilized water to remove any contaminant or dust particles, putted on filter paper to dry .the beaker washed with sterilized water and sterilized in oven at 200℃ for 30 min. The fenugreek seed putted in 50ml dionizd water at beaker and covered with plastic cover. Then it was incubate for 24h at room temperature.

After the incubation period the solution of the fenugreek was centrifuged at 6000 rpm for 15 min, than it was stored at 4℃, and use within 3 days for GNPs synthesis.

2.4 Biosynthesis of GNPs by Microwave Irradiation

In a typical experiment, to 200 ml beaker was added 120 mg of gum arabic powder, 10 ml of fenugreek seed extract and the volume increased to 20 ml by addition of an appropriate volume of deionised water. To the resulting mixture 28 ml aqueous solution of 10 mM [$HAuCl_4.3H_2O$] was immediately added.

Following this, the beaker was placed in the centre of a domestic microwave oven (MS3040S/00) at 2450MHZ. After just 30 s of microwave irradiation at the maximum power output of 850 W, the color of the stirred mixture turned purple-red from pale yellow indicating the formation of GNPs. The solution was then left to cool to room temperature and the rapid reduction is complete within 2 min as shown by stable light purple- red color of the solution which gives 10 ml colloid. To obtain 8 and 6 ml colloids the addition of the fenugreek seed extract is varied as 8, 6 ml, respectively.

3. Result and Discussion

In the present study, Gold nanoparticles exhibit a distinct optical feature commonly referred to as localized surface Plasmon resonance (LSPR), that is, the collective oscillation of electrons in the conduction band of gold nanoparticles in resonance with a specific wavelength of incident light. LSPR of gold nanoparticles results in a strong absorbance band in the visible region (500 nm-600 nm), which measured by UV-Vis spectroscopy .The LSPR spectrum is dependent both on the size, and shape of gold nanoparticles. The peak absorbance wavelength increases with particle diameter, and for uneven shaped particles such as gold nanourchins, the absorbance spectrum shifts significantly into the far-red region of the spectrum when compared to a spherical particle of the same diameter .Figure 1 below show UV-VIS curves for absorption of synthesized GNPS, the absorption at the wavelength range from 400nm – 700nm.

3.1. UV-VIS Result

The template is used to format your paper and style the text. All margins, column widths, line spaces, and text fonts are prescribed; please do not alter them. You may note peculiarities. For example, the head margin in this template measures proportionately more than is customary. This measurement and others are deliberate, using specifications that anticipate your paper as one part of the entire proceedings, and not as an independent document. Please do not revise any of the current designations.

3.2. TEM Result

The morphology of GNPs was characterizing using TEM images recorded at different magnifications of gold particles resulting from the reduction of chloroaurate ions by different amounts of the fenugreek extract. Figure2 (A),(B),(C) and (D) show GNPs reduce by 8ml fenugreek extract ,its consist of branched (multipods) hexagonal with spherical, triangular ,pentagon , and rod nanoparticles .when 10 ml fenugreek extract was used to reduce the aqueous HAuCl4, figure 3(A),(B),(C) and (D) consist of branched (multipods) spherical with triangular ,rod , and hexagonal nanoparticles .According to the size distribution of the spherical GNPs shown in figure 4 (A) and (B) the nanoparticles, the average size ca 13.71nm for 8 ml FSE and average of size ca. 11.85nm for 10ml FSE.

In conclusion, Biosynthesis of GNPs using fenugreek extract produce multiform GNPs.
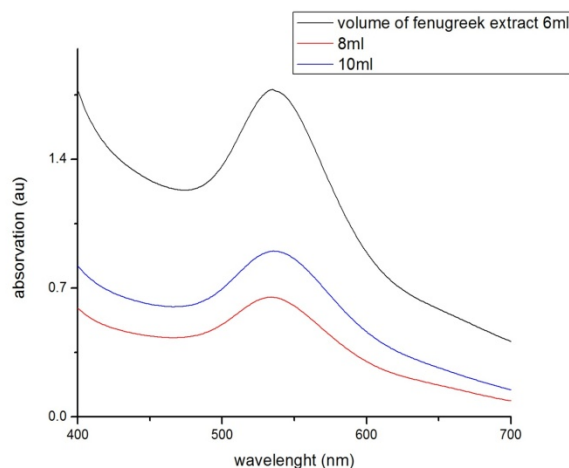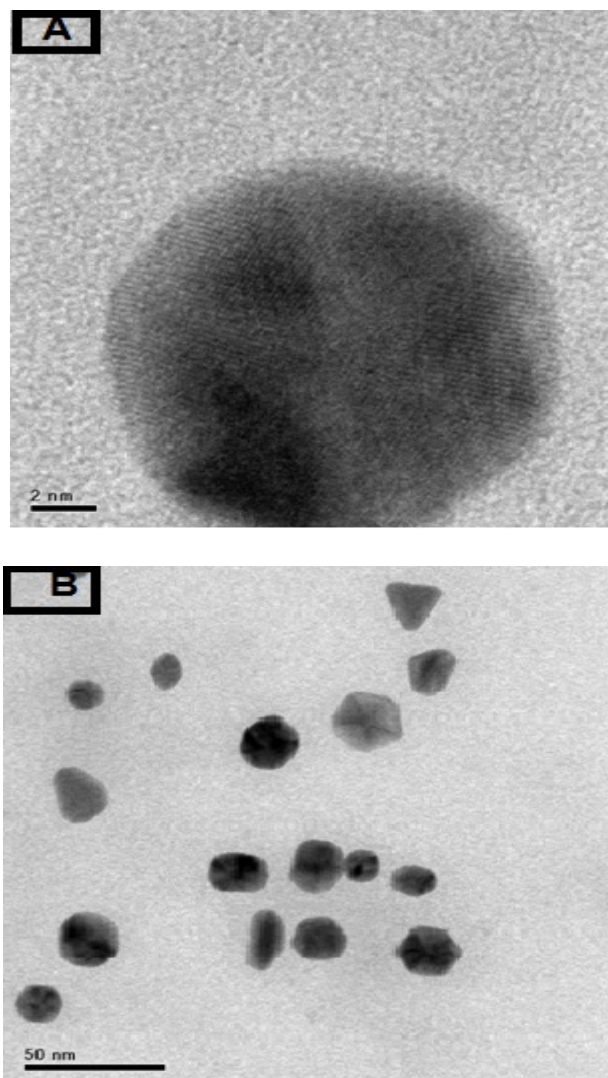

Figure 1 Absorption spectra of GNPs after bioreduction by fenugreek Extract of 6, 8 and 10 ml dosages were exposed to 28 ml, 10 mM Aqueous solution of $HAuCl_4$.
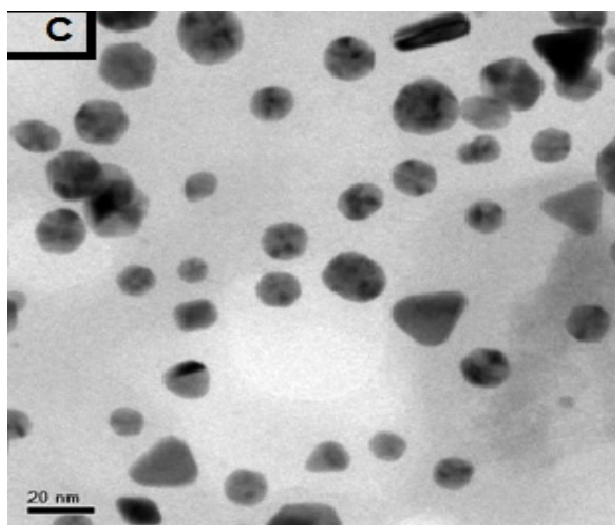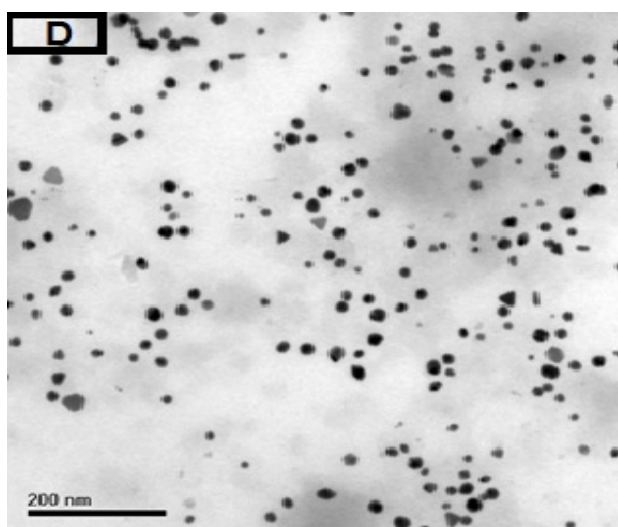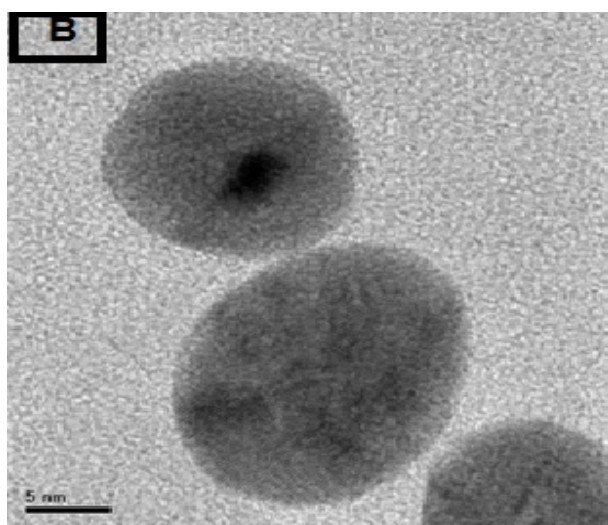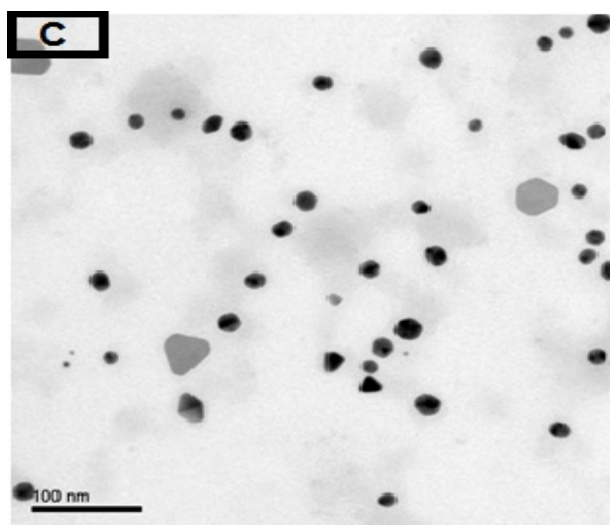
Figure 2 TEM images illustrating the biosynthesis of GNPs using microwave irradiation by exposing 8 ml FSE to 28 ml, 10 mM aqueous $HAuCl_4$, Scale bars (A) 2nm,(B) 50nm (C)100nm and (D)200nm.
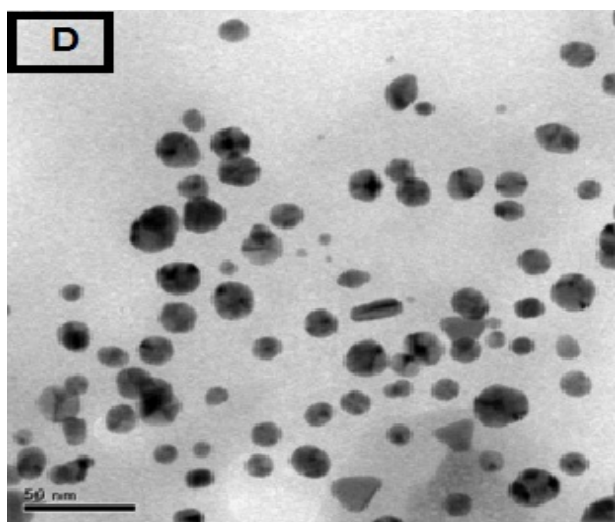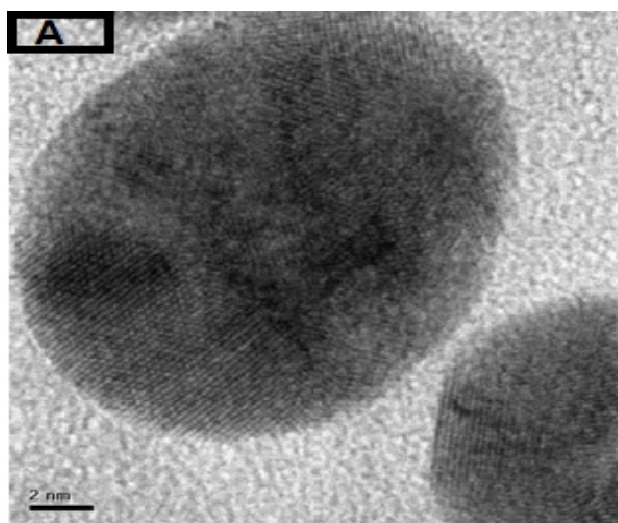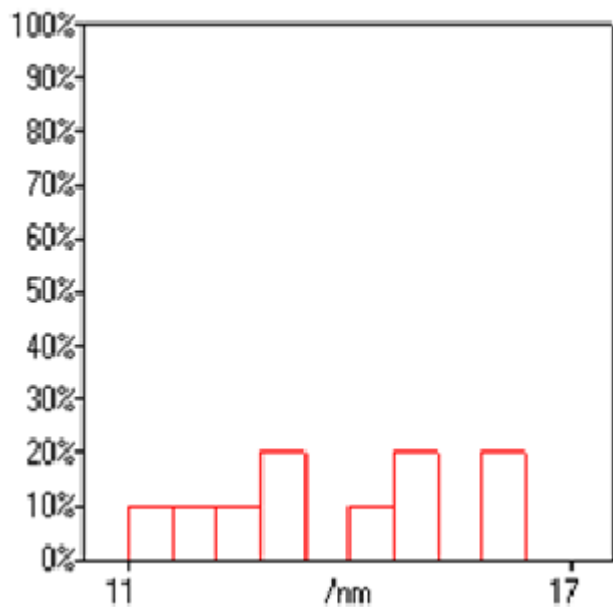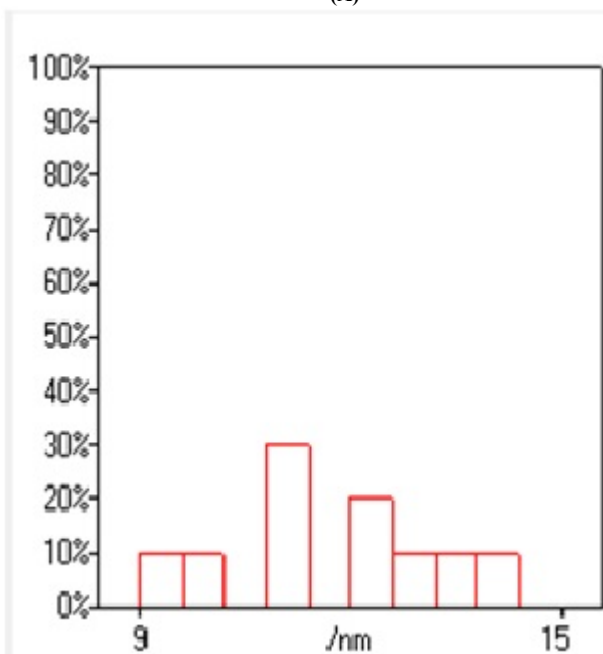

Figure 3 TEM images illustrating the biosynthesis of GNPs using microwave irradiation by exposing 10 ml FSE to 28 ml, 10 mM aqueous $HAuCl_4$, Scale bars (A) 2nm,(B) 5nm (C)20nm and (D) 50nm.

(A)

(B)

Figure 4 A histogram of size distribution of spherical GNPs synthesized using (A) 8 ml FSE (B) 10 ml FSE.

3.3. EDX Result

In the EDX spectrum of the GNPs, Figure5 (A) showed that a typical biogenic nanoparticle exhibited strong X-ray emission signals from the gold atoms and the Cu peaks were due to background signals from the supporting grid. This indicates that the biogenic GNPs are relatively pure in chemical composition.

XRD analysis figure5(B) show Three peaks observed at 38.3°, 40.6°,and 50.4°,can be indexed to the (111), (200),and (220) reflections of face-centered cubic (FCC) structure of metallic Au, respectively , showing the pure crystalline nature of the prepared

particles. The intensity ratio between the (200) and the (111) diffractions (I(200)/I(111)) of 1.43 for the prepared sample is larger than the conventional bulk intensity ratio (~0.53).
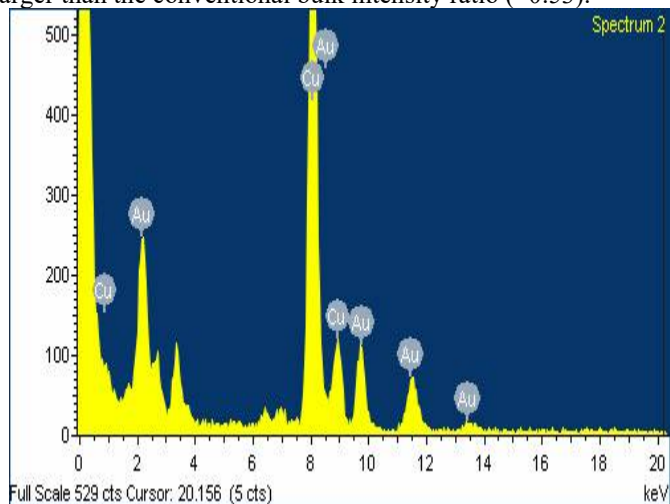
(A)
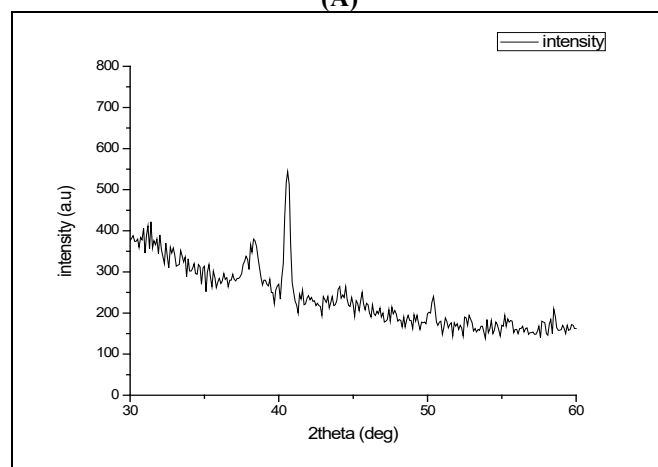
(B)

Figure 5 (A) EDX spectrum of GNPs from the inset image, (B) X-ray diffraction patterns of 8 ml FSE with 28 ml, 10 mM aqueous HAuCl$_4$.
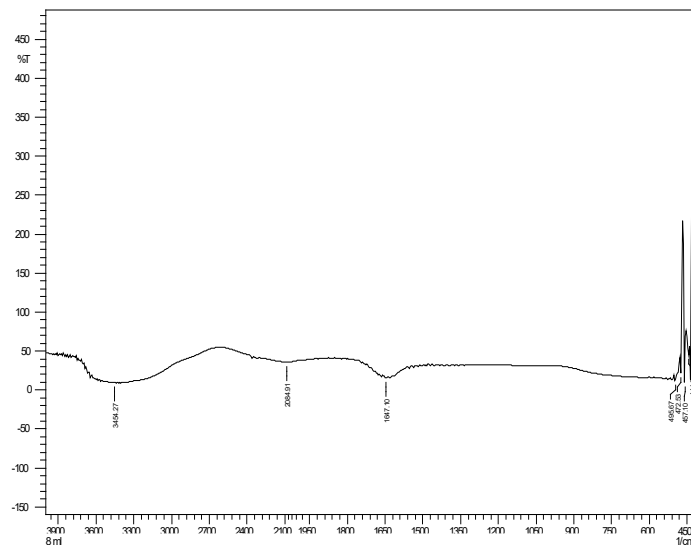

Figure 6 FTIR spectrum of FSE with 28 ml, 10 mM aqueous HAuCl$_4$.

3.4. Fourier transform infrared spectrum Result

Fourier transform infrared spectrum show the active components that have been detected Phenols and Alkaloid. The extracts of the fenugreek exhibit antioxidant activity, chemical composition and polar nature of FSE contains phenol compound. IR spectrum show peaks at 3454.27, 2084.91, 1647.10, 495.67 cm-1 correspond to (O–H stretch, H–bonded) phenols, (–C≡C–) stretch/ alkynes, (–C=C–) stretch/ alkenes. As figure 6 shows.

4. Conclusion

The work defines the synthesis of GNPs in aqueous solution of chloroaurate ions using fenugreek extract as reducing agent and gum arabic as stabilizer. This method produced biocompatible GNPs simply. One synthetic route, microwave irradiation his been used. The study finds that biosynthesis of GNPs using fenugreek extract produce multiform and uncontrollable gold nanoparticle .The study finds that as the amount of fenugreek extract increased the size diameter of GNPs increase. In further studies, these functional GNPs could be used in different medical application like vaccine storage indicator methods.

Acknowledgment

References

[1] Ahamed Fragoon, Amal Mamoun, Lamiaa Frah, Shahinaz Abd_Alwahab (biosynthesis of Gold Nanoparticle by Fenugreek Seed (Trigonella Foenum Extract) (2016).

[2] Kostoff, R. N.; Koytcheff, R. G.; Lau, C. G. Y. (Structure of the nanoscience and nanotechnology applications literature). The Journal of Technology Transfer, 1-13.

[3] Andrievskii, R. A. Directions in Current Nanoparticle Research. Powder Metallurgy and Metal Ceramics, **42** (11): 624-629 (2003).

[4] Liz-Marzan, L. M. (Nanometals: Formation and color). Materials Today, **7**(2): 26-31 (2004)

[5] Roco, M. C. (Nanoparticles and Nanotechnology Research) Journal of Nanoparticle Research, **1**(1): 1-6 (1999).

[6] Reibold, M.; Paufler, P.; Levin, A. A.; Kochmann, W.; Patzke, N.; Meyer, D. C. Materials: Carbon nanotubes in an ancient Damascus sabre. Nature 2006.

[7] Fredy Kurniawan (new analytical application of gold nanoparticale) Surabaya, Indonesia march 2008.

[8] U. Kreibig, M. Vollmer (Optical Properties of Metal Clusters), Springer-Verlag, Berli.

[9] S. Link, M.A. El-Sayed J. Phys. Chem. B, **103**: 8410 (1999).

[10] Luis M Liz_Marzan (Nanometals: Formation and color) materialstoday 23 January 2004.

[11] Pooja M. Tiwari, Komal Vig, Vida A. Dennis and Shree R. Singh (Functionalized Gold Nanoparticles and Their Biomedical Applications) Nanomaterials, **1**: 31-63 (2011).

[12] Rajesh Sardar, Alison M. Funston, Paul Mulvaney, and Royce W. Murray (Gold Nanoparticles: Past, Present, and Future) Langmuir, **25**(24): 13840–13851 (2009).

[13] V. Kumar and S. K. Yadav, J. Chem (Plant-mediated synthesis of silver and gold nanoparticles and their applications) **84**: 151 (2009).

[14] Abdel Moneim E. Sulieman1, Heba E. Ahmed2and Awad M. Abdelrahim(The Chemical Composition of Fenugreek (Trigonella Foenum graceum L) and the Antimicrobial Properties of its Seed Oil) Wad-Medani, Sudan **3**(2).

[15] Ghosh, Sourav; Sengupta, Jayeeta; Datta, Poulami; Gomes, Antony (Hematopoietic and Antioxidant Activities of Gold Nanoparticles Synthesized by Aqueous Extract of Fenugreek (Trigonella foenum-graecum) Seed), 546-5527 (2014).

[16] L. Huang, M. Wang, Y. Zhang, Z. R. Guo, J. F. Sun, and N. J. Gu,Phys. Chem. C **111**: 16154 (2007).

[17] D. V. Leff, P. C. Ohara, J. R. Health, and W. M. Gelbart, J. Phys.Chem. **99**: 7036 (1995).

[18] T. K.Sau, A. Pal, N. R. Jana, N. L. Wang, and T. Pal, J. Nanopart.Res. **3**: 257 (2001).

[19] R. N. Gedye, W. Rank, and K. C. Westaway, Can. J. Chem. **69**: 706 (1991).

[20] J. R. J. PareÂ, J. M. R. BeÂlanger, and S. S. Stafford, Trends Anal.Chem. **13**: 176 (1994).

[21] Fragoon, J.Li, J.Zhu, and J. Zhao (Biosynthesis of Controllable Size and Shape Gold Nanoparticles by Black Seed (Nigella Sativa) Extract) (2012).

Dynamic detection of abnormalities in video analysis of crowd behavior with DBSCAN and neural networks

Hocine Chebi[1], Dalila Acheli[2], Mohamed Kesraoui[3]

[1]*Doctoral student (Automatic and Industrials informatics), Faculté des hydrocarbures et de la chimie (FHC), Laboratoire d'automatique appliquée, University M'hamed Bougara Boumerdès, Algeria.*

[2]*Professor, Faculté des sciences (FS), Laboratoire d'automatique appliquée, University M'hamed Bougara Boumerdès, Algeria.*

[3]*HDR, Faculté des hydrocarbures et de la chimie (FHC), Laboratoire d'automatique appliquée, University M'hamed Bougara Boumerdès, Algeria.*

A B S T R A C T

Visual analysis of human behavior is a broad field within computer vision. In this field of work, we are interested in dynamic methods in the analysis of crowd behavior which consist in detecting the abnormal entities in a group in a dense scene. These scenes are characterized by the presence of a great number of people in the camera's field of vision. The major problem is the development of an autonomous approach for the management of a great number of anomalies which is almost impossible to carry out by human operators. We present in this paper a new approach for the detection of dynamic anomalies of very dense scenes measuring the speed of both the individuals and the whole group. The various anomalies are detected by dynamically switching between two approaches: An artificial neural network (ANN) for the management of group anomalies of people, and a Density-Based Spatial Clustering of Application with Noise (DBSCAN) in the case of entities. For greater robustness and effectiveness, we introduced two routines that serve to eliminate the shades and the management of occlusions. The two latter phases have proven that the results of the simulation are comparable to existing work.

1. Introduction

Recently, computer vision in the analysis of densely crowded environments has been very interesting. Problems such as segmenting, estimating, and determining the goal of individuals' crowd components have all been subjects of research [1-4]. This field of research is an important application in the video surveillance intelligences and visual crowd behavior analysis. In many of these researches, the purpose is not to analyze normal crowd behavior but to detect deviations and abnormal events.

The approach suggested in this paper differs from the existing approach [5-7] by relying on detection of dynamic anomalies,

which makes the detection of anomalies possible for both cases (a group or a single person).

It can be divided into three sublevels: the bottom level (the estimate of optical flow), the intermediate level (construction of the model magnitude) and the semantic level (the notification of operators).

The goal of this approach is to illustrate the detection of anomalies in very dense scenes based on the speed of the individuals and that of the group. The various anomalies are detected automatically by dynamic switching between two approaches which are the artificial neural networks for the management of anomalies in a group of people, while the DBSCAN method is used to detect the entities [8, 9]. For greater robustness and effectiveness, we have introduced two routines

Corresponding Author : HOCINE CHEBI, Faculté des hydrocarbures et de la chimie (FHC), Laboratoire d'automatique appliquée, University M'hamed Bougara Boumerdès, Algeria, chebi.hocine@yahoo.fr.

allowing the elimination of the shades [10, 11] and the management of occlusions [11].
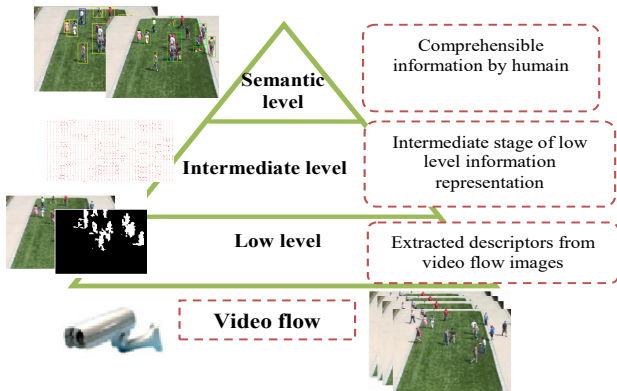

Figure 1: Global illustration of our solution for crowd behavior analysis.

The rest of this paper is organized as follows: in section 2 we present a brief background on the various approaches as well as the works related to this field, and our suggested approach in order to overcome certain problems encountered in the literature. Section 3 presents the mathematical formulation of the various methods used in order to detect anomalies of the race type and walk type in a crowded scene. Finally, the results are presented in section 4 and we can conclude that new prospects for future work are provided.

2. State of the art and approach description

Crowd behavior is classified in two categories: the first one consists of estimating the density of the crowd and the second of extracting motives for movement or detecting events in a scene of a crowd and following the abnormal behavior.

In the first category we distinguish the methods based on the analysis of behavior [7-11]. These methods supply an interesting static analysis of the surveillance of the crowds but do not detect abnormal events. There are also some techniques based on optical flow [1-4] that detect stationary crowds.

In the second category the purpose is to detect abnormal events in a crowd by basing itself on the motives for movement. The principle of extraction of the motives for movement is to model the most frequent behavior and to consider the abnormal events as absurd cases. The deviation from typical behavior is used to characterize the abnormality. Several techniques were proposed for this category [12]. Combine hidden Marcov models with analysis of the main vector components of the optical flow to detect scenarios of emergencies. However, the experiments concerned simulated data. Using the dynamics of tracking behavior one can recognize and locate present objects in a temporal sequence of images [13]. Within the framework of human crowds there is a particular interest in video surveillance where the follow-up of individuals allows checking automatically the comings and goings in a space. Just like in image recognition, a follow-up can be based on graphic properties such as colors or outlines [14, 15]. The added temporal dimension allows the possibility of a continuity of the presence and the position of the person in the scene, in spite of the occlusion. The temporal and spatial consistency of the followed characteristics can be obtained in certain cases by means of methods of clustering [16].

The proposed approaches contribute to the detection of major anomalies arising in a complex scene. They also contribute to the detection of events in the crowd by following groups instead of

following every person individually which facilitates the detection of events occurring in crowds.

The approaches usually used for the analysis of crowd behavior in video sequences generally comprise four essential stages: detection of movement, segmentation, classification and tracking.

In our work we propose the use of the detection movement technique by optical flow [12-15]. The latter makes it possible to detect groups which move in the same direction and to extract the reasons for movement. The major advantage of this method is that it doesn't need to be modeled, [4, 5], because it consists of detecting the movement by calculation in any point of the image of a mathematical quantity which is a function of the intensity or the color of the whole of the pixels and which is supposed to reflect the importance of the visible movement in the scene. Therefore we propose that the segmentation [16] be done by regrouping the areas with the aim of providing a more precise cutting of the borders of the areas. Afterwards, we propose to use a technique of classifying anomalies by a dynamic switching between the two approaches of artificial neural networks [17] for the management of anomalies in a group of people, and the DBSCAN [9] method for detecting the entities. Then we propose that the improvement of the results be obtained by adding techniques of elimination of shades and of occlusion which is due to position and the orientation of the camera and the degree of influence of the occlusion. Lastly, we propose the use of a particle filter, which is well adapted to follow disturbed trajectories with abrupt changes of movement, or a KALMAN filter [7] for the tracking.
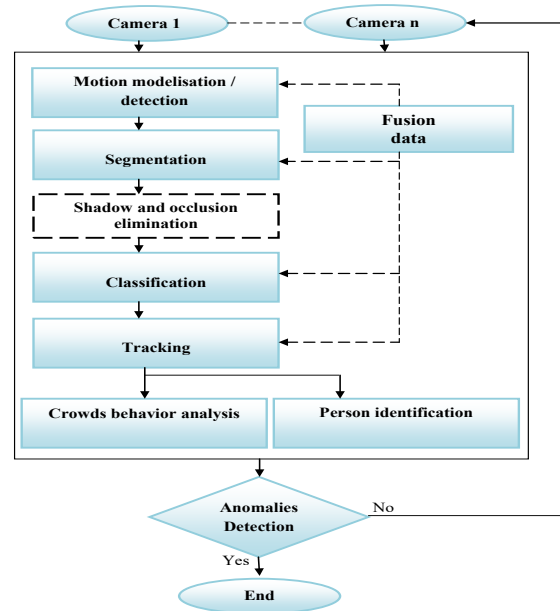

Figure 2: General architecture of automated video surveillance system.

According to the state of the art, the proposed approach is illustrated in the flow chart in (Figure 2). The first stage is for acquiring the image to be treated by the means of a camera. After that, we carried out detection by the optical flow; segmentation of the movements and classification, the last of which represents the new approach for the detection of abnormalities in very dense scenes while being based on the speed of the individuals and of the group. The various anomalies are first detected to be handled automatically without training by the DBSCAN method to detect the entities. The next stage is the tracking of the abnormalities. Finally a test is carried out in order to enable us to extract some

comprehensible information detecting normal and abnormal crowd behavior.

3. Mathematical formulation

The general architecture used will be detailed by the following sections:

3.1. Motion vector extraction

The investigated crowd activities are characterized by the movement of people. The examination of motion dynamics of crowds is based on the so called motion vectors obtained by the method of optical flow which is applied to each pair of subsequent video frames.

Applying optical flow returns a set of motion vectors in the form:

$$V_{i,t} = (x_{i,t}, y_{i,t}, m_{i,t}, \theta_{i,t}) \tag{1}$$

Where "$V_{i,t}$" is the motion vector "i" at frame "t", represented by the feature point at the coordinate $(x_{i,t}, y_{i,t})$, the magnitude "$m_{i,t}$" and the orientation angle "$\theta_{i,t}$".

3.2. Elimination of shade

The stage of the shades removal was achieved by a simple passage of colorimetric space RGB towards space HSV "for Hue / Saturation / Value", while eliminating the component brightness V. This space highlights the chromatic properties due to its components H, S and V.

The chromaticity of pixel (x, y) could be obtained by color normalization. For example the red channel:

$$C(r, x, y) = \frac{I(r, x, y)}{I(r, x, y) + I(g, x, y) + I(b, x, y)}, \tag{2}$$

where $I(r, x, y)$, $I(g, x, y)$, $I(b, x, y)$ are respectively the intensities of the channels red, green and blue.

It is the same for the two other channels green and blue. The chromaticity of a pixel is then

$$C(x, y) = (C(r, x, y), C(g, x, y), C(b, x, y)). \tag{3}$$

The difference in chromaticity ΔC, between the current $C'(x, y)$ chromaticity of the pixel and its chromaticity $C(x, y)$ in the model of the background makes it possible to measure the Mahalanobis distance $D(x, y)$ represented as follows:

$$D(x, y) = \sqrt{\Delta C(x, y)^T S^{-1} \Delta C(x, y)} \tag{4}$$

Where $S(x, y)$ the chromaticity covariance matrix of the pixel (x, y). Then, for each new image and each pixel, the Mahalanobis distance is calculated.

3.3. Management occlusion

The position and orientation of a camera influences the degree of occlusion. If the camera's optical axis is horizontal, then occlusion will occur in the segment parallel to the horizontal axis of the image plane. Occluded blobs will be indistinguishable due to overlap in depth. We developed a hybrid segmentation methodology to split occluded blobs using a histogram-based approach for horizontal occlusion and an ellipse-based approach for vertical occlusion (Figure 3).
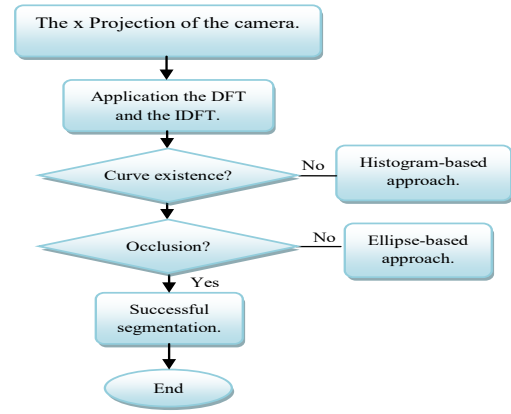

Figure 3: Segmentation flow chart.

Blobs, which become slightly occluded at the same depth such as these, usually have special shape-based features. When projected vertically onto a horizontal line the blobs change into the shapes shown. The curve is similar to a signal in the time domain where the horizontal line is the time axis, and thus discrete Fourier transformation "DFT" can be employed to transform the line into a frequency domain. Thereafter, the lowest frequency components are retained and the rest are set to zero by a filter. Using inverse discrete Fourier transformation "IDFT" they are then transformed back into the time domain. This process smoothes the original curve and benefits the following segmentation. On the smooth curve, the significant peaks are usually located at the horizontal position of the head, whereas the significant valleys are usually located at the effective cut points for segmenting the occlusion.

3.4. Motion vectors clustering

Among the many algorithms proposed in data mining field, DBSCAN is one of the most popular algorithms due to its high quantity of noiseless output clusters. It discovers clusters with arbitrary shape with minimal number of input parameters.

The input parameters are the radius of the cluster "Eps" and minimum points required inside the cluster "Minpts". Complete algorithm of DBSCAN is given by [18].

In order to determine the membership of each element to a cluster and make decisions we need a measure function. Minkowski distance is widely used:

$$d(i, j) = \sqrt[q]{|x_{i1} - x_{j1}|^q + |x_{i2} - x_{j2}|^q + \cdots + |x_{in} - x_{jn}|^q} \tag{5}$$

Many variants are used, mostly with q=1 or q=2. In our case, we have used q=2, which represents the Euclidean distance. From the latter distance, we have derived the next equation. Using a simple difference between the position coordinates, and the magnitudes:

$$\sqrt[2]{(x_p - x_q)^2 + (y_p - y_q)^2 + (m_p - m_q)^2} < \varepsilon \tag{6}$$

Where: (x_p, y_p) and (x_q, y_q) are the coordinates of the point's p and q; "m_p" and "m_q" are magnitudes of the motion vectors at the point's p and q;

As using DBSCAN by one of these three distance measurements, we can cluster motion vectors into diverse groups of data points which have similar coordinates, similar magnitudes

and similar orientation. Each group of motion vectors represents a motion pattern.

3.5. Motion vectors clustering

The neuronal network is used to classify the crowd behavior. Classification is made for each sequence of images in order to detect the various behaviors of a group of people. The classifier is based on a set of neurons which contain three layers. Each type of behavior is individually detected by a network. The structure of each network is defined so that the number of neurons in the input layer is equal to the number of input parameters, and the number of neurons in the hidden layer can be experimentally determined. In this work, two classes of behavior are considered, the normal and abnormal classes, each type of behavior is represented by a neuron in the output layer. Neurons in the hidden layer are represented by a sigmoid function. The model is represented by the following equation:

$$e_k^{(i)} = \sum_j w_{j,k}^{(i-1)} s_j^{(i-1)} + b_k^{(i-1)} \qquad (7)$$

In output, we have $s_k^{(i)} = a_k^{(i)}\left(e_k^{(i)}\right) = \frac{1}{1+\exp\left(-e_k^{(i)}\right)}$ which is related to the applied activation in the network. The value $b_k^{(i-1)}$ is a skew added to the entry of the kth neuron. The function of error, which represents the Euclidean distance between the output of the network and the target, is given as follows:

$$E = \frac{1}{2}\|y - c\|_2^2 = \frac{1}{2}\sum_{i=1}^{m}(y_i - c_i)^2 \qquad (8)$$

It is now necessary to minimize the average of the errors given by the function E on the whole of the data provided in input $E_{average} = \frac{1}{N}\sum_{t=1}^{N} E_t$, Where N is the number of couples given and E_t represents the t-th error of training.

3.6. Detection of events

In this section, we describe the detection of anomalies in a dense scene. The selected scenarios belong to the events described in the video [19, 20].

Run and walk behavior: The principal idea consists of calculating the average magnitude of the movement vectors in each image. A high magnitude means the event runs, while low magnitude means the event goes.

$$M_{mean} = \frac{\sum_{i=1}^{nxm} mag(i)}{nxm} \qquad (9)$$

With n and m numbers it points to movement in the image, and $mag(i) = \sqrt[2]{Rel_i^2 + Img_i^2}$ is the magnitude of each point of movement.

Where Rel and Img are the real and imaginary components of the movement vector.

We considered that the characteristic of the state of a collapse situation is a signal of sudden change with a high peak height of duration. If there is such a signal then there is an abnormal event. The decision for normal or abnormal events is to be taken by comparing the calculated and normalized measure with a specific threshold defined by:

$$T_N = \max_{k=1\ldots F}\{N(d(M_t, M_{t+1}))\}_k \qquad (10)$$
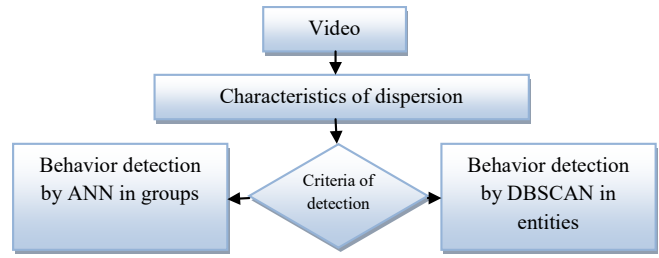

Figure 4: Dynamics strategy of detection.

The strategy of detection in (Figure 4) represents the unusual way of detecting crowd behavior by two approaches (DBSCAN and ANN). This dynamic strategy is always in the case of entity and group of people. The results of simulation of this new approach will be presented in the following section.
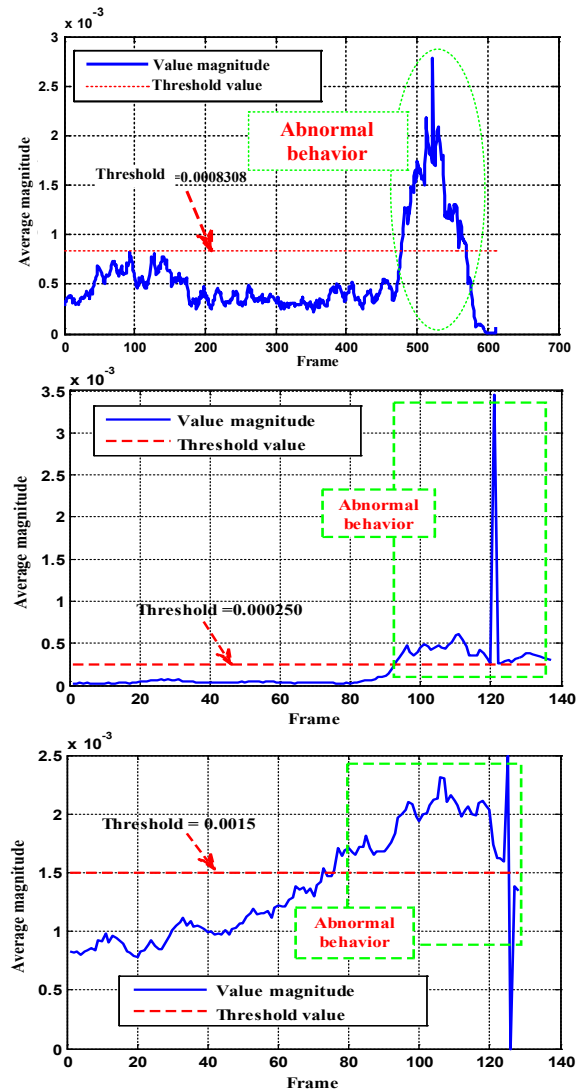

Figure 5: Examples of average speed of a group of people.

4. Results

In this section, the proposed method of detection by switching in a dynamic way between two approaches, the artificial neurons networks (ANN) for the management of group anomalies of people, and the Density Based Spatial Clustering of Application

with Noise (DBSCAN) in the case of entities. The videos are mainly collected from the UMN dataset [19]. The BEHAVE video dataset and the PETS2009 dataset [20] for performance evaluation are adopted in anomalous frame behavior detection experiments.

The proposed approach is based on computing the magnitude of the motion vector which presents the optical flow in the Cartesian frame. The point $P(x, y)$ is the position of its interests point at time "t" , where $Q(x, y)$ is the position of the same point at time "t + 1", we use the Euclidean distance.

We calculate the average magnitude of each sequence of images with an aim to determine the running and walking events (Figure 5). These events can be identified by using the magnitude of the vectors of optical flow. Therefore the principal idea consists of calculating the average magnitude of the movement vectors in each image. A high magnitude indicates a running event while low magnitude indicates a walking one. The detection is performed using DBSCAN in the case of entities, and ANN for the management of people in a group, the classifiers based on the average speed as criteria. The results of the approach suggested are represented in (Figure 6) and (Figure 7).

Figure 6: Behaviors detection by NNA, (a) normal behavior, (b) abnormal Behavior.

In our work, we suppose that the number of people in an occulted group is not limited. Moreover, we compare our results with other methods (Figure 8), such as the function of probabilistic density [21] and [22], the social force model (SFM) [23], and the metric ones of similarities based on the speed and the orientation of decoupling 2D of histograms [24] and [23]. The obtained results are encouraging when the automatic detection of anomalies is close to the real time measurement. The approach suggested shows a great robustness against false alarm detection since the automatic detection of anomaly occurs after the real release of the anomaly.

These results prove that our method gives the satisfactory results comparable to ones concerning the other three methods (Figure 8).

In (Figure 9) and (Figure 10) is present some results that illustrate the case of occlusion management and elimination of shades. Our approach has some advantages as it presents a positive contribution for the detection of the movement in a complex environment. However it requires the estimation of temporal time for each sequence of image and at every moment of the video sequence which makes it very greedy in computing power consumption. Moreover the optical flow occupies only about 84 % of movement surface detection in opposition to the advection of particles of social forces model which is used to locate a large surface (more than 96 %). Our approach reached a flow of 4 images per second on an INTEL Pentium 2.16 GHz processor (which can be seen as a weak processor) simulated under MATLAB "R2014a".
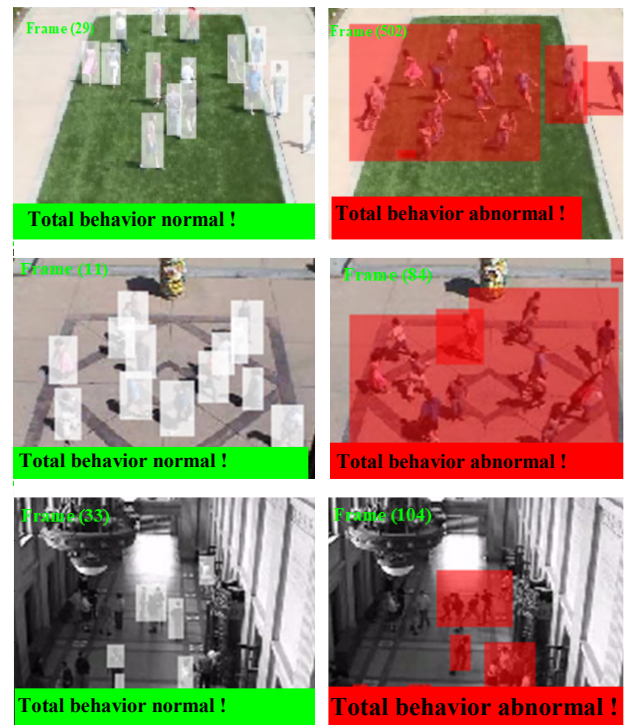

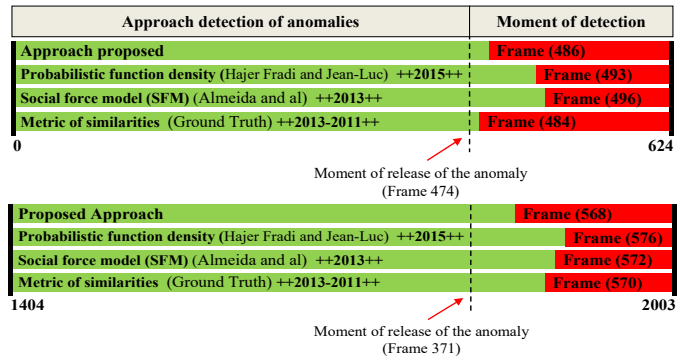Figure 7: Examples of behaviors analysis by DBSCAN.

Figure 8: Moment's anomalies detection for video 1 and 3 in data UMN [19] (green: Normal events, red: Abnormal events).
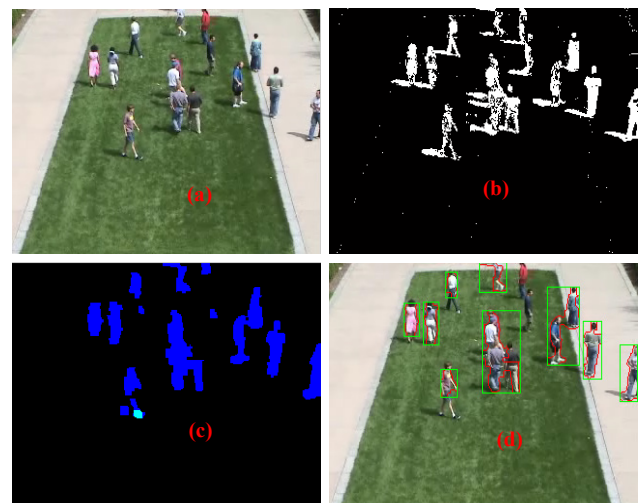

Figure 9: Results before and after the removal of shades. (a) Original image, (b) Binary image, (c) and (d) Results of shadow elimination.
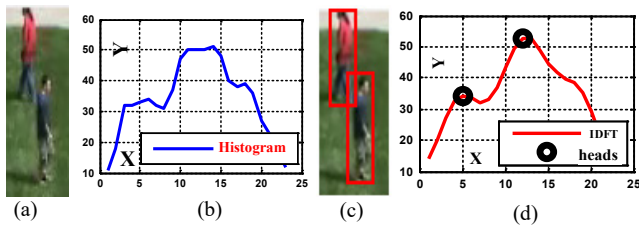
Figure 10: States of occlusion (a) Occlusion (b) Histogram of image (c) Result of occlusion (d) Smoothing of the histogram.

We have some illustrative results in (Figure 11) expressing the case of elimination of shade. We note that our described approach favors as it presents a positive contribution for the detection of the reasons for movement in a complex environment. The results of (Figure 11) show that our system has a good robustness with a precision of more than 0.75.
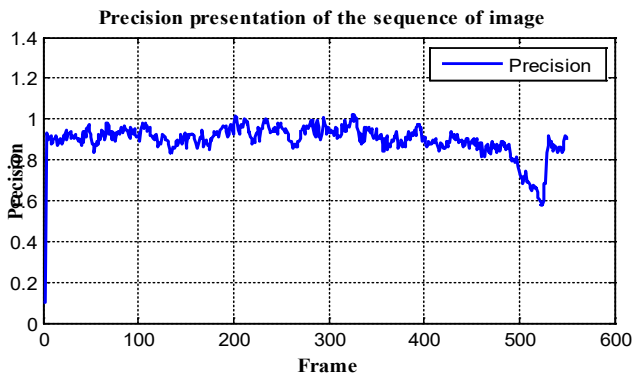

Figure 11: Example Results of Precision presentation of shadow elimination.

To clarify other advantages of the algorithm we simulated the video according to:

The blue colored curve below (Figure 12) presents the output of the algorithm proposed previously. Different sequences from the image in the normal and abnormal situations were differentiated by a label from one or zero respectively, according to classification by neural networks.

To show the effectiveness of the method ran a simulation using the data from [20] which showed satisfactory results in another behavior situation i.e. in the case of the presence of a vehicle, unusual crossing of a road at a faster pace (Figure 13).
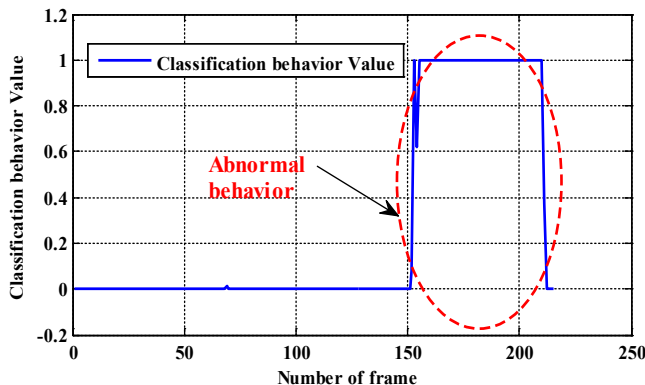

Figure 12: Example of total video analysis contains abnormal behavior and classification by neural networks.
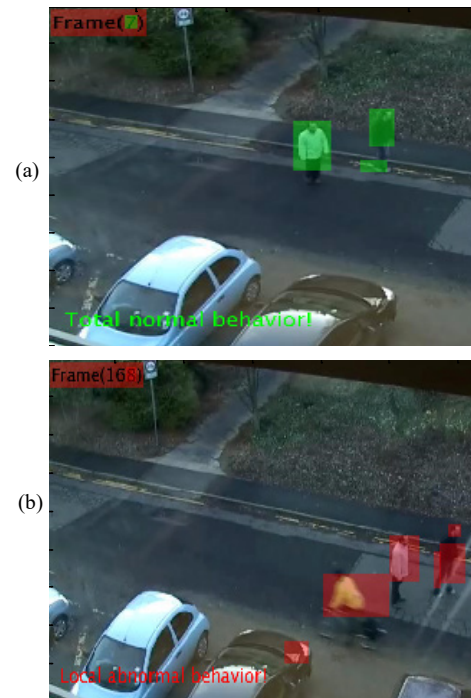

Figure 13: Detection of behavior by NNA in data [20], (a) normal behavior, (b) abnormal behavior.

For the identification of events of crowd evaluation, we examine the calculation of the performances of the strategy and we obtain these following results:

TABLE 1. COMPUTING TIME OF THE CLUSTERS.

NUMBERS POINTS	COMPUTING TIME OF THE CLUSTERS (SEC)
484	0.112150
891	0.302466
1203	0.610144
1433	0.687086
2051	1.508658
2357	1.958189
2873	2.498675
3412	3.749445
3632	3.831626
3776	4.157234
4406	5.663246
4956	7.070499
5396	8.723374

The results of our experiments show that with time the execution by contribution with the number of points of DBSCAN is close to the quadratic equation as seen in Table 1, and the numbers of the points on top is almost linear as seen in (Figure 14). The Figure 14 illustrates the efficiency of DBSCAN. Figure 15 is the following different watch examples of the images with behavior abnormal.

We noticed that the adopted algorithm manages to detect an abnormal behavior when it appears. This algorithm functions in the majority of cases. Nevertheless, in certain cases it shows its imperfections. It is judged sufficiently effective to supervise the behavior of crowds where there is movement of the crowd in a linear direction like the example of a population crossing the road.
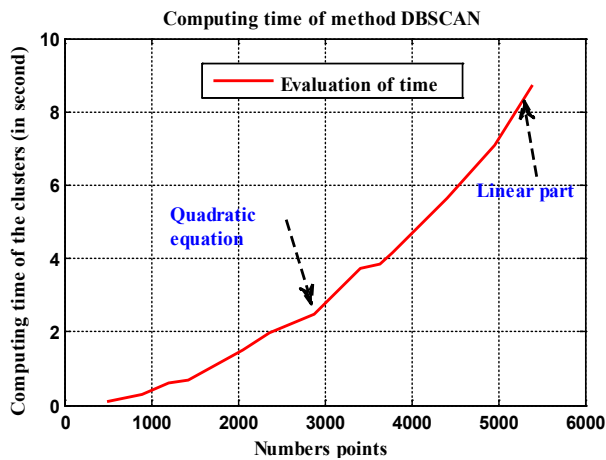
Figure 14: Results of computing time by the DBSCAN method.

Figure 15: Another examples of the images with behavior abnormal.

5. Conclusion

In this article, we described a new method based on dynamics of the detection of abnormal crowd behavior. We are interested in the analysis of crowd behavior and its entities in a dense scene. The approach is composed of two components: the calculation of the dispersion parameters and the behavior classification. The various anomalies are detected while dynamically switching between two approaches: artificial neural networks (ANN) for the detection of anomalies of a group of people, and the Density Based Spatial Clustering of Application with Noise (DBSCAN) in the entities case. In order to examine the effectiveness of the detection algorithm proposed, several synthetic and public scenes are employed. In conclusion, the experiments prove that the algorithm proposed in detection was examined on several scenes depending on the successful detection of abnormal behaviors.

The method suggested is applied to detect the abnormal crowd behavior to imply the dynamics of detection. Behaviors of escape from the crowd in the low ones or average crowd scenes density can be identified remarkably, but the results in the scene with high crowd density can be insufficient. The method suggested can be estimated exactly only for the strongly distinguishable areas. And one of the main problems of the method suggested is an execution in weak real time. As an element of future work the authors' aim

is to study the factors affecting the speed of the algorithm and improve the execution of the algorithm in real time and its exactitude.

References

[1] H. Chebi, D. Acheli, "Dynamic detection of anomalies in crowd's behavior analysis", International Conference on (ICEE'2015), Algeria, (2015).

[2] Y. Zhang; L. Qin; R. Ji; S. Zhao; Q. Huang; J. Luo, "Exploring Coherent Motion Patterns via Structured Trajectory Learning for Crowd Mood Modeling," in IEEE Transactions on Circuits and Systems for Video Technology , **PP**(99): 1-1.

[3] M. Zhou, H. Dong, D. Wen, X. Yao and X. Sun, "Modeling of Crowd Evacuation With Assailants via a Fuzzy Logic Approach," in IEEE Transactions on Intelligent Transportation Systems, **17**(9): 2395-2407 (2016).

[4] S. Yi, H. Li and X. Wang, "Pedestrian Behavior Modeling From Stationary Crowds With Applications to Intelligent Surveillance," in IEEE Transactions on Image Processing, **25**(9): 4354-4368 (2016).

[5] S. Wang, Z. Miao, "Anomaly detection in crowd scene," 2010 IEEE 10th International Conference on Signal Processing (ICSP), 1220-1223 (2010).

[6] S.S. Pathan, A. Al-Hamadi, B. Michaelis, "Crowd behavior detection by statistical modeling of motion patterns," 2010 International Conference of Soft Computing and Pattern Recognition (SoCPaR), 81,86 (2010).

[7] T. Ko, "A survey on behavior analysis in video surveillance for homeland security applications," 37th IEEE Applied Imagery Pattern Recognition Workshop, 2008. 1-8 (2008).

[8] M. Szczodrak, J. Kotus, K. Kopaczewski, K. Lopatka, A. Czyzewski, H. Krawczyk, "Behavior Analysis and Dynamic Crowd Management in Video Surveillance System", 2011 22nd International Workshop on Database and Expert Systems Applications (DEXA), 371-375 (2011).

[9] A. El Maadi, M.S. Djouadi, "Suspicious motion patterns detection and tracking in crowded scenes," 2013 IEEE International Symposium on Safety, Security, and Rescue Robotics (SSRR), 1-6 (2013).

[10] J. Li, G. Wang, "A shadow detection method based on improved Gaussian Mixture Model", 2013 IEEE 4th International Conference on Electronics Information and Emergency Communication (ICEIEC), 62-65 (2013).

[11] H. Qian, X. Wu, Y. Ou; Y. Xu, "Hybrid algorithm for segmentation and tracking in surveillance", IEEE International Conference on Robotics and Biomimetics, 395-400 (2009).

[12] J. Shi, C. Tomasi, "Good features to track", Computer Vision and Pattern Recognition, 1994. 1994 IEEE Computer Society Conference on Proceedings CVPR '94., 593,600 (1994)

[13] B. Atcheson, W. Heidrich, I. Ihrke, "An evaluation of optical flow algorithms for background oriented schlieren imaging" Experiments in Fluids, vol. 46, pp. 467-476, 2009.

[14] P. Burt, E. Adelson, "The Laplacian Pyramid as a Compact Image Code," IEEE Transactions on Communications, **31**(4): 532, 540 (1983).

[15] B.K. Horn, B.G. Schunck. "Determining optical flow." 1981 Technical Symposium East. International Society for Optics and Photonics, (1981).

[16] C. Demonceaux, "Etude du mouvement dans les séquences d'images par analyse d'ondelettes et modélisation markovienne hiérarchique. Application à la détection d'obstacles dans un milieu routier". Diss. Université de Picardie Jules Verne, (2004).

[17] H. A. ROWLEY, S. BALUJA, "Takeo KANADE: Neural network-based face detection". IEEE Transactions on Pattern Analysis and Machine Intelligence (TPAMI), **20**:23–38 (1996).

[18] M. Parimala, D. Lopez, N.C. Senthilkumar: "A Survey on Density Based Clustering Algorithms for Mining Large Spatial Databases", International Journal of Advanced Science and Technology, **31**: (2011).

[19] UMN, Minneapolis, MN, USA. (2006). Unusual Crowd Activity Dataset of University of Minnesota. [Online]. Available: http:// mha.cs.umn.edu/movies/crowd-activity-all.avi.

[20] S. J. Blunsden, R. B. Fisher, "The BEHAVE video dataset: ground truthed video for multi-person behavior classification", Annals of the BMVA, Vol **4**:1-12 (2010), http://groups.inf.ed.ac.uk/vision/BEHAVEDATA/INTERA CTIONS/.

[21] H. Fradi, J. L. Dugelay, "Towards crowd density-aware video surveillance applications", Contents lists available at ScienceDirect, Information Fusion **24:** 3–15 (2015).

[22] R. MEHRAN, A. OYAMA, M. SHAH. "Abnormal crowd behavior detection using social force model". In IEEE Conference of Computer Vision and Pattern Recognition, 935-942 (2009).

[23] I. R. DE ALMEIDA, C.R. JUNG. "Change detection in human crowds". In 2013 26th SIBGRAPI-Conference on Graphics, Patterns and Images (SIBGRAPI), 63-69 (2013).

[24] D.Y. CHEN, P.C. HUANG, "Motion-based unusual event detection in human crowds". Journal of Visual Communication and Image Representation, **22**(2): 178-186 (2011).